Politecnico di Milano

SCHOOL OF INDUSTRIAL AND INFORMATION ENGINEERING
Master of Science – Nuclear Engineering

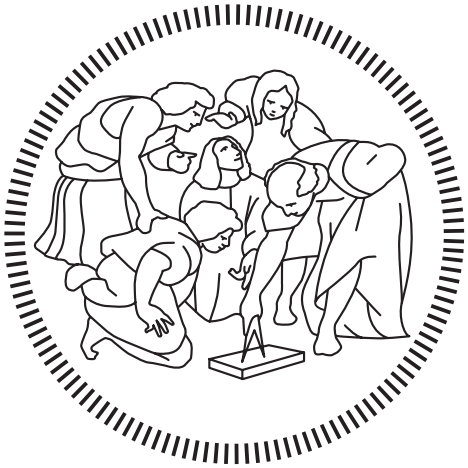

Modelling and assessment of the release of gaseous and volatile fission products from oxide fuel

Supervisor
Davide PIZZOCRI

Co-Supervisor
Lelio LUZZI

Candidate
Giovanni ZULLO – 898393

Academic Year 2019 – 2020

Contents

Abstract

The subject of the present work concerns the modelling and assessment of radioactive gaseous and volatile Fission Products (FPs). These are of primary importance in radiological risk analysis and licensing process of a Nuclear Power Plant (NPP). The state-of-the-art methodology available to evaluate the *source term*, that is the amount of radioactive material which can leakage from the reactor containment, is the American Nuclear Society (ANS) *Method for Calculating the Fractional Release of Volatile Fission Products from Oxide Fuel*, ANS 5.4. If coupled with isotopic yields, it provides the *gap activity*, namely the inventory of radioactive gaseous and volatile FPs that are released from the fuel rod if the cladding is breached. The output of ANS 5.4 is the fractional release of radioactive isotopes from the fuel. The ANS 5.4 predictions for fractional release, with respect to the validation database, are higher of at least one order of magnitude, as a consequence of the basic assumptions of the model. ANS 5.4 methodology has been developed for stationary conditions of the reactor. Therefore, it should not be applied to accidents which involve abrupt temperature variations.

In this work, the stationary hypothesis of the reactor has been circumvented by developing a spectral solver for an improved intra-granular diffusion-decay problem, able to describe transient conditions. The spectral solver has been integrated in the 0D meso-scale code SCIANTIX and verified via Method of Manufactured Solutions (MMS), a technique for testing the consistency of numerical algorithms. This step is fundamental in Verification and Validation (V&V) framework. At inter-granular level, bubble interconnection and subsequent release is described in ANS 5.4 through an empirical correlation, the Vitanza threshold, function of fuel burnup and temperature. The replacement of the Vitanza threshold with a physics-based model constitutes a substantial improvement for inter-granular description. Such a model has been integrated in the spectral solver in order to consider inter-granular bubble growth, coalescence, interconnection and release, through a set of evolutionary equations.

The complete spectral solver for intra- and inter-granular description has been implemented in SCIANTIX. A validation of the model has been carried out against fractional release measurements obtained during VERCORS tests, a set of out-of-pile experiments representative of transient Loss-of-Coolant Accident (LOCA) conditions. The results obtained confirm that the improved model is able to predict the global fractional releases of gaseous and volatile FPs during accident conditions. In addiction, the model is able to provide a conservative description of the release kinetics throughout the transient phase.

Sommario

Il comportamento dei prodotti di fissione gassosi e volatili è di importanza cruciale nella valutazione della radioattività potenzialmente emessa da un impianto nucleare di potenza. Attualmente è possibile valutare il *termine di sorgente*, cioè la quantità di radioattività interna ad un reattore che potentialmente ne può fuoriuscire, grazie alla metodologia ANS 5.4. Questa, se accoppiata ai rendimenti isotopici di fissione, permette di calcolare l'*attività di gap*, cioè l'inventario di isotopi radioattivi che si accumulano nell'intercapedine della barra di combustibile e che in presenza di fratture possono contaminare il fluido termovettore.

ANS 5.4 viene usato per calcolare il rilascio frazionario degli isotopi radioattivi di interesse radiologico dal combustibile nucleare. Vale a dire quelli gassosi e volatili, con emivita sufficientemente breve (minore di un anno). Le predizioni dei rilasci frazionari della metodologia ANS 5.4 sono spesso conservative. Rispetto database di validazione, il modello sovrastima le misure di almeno un'ordine di grandezza, conseguentemente alle ipotesi presenti nel modello. La metodologia ANS 5.4 è stata sviluppata per reattori in condizioni stazionarie. Per questo motivo non dovrebbe essere applicata a condizioni incidentali che coinvologono variazioni improvvise di temperatura.

In questo lavoro la descrizione intra-granulare è stata migliorata. L'ipotesi di stazionarietà è stata rimossa sviluppando un risolutore spettrale per l'equazione di diffusione-decadimento. Il risolutore è stato implementato nel codice SCIANTIX, e la sua consistenza è stata verificata grazie al metodo della soluzione manufatta (MMS). La descrizione inter-granulare di ANS 5.4 è basata su una correlazione empirica che modellizza la saturazione delle bolle a bordo grano ed il conseguente rilascio. Tale correlazione, nota come *soglia di Vitanza*, dipende dai valori di temperatura e bruciamento del combustibile. La soglia di Vitanza è stata sostituita da un modello meccanicistico per l'evoluzione delle bolle a bordo grano. Tale modello include i fenomeni di crescita delle bolle, coalescenza, interconnessione e successivo rilascio di prodotti di fissione.

Nell'ultima fase di validazione, il risolutore spettrale completo di descrizione intra- e inter-granulare è stato impiegato per simulare i test VERCORS. Questi test sono rappresentativi di condizioni incidentali. In particolare, variazioni improvvise di temperatura tipiche nei LOCA con conseguente rilascio di radioattività. Il modello risulta in grado di predire i rilasci frazionari dei prodotti di fissione volatili con errori inferiori all'1%. In aggiunta il modello riesce a fornire una descrizione conservativa della cinetica rilascio, durante tutto il transitorio.

Estratto in Italiano

Introduzione

Nel combustibile dei reattori nucleari si formano normalmente degli isotopi radioattivi. La loro produzione è naturale conseguenza delle reazioni di fissione nucleare da parte dei neutroni sull'uranio 235. Gli isotopi prodotti si chiamano gas o prodotti di fissione, a seconda delle loro proprietà fisiche.

Il nocciolo di un reattore nucleare termico tipicamente è composto da diverse barre di combustibile. Queste, a loro volta, contengono delle pastiglie di diossido di uranio (UO_2). Queste pastiglie vengono prodotte per sinterizzazione di una polvere. Il solido ottenuto ha una struttura policristallina al cui interno sono presenti delle strutture micrometriche dette *grani* [Olander, 1976].

I prodotti di fissione si formano durante l'irraggiamento neutronico all'interno dei grani di UO_2. Nel corso degli anni, differenti osservazioni sperimentali hanno permesso di stabilire un modello valido del comportamento dei prodotti di fissione [Booth, 1957, Turnbull et al., 1982, White and Tucker, 1983, White, 2004, Pastore et al., 2013]. In prima approssimazione, a livello intra-granulare la maggior parte degli isotopi prodotti tende a diffondere verso il bordo grano. Sul bordo grano sono presenti delle bolle che assorbono i prodotti di fissione, che si ingrandiscono e possono arrivare a coalescere. Successivamente avviene la formazione di una rete di bolle interconnesse che collega l'interno della pastiglia con la sua superficie. In tal caso i prodotti di fissione gassosi e volatili, diffondono attraverso questo percorso, e possono fuoriuscire dall'UO_2.

La presenza dei prodotti di fissione limita il tempo di vita utile delle barre di combustibile. Il loro accumulo può provocare rigonfiamenti delle pastiglie, interazioni meccaniche dannose con la guaina della barra, fenomeni di microfessurazione e infine rilascio di radioattività all'interno del reattore. La fissione nucleare produce xeno, kripton, cesio, tellurio, iodio e altri isotopi. Gli isotopi elencati appartengono alla categoria dei prodotti di fissione gassosi e volatili [Kleykamp, 1985]. Solitamente sono radioattivi e devono essere considerati potenzialmente pericolosi da un punto di vista radiologico. Infatti, in condizioni incidentali, possono disperdersi nell'ambiente e contribuire ad aumentare la dosa assorbita dalla popolazione.

In particolare, di un reattore è necessario valutare il *termine di sorgente* e la *attività di gap*. Il primo è un indicatore della quantità di materiale radioattivo presente all'interno del reattore, che può essere rilasciata nell'ambiente esterno. La seconda si riferisce all'inventario dei prodotti di fissione accumulati nell'intercapedine della barra di combustibile e che possono essere messi in circolo all'interno dell'impanto [Housiadas et al., 2012, American Nuclear Society, 2016].

Allo stato dell'arte esiste una metodologia per compiere questo tipo di valutazione. Il suo nome completo è *Method for Calculating the Fractional Release of Volatile Fission Products from Oxide Fuel*, abbreviato in ANS 5.4 [Turnbull and Beyer, 2009]. La metodologia ANS 5.4 permette di stimare il *rilascio frazionario* di alcuni prodotti di fissione radioattivi, quelli gassosi e volatili. È stata sviluppata per reattori ad acqua leggera, che utilizzano diossido di uranio come combustibile e che operano in condizioni stazionarie. In particolare è applicabile in assenza di transitori improvvisi di potenza, a cui normalmente sono associati dei fenomeni di rilascio repentino. Questa ipotesi di stazionarietà è anche nota come regime di equilibrio secolare. Il modello su cui si basa ANS 5.4 è duplice.

A livello intra-granulare considera la matrice di UO_2 come un insieme di grani sferici [Booth, 1957]. A livello inter-granulare considera il fenomeno dell'interconnessione delle bolle a bordo grano attraverso una correlazione empirica tra temperatura e bruciamento del combustibile, nota come *soglia di Vitanza* [Vitanza et al., 1979].

La metodologia ANS 5.4 generalmente sovrastima i valori di rilascio frazionario per gli isotopi di interesse. Il database di validazione di ANS 5.4 include un campione di alcune barrette irraggiate (IFA-504, IFA-558 e IFA-633). I valori di rilascio frazionario predetti dal modello, per gli isotopi ^{85m}Kr e ^{131}I, superano di almeno un ordine di grandezza le misurazioni sperimentali [Turnbull, 2001, Turnbull and Beyer, 2009].

Il presente lavoro di tesi si inserisce in questo contesto. Cercando di analizzare gli aspetti più limitanti della metodologia ANS 5.4 e di sopperirne alcune mancanze. Le principali ipotesi che vengono revisionate durante questo lavoro sono l'equilibrio secolare e la descrizione del bordo grano (Capitolo 1). Si riscrive il problema intra-granulare sfruttando l'ipotesi di decomposizione spettrale della variabile concentrazione. Questa strada permette di superare l'ipotesi di equilibrio secolare e di implementare un nuovo risolutore in SCIANTIX [Pizzocri et al., 2020], un codice 0D di performance del combustibile.

Questo nuovo risolutore risulta in grado di descrivere l'andamento temporale della concentrazione dei vari isotopi e permette di estrarne il relativo rilascio frazionario (Capitolo 2). Nell'ambito della simulazione numerica possiede importanza anche la verifica di un algoritmo appena sviluppato. Perciò il risolutore pocanzi introdotto viene verificato numericamente grazie al metodo della soluzione manufatta (MMS). Infine, la soglia di Vitanza viene sostituita da una descrizione fisica del comportamento delle bolle a bordo grano (Capitolo 3). La bontà del modello completo intra- ed inter-granulare viene validata contro i risultati di rilascio ottenuti nei test sperimentali VERCORS [Ducros et al., 2013], rappresentativi di condizioni incidentali (LOCA).

Naturalmente la metodologia ANS 5.4 presenta ulteriori limitazioni che non saranno affrontate in questo momento. Ad esempio, non descrive l'eventuale trasporto di isotopi radioattivi dalla barra di combustibile al fluido termovettore. Non considera fenomeni chimici di ossidazione che aumentano il rilascio radioattivo. Tali miglioramenti sono oggetto di sviluppi futuri, partendo dai risultati qui ottenuti.

Revisione della metodologia ANS 5.4

All'interno del Capitolo 1 si è cercato di portare alla luce l'impalcatura matematica su cui è basato ANS 5.4. Viene ricavata l'equazione del rilascio frazionario, noto come R/B, partendo dalla descrizione a sfere equivalenti del combustibile [Booth, 1957, Beck, 1960].

Il diossido di uranio viene modellizato come un insieme di grani sferici, identici, omogenei, di raggio a. All'interno di ogni grano vengono generati dei prodotti di fissione radioattivi il cui tasso di produzione è pari a B ($\mathrm{at\,m^{-3}\,s^{-1}}$). A sua volta $B = y\dot{F}$, in cui y ($\mathrm{at\,fiss^{-1}}$) è il rendimento isotopico della specie e $\dot{F}$ ($\mathrm{fiss\,m^{-3}\,s^{-1}}$) è il tasso di fissioni nel nocciolo del reattore. Se la specie descritta è caratterizzata da una constante di decadimento λ ($\mathrm{s^{-1}}$) ed il coefficiente di diffusione nella matrice di combustibile è D ($\mathrm{m^2\,s^{-1}}$), allora il problema di Cauchy che governa l'evoluzione della concentrazione C ($\mathrm{at\,m^{-3}}$) nel combustibile è il seguente

$$\begin{cases} \dfrac{\partial C(r,t)}{\partial t} = \alpha D \nabla^2 C(r,t) - \lambda C(r,t) + B & \\ C(r,0) = 0 & 0 < r < a \\ C(a,t) = 0 & t > 0 \\ C(0,t) = C_0 & t > 0 \end{cases}$$

Il coefficiente di diffusione D del modello dipende dalla temperatura T (K) del combustibile e dal tasso di fissioni $\dot{F}$, secondo la formula introdotta da [Turnbull et al., 1982]

$$D = 7.6 \times 10^{-11} e^{-35000/T} + 1.41 \times 10^{-25} \sqrt{\dot{F}} e^{-13800/T} + 2 \times 10^{-40} \dot{F}$$

in cui i coefficienti numerici sono stati calibrati per interpolare meglio i dati sperimentali disponibili [Turnbull and Beyer, 2009].

In ANS 5.4 è stato introdotto il parametro adimensionale α, noto come *termine del precursore*. Il suo effetto è quello di evidenziare l'effetto che alcuni precursori (p) hanno sull'isotopo in questione (n) nell'amplificare in maniera più o meno importante il processo di diffusione. La formula messa a disposizione in ANS 5.4 è la seguente [Friskney and Speight, 1976, Turnbull and Beyer, 2009]

$$\alpha = \left(\frac{1 - (y_0/x_0)^3}{1 - (y_0/x_0)^2} \right)^2$$

in cui $y_0 = \sqrt{D_\mathrm{p}/\lambda_\mathrm{p}}$ and $x_0 = \sqrt{D_\mathrm{n}/\lambda_\mathrm{n}}$. Infatti è stato osservato [Friskney and Speight, 1976] che il rilascio frazionario di un isotopo aumenta considerevolmente quando il suo coefficiente di diffusione è piccolo rispetto a quello del precursore. Come se ci fosse un effetto di rinculo tra nuclei padre e figlio. L'effetto è ovviamente evidente quando le emivite considerate sono comparabili al tempo di irraggiamento.

Una volta descritto il problema intra-granulare, la metodologia ANS 5.4 esplicita il rilascio frazionario come[1]

$$\left(\frac{R}{B} \right)_\infty = \frac{3}{\sqrt{\mu}} \left(\coth \sqrt{\mu} - \frac{1}{\sqrt{\mu}} \right)$$

[1] D'ora in poi, per chiarezza, il rilascio frazionario utilizzato da ANS 5.4 verrà sempre scritto come $(R/B)_\infty$, per evidenziare il fatto che la formula è valida in regime di equilibrio secolare.

Il rilascio frazionario all'equilibrio dipende solamente da $\mu = \lambda a^2/\alpha D$. Un gruppo adimensionale proprio del problema e dell'isotopo considerato.

La metologia ANS 5.4 non risolve l'equazione di diffusione-decadimento per la concentrazione. La soluzione analitica è stata fornita nel Capitolo 1. Brevemente, il legame tra concentrazione $C(r,t)$ e rilascio frazionario $(R/B)_\infty$ passa per la definizione del *tasso di rilascio* R di isotopi a bordo grano ($\mathrm{at\,m^{-3}\,s^{-1}}$)

$$R = -\alpha D \frac{3}{a} \left.\frac{\partial C(r,t)}{\partial r}\right|_{r=a}$$

Si ricava la seguente espressione tempo-dipendente per R/B

$$\frac{R}{B} = \frac{3}{\sqrt{\mu}}\left(\coth\sqrt{\mu} - \frac{1}{\sqrt{\mu}}\right) - \frac{6}{\pi^2}\sum_{n=1}^{\infty}\frac{e^{-(n^2\pi^2/\mu+1)\tau}}{n^2+\mu/\pi^2}$$

in cui $\tau = \lambda t$. La formula evidentemente coincide con $(R/B)_\infty$ nel limite $t \to \infty$.

Il vantaggio di aver sviluppato analiticamente il problema di diffusione-decadimento ha permesso l'introduzione della media integrale sul volume di grano sferico di $C(r,t)$. La media integrale viene indicata con $\bar{C}(t)$ e dipende solamente dall'istante di tempo di considerato (Eq. 1.28). Il suo limite asintotico è finito e può essere indicato con C_∞. La media integrale della concentrazione sarà utile perché legata ad $(R/B)_\infty$ dalla relazione

$$\left(\frac{R}{B}\right)_\infty = 1 - \frac{\lambda C_\infty}{B}$$

Fino a qui è stato chiarito che il modello intra-granulare su cui poggia ANS 5.4 introduce la richiesta di equilibrio secolare. Adesso si può descrivere il criterio di interconnessione delle bolle sul bordo grano. Come già detto, quando le bolle sul bordo grano fanno coalescenza possono formare un percorso tra l'interno della pastiglia e la sua superficie. Allora i prodotti di fissione gassosi e volatili possono diffondere e fuoriuscire dalla pastiglia. Prima dell'interconnessione si assiste ad un periodo di incubazione durante il quale il rilascio è trascurabile [Vitanza et al., 1979, White and Tucker, 1983].

ANS 5.4 adotta la soglia di Vitanza per modellizzare il periodo di incubazione prima del rilascio ed il fenomeno di interconnessione delle bolle. Sulla base del bruciamento β ($\mathrm{GWd/tUO_2}$) viene calcolata una temperatura di soglia T_{IC}

$$T_{\mathrm{IC}} = \frac{9800}{\ln(176\beta)}\ ^\circ\mathrm{C} \qquad \beta < 18.2\ \mathrm{GWd/tUO_2}$$
$$T_{\mathrm{IC}} = 1434 - 12.85\beta\ ^\circ\mathrm{C} \qquad \beta \geq 18.2\ \mathrm{GWd/tUO_2}$$

Quando $T_{\mathrm{IC}} = T$ avviene l'interconnessione delle bolle ed il rilascio frazionario aumenta, secondo

$$\left(\frac{S}{V}\right) = 120\ \mathrm{cm^{-1}} \quad T < T_{\mathrm{IC}}$$
$$\left(\frac{S}{V}\right) = 650\ \mathrm{cm^{-1}} \quad T \geq T_{\mathrm{IC}}$$

ANS 5.4 esprime l'aumento di $(R/B)_\infty$ in funzione del rapporto superficie-volume legato al raggio del grano sferico dalla relazione $S/V = 3/a$.

A titolo di esempio, viene mostrato il funzionamento della metodologia ANS 5.4 per alcuni prodotti di fissione (Tab. 1, Fig. 1). Si considera un reattore ad acqua leggera che opera in condizioni stazionarie per quattro anni e mezzo, circa 60000 ore. Il tasso di fissione e la temperatura della pastiglia sono scelte rispettivamente come $\dot{F} = 1 \times 10^{19}$ fiss $\mathrm{m}^{-3}\,\mathrm{s}^{-1}$ e $T = 1000$ K. In queste condizioni il coefficiente di diffusione vale circa $D \approx 2.453 \times 10^{-21}$ $\mathrm{m}^2\,\mathrm{s}^{-1}$. In condizioni stazionarie il bruciamento β è lineare nel tempo, secondo la relazione β (GWd/tUO_2) ≈ 0.001185 t(h) (Eq. 1.40). In accordo con la soglia di Vitanza, l'interconnessione ha luogo quando $\beta \approx 55$ GWd/tUO_2.

Table 1. In tabella sono elencati i prodotti di fissioni considerati in esempio. I rilasci frazionari prima e dopo l'interconnessione vengono indicati rispettivamente come $(R/B)_{\infty,i}$ e $(R/B)_{\infty,f}$. Sono stati calcolati tramite la formula analitica della metologia ANS 5.4.

Nuclide	λ (s^{-1})	α	$(R/B)_{\infty,i}$	$(R/B)_{\infty,f}$
^{85m}Kr	4.30×10^{-5}	1.31	1.037×10^{-4}	5.618×10^{-4}
^{131}I	9.98×10^{-7}	1.00	5.948×10^{-4}	3.219×10^{-3}
^{133}I	9.26×10^{-6}	1.21	2.148×10^{-4}	1.163×10^{-3}
^{133}Xe	1.53×10^{-6}	1.25	5.371×10^{-4}	2.907×10^{-3}
^{135m}Xe	7.55×10^{-4}	23.5	1.048×10^{-4}	5.678×10^{-4}
^{135}Xe	2.12×10^{-5}	1.85	1.756×10^{-4}	9.507×10^{-4}

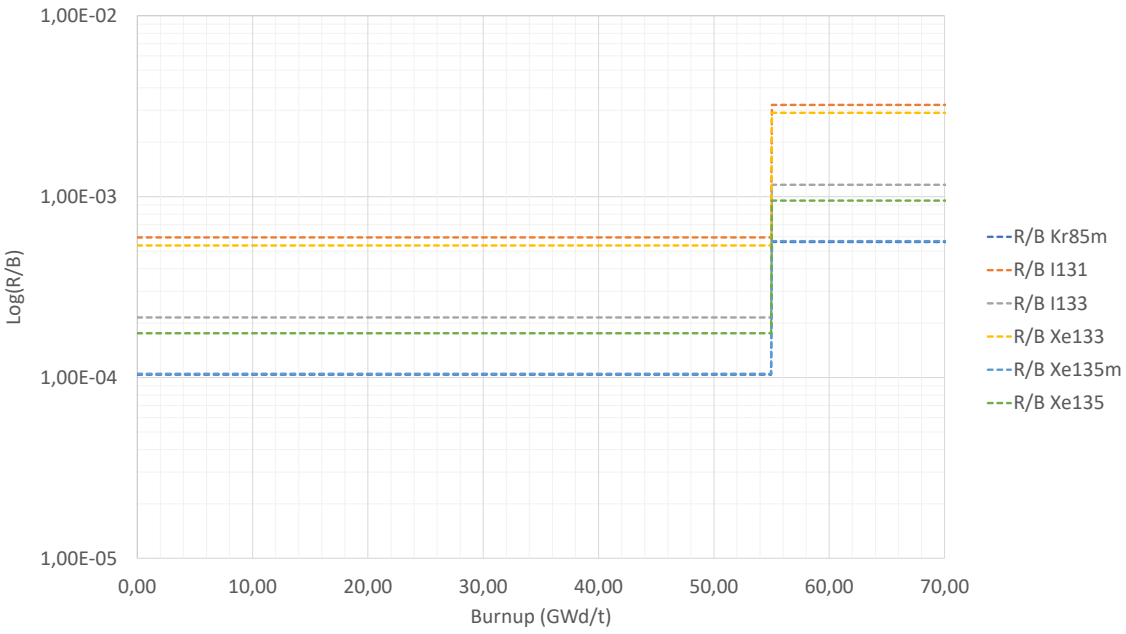

Figure 1. Rilascio frazionario calcolato applicando la metodologia ANS 5.4. Per chiarezza, il grafico è semi-logaritmico. Si può apprezzare il periodo di incubazione, che dura circa 46440 ore. In seguito avviene interconnessione delle bolle a bordo grano, quando $\beta \approx 55$ GWd/tUO_2, con conseguente aumento a gradino del rilascio frazionario.

Il modello su cui si basa la metodologia ANS 5.4 è stato calibrato e validato contro misure di rilascio frazionario provenienti dagli esperimenti IFA-504, IFA-558 e IFA-558. Le misure reperibili riguardavano principalmente ^{85m}Kr e ^{131}I. Per il ^{85m}Kr erano disponibili un centinaio di misure mentre per lo ^{131}I si sono potute utilizzare solamente 21 misure indirette, ricavate da misure del figlio ^{131}Xe. Contro queste misure sperimentali, la metodologia ANS 5.4 prevede rilasci frazionari di circa un'ordine di grandezza superiore, per ^{85m}Kr, e di circa due ordini di grandezza superiori, per ^{131}I. In questo senso risultano evidenti due limitazioni riguardanti ANS 5.4.

La prima riguarda la possibilità di essere applicato solo a reattori che operano in regime stazionario per sufficiente tempo. Questa richiesta esclude l'applicazione della metodologia a condizioni incidentali, che poi sono quelle per cui è più importante valuatare il rilascio di sostanze radioattive.

La seconda limitazione concerne le correlazioni empiriche impiegate nel modello. Come prima cosa, la soglia di Vitanza proposta in ANS 5.4 è stata modificata ad alti bruciamenti per interpolare meglio le misure da IFA [Turnbull and Beyer, 2009]. Non è detto quindi che nuovi dati disponibili possano entrare automaticamente nella gamma di validazione. Inoltre, come è tipico dei modelli basati su correlazioni, non possono essere adoperati per materiali differenti. Non senza modifiche importanti del modello. Va comunque sottolineato che i modelli basati su correlazioni sono più facilmente implementabili e richiedono minore costo computazionale, rispetto ai modelli meccanicistici. Questi ultimi hanno a che fare generalmente con diverse equazioni evolutive, ognuna discretizzata in tempo. Da qui, il maggior costo computazionale.

Sviluppo di un nuovo risolutore per l'equazione di diffusione-decadimento

Come già accennato in precedenza, esiste un'altra strada percorribile per risolvere l'equazione di diffusione-decadimento in simmetria sferica. Il Capitolo 2 sarà dedicato a questa derivazione ed alle sue applicazioni. Rispetto al problema di Cauchy precedente, si modifica una condizione al contorno. La modifica comunque non cambierà il risultato del sistema.

$$\begin{cases} \dfrac{\partial C(r,t)}{\partial t} = \dfrac{\alpha D}{r^2}\dfrac{\partial}{\partial r}\left(r^2\dfrac{\partial C(r,t)}{\partial r}\right) - \lambda C(r,t) + B & \\ C(r,0) = C_0, & 0 < r < a \\ C(a,t) = 0, & t > 0 \\ \left.\dfrac{\partial C(r,t)}{\partial r}\right|_{r=0} = 0, & t > 0 \end{cases}$$

Essenzialmente si sfrutta l'*ansatz* di decomposizione spettrale della concentrazione [Friskney and Speight, 1976, Pastore et al., 2018] scritto come

$$C(r,t) = \sum_{k=1}^{\infty} x_k(t)\psi_k(r)$$

Le funzioni $\psi_k(r)$ rappresentano le autofunzioni dell'operatore di Laplace in coordinate sferiche, cioè dei seni cardinali normalizzati opportunamente. I coefficienti temporali

dell'espansione $x_k(t)$ invece sono incogniti. Ognuno viene determinato risolvendo un'equazione di puro decadimento, alla quale si arriva sostituendo la decomposizione di $C(r,t)$ nel sistema di partenza.

Alla fine, quello che interessa non è la quantità $C(r,t)$ ma esattamente la sua media integrale sul volume del grano

$$\bar{C}(t) = \frac{3}{4\pi a^3} \int_0^a C(r,t) 4\pi r^2 dr$$

La formula analitica per $\bar{C}(t)$ coincide con quella ricavata nel Capitolo 1 (Eq. 1.28). In virtù di questa equivalenza, il risultato ottenuto dalla decomposizione spettrale si può dire coerente con quanto trovato in precedenza.

Risulta semplice implementare nel codice di performance SCIANTIX la controparte numerica di quanto sviluppato finora. Schematicamente, per ogni coefficiente temporale $x_k(t)$ si risolve l'equazione di puro decadimento in tempo con il metodo di Eulero implicito. Si ricostruisce poi un'approssimazione di $\bar{C}(t)$, indicata con C^K, sommando un numero K di modi finito.

Grazie all'implementazione del modello in SCIANTIX è possibile migliorare ulteriormente la descrizione intra-granulare. È noto che i fenomeni di trapping e resolution modificano la diffusione dei prodotti di fissione verso il bordo grano [Speight, 1969, White and Tucker, 1983, Pizzocri et al., 2018]. Questi meccanismi influenzano il coefficiente di diffusione D attraverso i loro rispettivi tassi di accadimento g (s^{-1}) e b (s^{-1}), risultando in un coefficiente di diffusione efficace per ogni isotopo

$$D_{\mathrm{eff}} = \frac{b+\lambda}{b+\lambda+g} D$$

Il vantaggio dell'utilizzo di SCIANTIX è che i parametri b e g sono determinati da un'equazione evolutiva per la densità di bolle intra-granulari N_{ig} ($\mathrm{bub\,m}^{-3}$), già presente nel modello (Eq. 2.9).

Metodo della soluzione manufatta

Il risolutore è stato sottoposto ad una verifica numerica. Si è scelto di utilizzare il metodo della soluzione manufatta [Oberkampf et al., 2004] perché permette di controllare l'accuratezza e la consistenza del codice numerico. Questo metodo si sviluppa in tre fasi.

1. Si sceglie una soluzione analitica arbitraria dell'equazione di partenza.

2. Si riarrangia l'equazione di partenza in maniera tale da far emergere i cosiddetti coefficienti manufatti (nel nostro caso, una costante di decadimento , un coefficiente di diffusione ed una sorgente manufatta).

3. Questi coefficienti manufatti vengono inseriti nel risolutore numerico e si compara la soluzione numerica ottenuta con quella analitica scelta al punto 1.

In Fig. 2 si può osservare il risultato del metodo della soluzione manufatta. In Fig. 3 la stima dell'errore di convergenza del risolutore. Per eseguire una stima dell'ordine di convergenza, sono state calcolate due soluzioni manufatte, una con

passo di discretizzazione temporale doppio rispetto all'altra. Come previsto, la soluzione numerica più vicina alla soluzione esatta è quella calcolata con passo di discretizzazione temporale minore (in Fig. 2, la linea arancione). Inoltre si ritrova l'ordine di convergenza unitario del metodo di Eulero implicito (Fig. 3), lo schema numerico adoperato per la discretizzazione della derivata temporale.

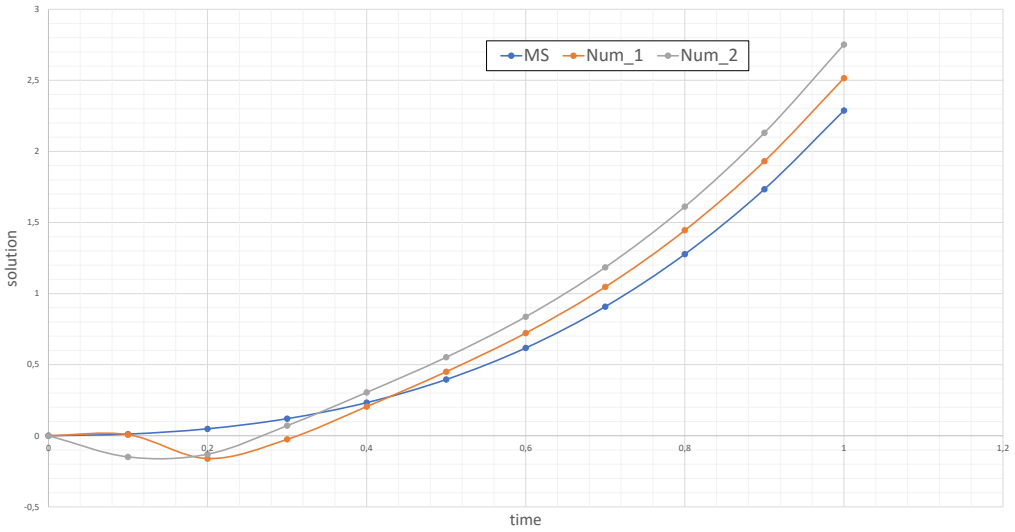

Figure 2. Confronto tra la soluzione analitica (linea blu) e le due soluzioni manufatte. La soluzione in arancione è stata calcolata con un passo di discretizzazione temporale pari alla metà di quello utilizzato per la soluzione in grigio.

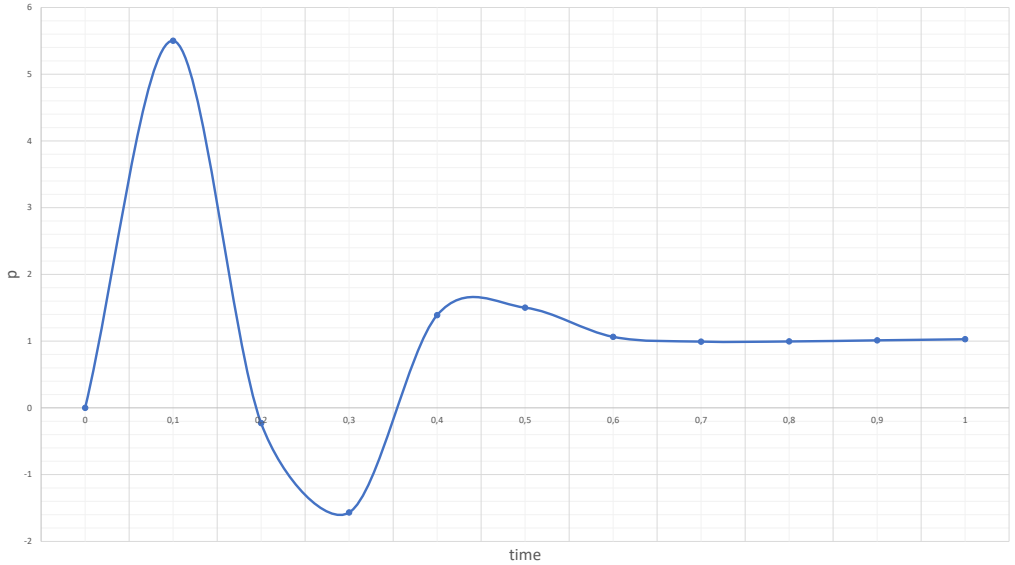

Figure 3. Andamento dell'ordine di convergenza p. Nonostante le oscillazioni iniziali, lo schema numerico rivela un ordine di convergenza unitario. Come previsto, poiché dipende dal metodo di Eulero implicito di ordine 1.

Confronto con il modello ANS 5.4

A questo punto è disponibile un risolutore spettrale verificato per l'equazione di diffusione-decadimento. Poiché si vogliono confrontare le previsioni del modello ANS 5.4 con le previsioni del risolutore spettrale, è stata implementata la soglia di Vitanza in SCIANTIX. Questa fase operativa procede secondo lo schema presentato in Fig. 4.

Per semplicità si è scelto di simulare l'esempio rappresentato in Fig. 1 con il risolutore spettrale integrato in SCIANTIX. Bisogna tuttavia precisare che, benchè l'andamento temporale di $C^K \approx \bar{C}(t)$ sia corretto (Fig. 5), la stima del rilascio frazionario sia corretta solo all'equilibrio (Fig. 6)

Per giustificare quanto detto bisogna riportare il legame analitico tra rilascio frazionario R/B e media integrale della concentrazione $\bar{C}(t)$ ottenuto nel Capitolo 1

$$\frac{R}{B} = 1 - \frac{\lambda \bar{C}(t)}{B} - \frac{6}{\pi^2} \sum_{k=1}^{\infty} \frac{e^{-(1+n^2\pi^2/\mu)\lambda t}}{n^2}$$

Per tempi sufficientemente lunghi gli esponenziali diventano trascurabili e si rende possibile calcolare il rilascio frazionario all'equilibrio dalla media della concentrazione

$$\left(\frac{R}{B}\right)_{\infty} = 1 - \frac{\lambda C_{\infty}}{B}$$

La medie integrali delle concentrazioni calcolate all'equilibrio sono rappresentate dalle linee tratteggiate orizzontali in Fig. 5. Le linee continue indicano invece quelle calcolate con il risolutore spettrale. È evidente come sul finire del transitorio iniziale queste ultime tendano verso i corretti valori di equilibrio. Inoltre si nota anche come l'effetto di interconnesione delle bolle abbia un impatto molto ridotto sui valori numerici delle concentrazioni, a differenza di quanto accade per il rilascio frazionario (Eq. 1.42 e Eq. 1.43).

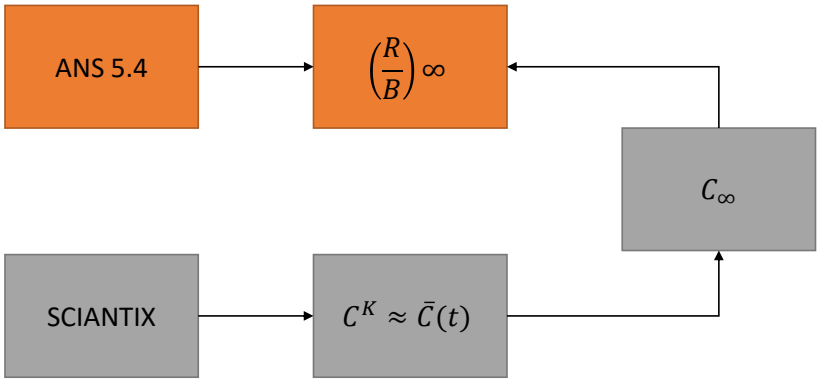

Figure 4. Il confronto tra i risultati di ANS 5.4 e quelli previsti dal risolutore spettrale si divide in fasi differenti. SCIANTIX restituisce un'approssimazione della media integrale della concentrazione C^K. All'equilibrio, questa grandezza può essere utilizzata per stimare il rilascio frazionario numerico $(R/B)^K_{\infty} = 1 - \lambda C^K_{\infty}/B$. Quest'ultima quantità sarà confrontata con il risultato analitico di ANS 5.4, $(R/B)_{\infty}$.

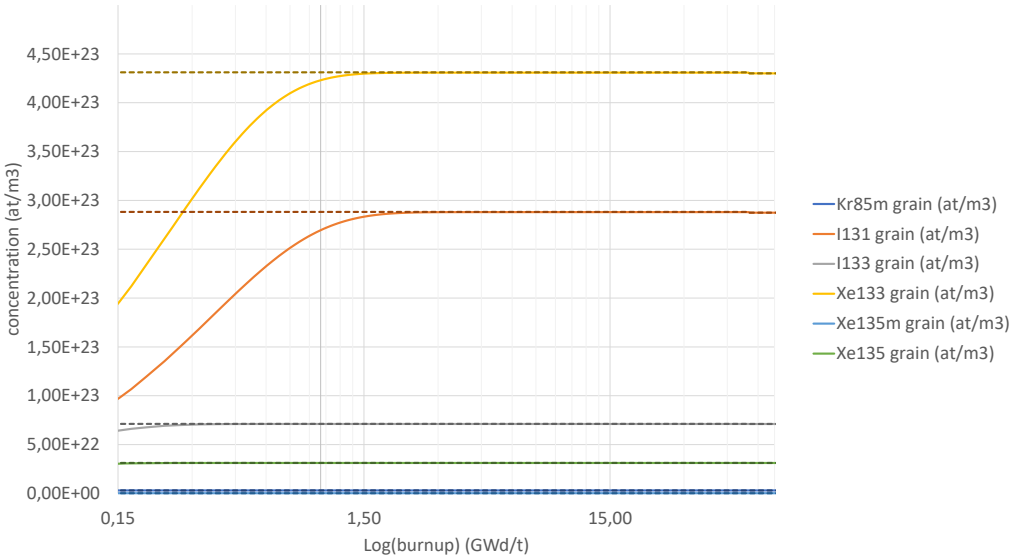

Figure 5. Calcolo della concentrazione media in funzione del bruciamento del combustibile. Le bolle a bordo grano interconnettono secondo la soglia di Vitanza. Le linee tratteggiate rappresentano le previsioni del modello ANS 5.4, le linee continue invece corrispondono alle soluzioni calcolate con il risolutore spettrale in SCIANTIX.

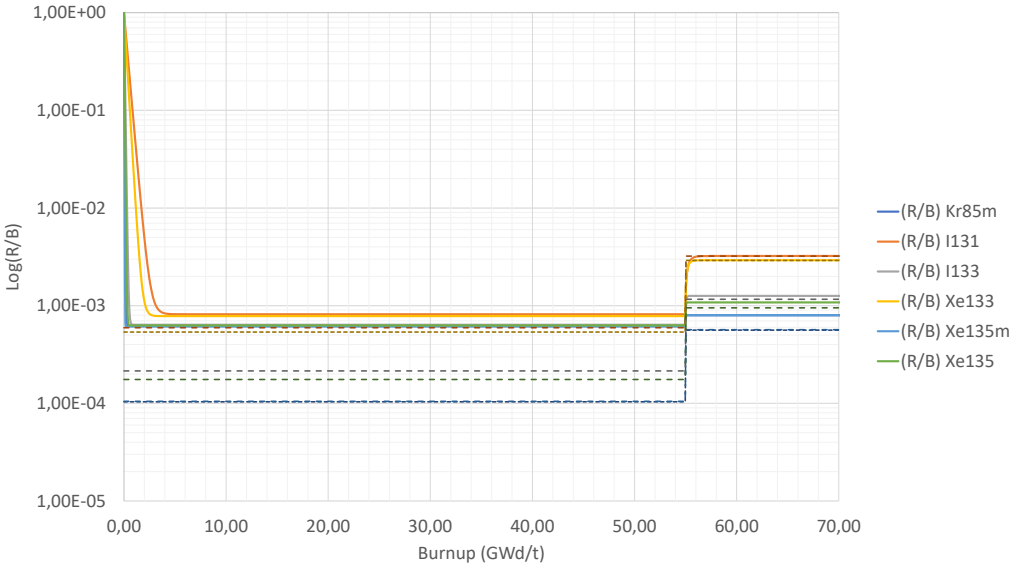

Figure 6. Calcolo dei rilasci frazionari in funzione del bruciamento del combustibile. Le bolle a bordo grano interconnettono secondo la soglia di Vitanza. Le linee tratteggiate rappresentano le previsioni del modello ANS 5.4, le linee continue invece corrispondono alle soluzioni calcolate con il risolutore spettrale in SCIANTIX.

I rilasci frazionari all'equilibrio calcolati con SCIANTIX, indicati con $(R/B)^K_\infty$, sono rappresentati in Fig. 6, con linee continue. La previsione del modello ANS 5.4 invece è reppresentata da linee tratteggiate. Come accennato, la soluzione del risolutore spettrale a inizio transitorio non è corretta. Il fatto che il rilascio frazionario parta da 1 non è fisicamente accettabile. Tuttavia la discrepanza è stata formalmente giustificata.

È stata condotta un'analisi dell'errore relativo esistente tra le predizioni numeriche estratte da SCIANTIX e i valori asintotici esatti di concentrazione media e rilascio frazionario. Al prim'ordine valgono le seguenti stime per gli errori relativi $u_{R/B}$ e u_C

$$u_{R/B} \approx (R/B)^K_\infty \frac{\sqrt{\mu}}{3} - 1, \quad u_C \approx -u_{R/B} \frac{3}{\sqrt{\mu}}$$

Queste formule sono interessanti per vari motivi. Per prima cosa esplicitano la dipendenza da μ, gruppo adimensionale del problema. In secondo luogo includono la dipendenza dell'errore dal numero di modi usati nella decomposizione spettrale. Idealmente, se $K \gg 1$ allora $(R/B)^K_\infty \approx 3/\sqrt{\mu}$ e $u_{R/B} \approx 0$. Infine legano le due incertezze in un rapporto di proporzionalità diretta. Poichè solitamente $\mu \gg 1$, allora $u_C \ll -u_{R/B}$. Inoltre le due incertezze hanno per forza segno opposto. Se una grandezza sovrastima la predizione numerica, l'altra la sottostima.

In Tab. 2 sono stati riportati i parametri più interessanti per il caso in questione. Poichè lo scopo di questa fase era il confronto dei risultati di ANS 5.4 con le predizioni del risolutore spettrale, bisogna osservare $u_{R/B}$.

La situazione peggiore è quella precedente all'interconnessione. Gli errori relativi possono a sovrastimare il rilascio frazionario quasi di 5 ordini di grandezza. Si nota che l'errore relativo maggiore caratterizza gli isotopi a μ più elevato. Questa imprecisione però è pienamente giustificata dagli errori effettuati dal codice numerico, sia in termini di troncamento delle cifre significative che in termini di modi presenti nell'approssimazione. Ricordiamo quindi che il cui risultato del codice è C^K e non $(R/B)^K_\infty$. L'inaccuratezza può essere quindi facilmente arginata considerando un numero K di modi maggiore ed aumentando le cifre significative, Dopo l'interconnessione l'errore diminuisce di almeno un ordine di grandezza, coerentemente con la diminuzione di μ. Viceversa, i risultati numerici per le medie delle concentrazioni sottostimano in maniera trascurabile i valori esatti, sia prima che dopo l'interconnesione delle bolle.

Table 2. Risultati della simulazione del comportamento intra-granulare degli isotopi radioattivi e confronto con i risultati analitici del modello di ANS 5.4.

Nuclide	$\mu = \lambda a^2/\alpha D$	C^K_∞ (at m^{-3})	$u_C \approx u_{R/B} 3/\sqrt{\mu}$	R/B^K_∞	$u_{R/B} \approx 1 - (R/B)^K_\infty \sqrt{\mu}/3$
Prima dell'interconnessione	$S/V = 3/a = 120$ cm^{-1}				
^{85m}Kr	8.36×10^8	3.0284×10^{21}	-5.110×10^{-4}	6.147×10^{-4}	4.926
^{131}I	2.54×10^7	2.8814×10^{23}	-2.228×10^{-4}	8.175×10^{-4}	0.374
^{133}I	1.95×10^8	7.1121×10^{22}	-4.230×10^{-4}	6.377×10^{-4}	1.968
^{133}Xe	3.12×10^7	4.3104×10^{23}	-2.449×10^{-4}	7.819×10^{-4}	0.455
^{135m}Xe	8.19×10^8	1.6149×10^{20}	-5.101×10^{-4}	6.149×10^{-4}	4.864
^{135}Xe	2.92×10^8	3.1160×10^{22}	-4.523×10^{-4}	6.278×10^{-4}	2.576
Dopo l'interconnessione	$S/V = 3/a = 650$ cm^{-1}				
^{85m}Kr	2.85×10^7	3.0278×10^{21}	-2.349×10^{-4}	7.968×10^{-4}	0.418
^{131}I	8.67×10^5	2.8745×10^{23}	-3.793×10^{-4}	3.226×10^{-3}	0.001
^{133}I	6.65×10^6	7.1077×10^{22}	-9.516×10^{-4}	1.259×10^{-3}	0.082
^{133}Xe	1.06×10^6	4.3011×10^{23}	-8.986×10^{-6}	2.919×10^{-3}	0.003
^{135m}Xe	2.79×10^7	1.6146×10^{20}	-2.325×10^{-4}	8.005×10^{-4}	0.410
^{135}Xe	9.95×10^6	3.1146×10^{22}	-1.283×10^{-4}	1.079×10^{-3}	0.135

Concludendo, analiticamente il risolutore spettrale accoppiato alla soglia di Vitanza è in grado di predire i rilasci frazionari analitici di ANS 5.4. A patto di ridurre opportunamente gli errori di troncamento e di aumentare il numero di modi considerati nell'espansione.

Sviluppo di un modello di bordo grano

Nel Capitolo 3 viene introdotto un modello meccanicistico per desrivere il comportamento delle bolle a bordo grano. L'obiettivo è quello di sostituire la soglia empirica di Vitanza. La descrizione si fonda su validi modelli esistenti [Speight and Beeré, 1975, White and Tucker, 1983, White, 2004, Veshchunov, 2008, Pastore et al., 2013]. In sintesi, si considera l'azione della pressione interna alle bolle a bordo grano. L'assorbimento dei prodotti di fissione da parte delle bolle produce un incremento di pressione ed uno stato di non-equilibrio. Le bolle in pressione tendono ad assorbire vacanze per ritornare nello stato di equilibrio. La loro dimensione aumenta fino ad una soglia di coalescenza. Al raggiungimento di questa soglia inizia il rilascio del gas.

All'interno dei grani sono presenti prevalentemente isotopi di xeno e krypton stabili. Le concentrazioni degli isotopi radioattivi di interesse radiologico sono sufficientemente piccole affinchè l'interconnessione del bordo grano non venga regolata da questi ultimi.

Stabilito il comportamento base delle bolle a bordo grano, descritto in maniera più dettagliata nel Capitolo 3, si può passare al suo accoppiamento in SCIANTIX con il modello di diffusione-decadimento.

Fondamentalmente, l'approccio scelto è basato su un bilancio di massa. Per ogni isotopo viene considerata la sua concentrazione prodotta P ($\mathrm{at\,m^{-3}}$), la concentrazione intra-granulare C ($\mathrm{at\,m^{-3}}$), la concentrazione assorbita a bordo grano U ($\mathrm{at\,m^{-3}}$), la concentrazione di isotopi decaduti L ($\mathrm{at\,m^{-3}}$) e la concentrazione di isotopi rilasciati X ($\mathrm{at\,m^{-3}}$). In ogni istante di tempo deve valere la seguente legge di conservazione

$$P = C + L + U + X$$

In cui P, C e L sono governate rispettivamente da

$$\begin{aligned}
\frac{\partial P}{\partial t} &= y\dot{F} \\
\frac{\partial C}{\partial t} &= \alpha D_{\mathrm{eff}} \nabla^2 C - \lambda C + y\dot{F} \\
\frac{\partial L}{\partial t} &= \lambda P - \lambda L
\end{aligned}$$

Prima che avvenga l'interconnessione $X = 0$ e

$$U = P - L - C$$

Dopo l'interconnessione, U diminuirà (a seguito del rilascio di isotopi) e si potrà scrivere

$$X = P - L - C - U$$

Il meccanismo che causa la diminuzione di U dopo l'interconnessione delle bolle verrà accennato nel Capitolo 3. Sulla base di queste definizioni è stato possibile definire una

nuova espressione per il rilascio frazionario di un isotopo. Infatti considerando che il gas disponibile per il rilascio è il termine di bordo grano (U), la nuova definzione di R/B è

$$\frac{R}{B} = \frac{X}{X+U}$$

che possiede il vantaggio di essere di facile utilizzo e corretta in ogni istante di tempo.

A questo punto è disponibile in SCIANTIX una routine completa. La parte intragranulare è gestita da un risolutore spettrale e la parte inter-granulare è accoppiata all'evoluzione delle bolle a bordo grano. Poiché il codice è in grado di elaborare transitori di temperatura repentini, è stato scelto confrontare le predizioni numeriche con i risultati sperimentali dei testi VERCORS [Ducros et al., 2013]. Questa serie di esperimenti è stata effettuata su una gamma di barre di combustibile prelevata da reattori ad acqua pressurizzata. I campioni di combustibile venivano re-irraggiati a bassa potenza per ricostruire l'inventario dei prodotti di fissione radioattivi senza causarne diffusione. In seguito venivano sottoposti a transitori di temperatura caratteristici di LOCA per causare il completo rilascio radioattivo degli isotopi e nella maggior parte dei casi anche il collasso del campione.

Solamente alcuni test sono stati effettuati su UO_2. Inoltre non tutti i transitori di temperatura sono disponibili. Per questo motivo non è stato possibile considerare tutti i 17 test ma solo 6. In Tab. 3 sono stati riportati i dettagli necessari per ripetere le simulazioni e i rilasci frazionari misurati e predetti a fine transitorio.

Nonostante sia stato sottolineato come ANS 5.4 di regola non venga applicato a condizioni incidentali, si è scelto comunque di eseguire un test indipendente. La formula per il rilasio frazionario di ANS 5.4 è stata utilizzata scegliendo conservativa-

Table 3. Caratteristiche dei test VERCORS considerati [Ducros et al., 2013]. Vengono riportate le caratteristiche degli irraggiamenti condotti, dei campioni di combustibile usato e dei transitori di temperatura effettuati. Inoltre si riportano le misure di rilascio frazionario a fine transitorio, le predizioni del codice SCIANTIX e del modello ANS 5.4.

	VERCORS 4	VERCORS 5	VERCORS 6	VERCORS RT1	VERCORS RT3	VERCORS RT6
PWR irradiation	Bugey	Bugey	Grave lines	Grave lines	BR3	Grave lines
Fuel burnup (GWd/tU)	38.3	38.3	60	47.3	39	71.8
Re-irradiation	Siloe	Siloe	Siloe	No	Yes (partly)	Yes
Max fuel temperature (°C)	2300	2300	2350	2300	2700	2200
Atmosphere (end of test)	Hydrogen	Steam	$H_2O + H_2$	$H_2O + H_2$	Mixed "reducing"	$H_2O + H_2$
Last plateau duration (min)	30	30	30	*c*	*c*	*c*
VERCORS fractional releases (%)						
Kr (via ^{85}Kr)				100	100	100
Te (via ^{132}Te)	100	98-100	98-100		100	99.5
I (via ^{131}I and ^{133}I)	87	93	98-100		100	100
Xe (via ^{133}Xe)	86	87	100		100	100
Cs (via ^{134}Cs and ^{137}Cs)	93	93	97	100	99.8	100
SCIANTIX fractional releases (%)						
Kr (via ^{85}Kr)				98.8	98.7	97
Te (via ^{132}Te)	97.9	97.9	99		99.1	97.3
I (via ^{131}I and ^{133}I)	98	98	98.5		99.2	97
Xe (via ^{133}Xe)	97.8	97.8	98		98.9	97.2
Cs (via ^{134}Cs and ^{137}Cs)	97.7	97.7	98	98.8	98.7	97.2
ANS 5.4 fractional releases (%)						
Kr (via ^{85}Kr)				100	100	100
Te (via ^{132}Te)	95.8	95.8	96.7		99.3	93
I (via ^{131}I and ^{133}I)	93.4	93.4	94.8		98.8	89.7
Xe (via ^{133}Xe)	97.9	97.9	98.4		99.7	96.4
Cs (via ^{134}Cs and ^{137}Cs)	100	100	100	100	100	100

c = la temperatura massima è stata raggiunta attraverso rampe successive di 100 °C, durate 10 minuti ciascuna.

mente la temperatura massima raggiunta durante il transitorio. Così si sono potute confrontare le predizioni di SCIANTIX con quelle di ANS 5.4 e dei VERCORS, a fine transitorio. Per entrambe le simulazioni, i risultati a fine transitorio si rivelano simili alle misurazioni. In media l'errore commesso è inferiore all'1%. Infatti i rilasci quasi totali, sollecitati dalle alte temperature, vengono correttamente modellati. Riguardo invece alla cinetica del rilascio frazionario durante il transitorio, la definizione introdotta in precedenza consente di monitorare il suo andamento nel tempo.

Si mostra la simulazione del caso VERCORS 4. Per i restanti casi si rimanda al Capitolo 3. Nella Fig. 7 ([Pontillon and Ducros, 2010a]) si mostra il transitorio di temperatura a cui è stato sottoposto il campione di UO_2 irraggiato. Si possono apprezzare le cinetiche del rilascio di tellurio, cesio. In Fig. 8, assieme all'interpolazione del transitorio di temperatura, sono presenti i rilasci frazionari in funzione del tempo per ^{132}Te e ^{137}Cs.

In generale, per temperature inferiori a 1200 °C non si osservano rilasci di alcun tipo. Per temperature intermedie, tra 1200 °C a 1500 °C il rilascio frazionario predetto anticipa quello osservato e i suoi valori sono più elevati durante il transitorio. A temperature più elevate la cinetica del rilascio ed i rispettivi valori sono descritti in maniera più accurata. Le differenze che si osservano sono inputabili a interazioni chimiche con i materiali strutturali del campione e della strumentazione. Ad esempio, il tellurio interagisce con lo stagno contenuto nella guaina e resta immagazzinato al suo interno, fino a quando temperature superiori ai 1500 °C non vengono raggiunte. In alcuni esperimenti invece è stata raggiunta la liquefazione del campione. In queesti casi una piccola frazione di cesio ($< 1\%$) può rimanere all'interno del *corium* sottoforma di uranati o zirconati e di conseguenza il rilascio di cesio non è totale. Questo tipo di interazioni non sono state incluse del modello.

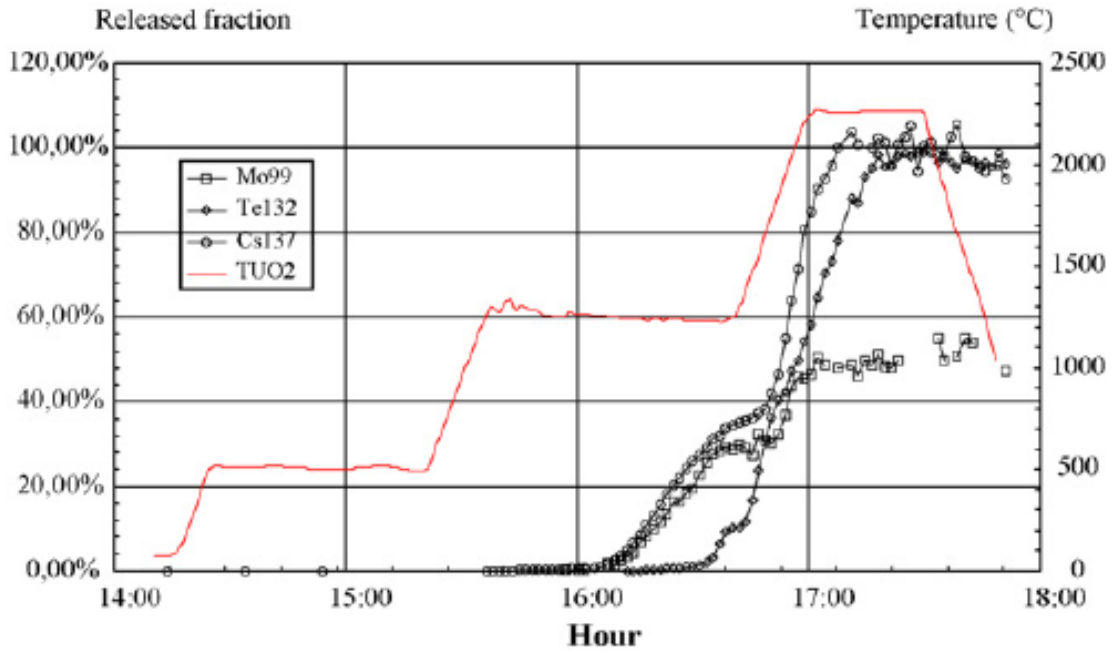

Figure 7. VERCORS 4: cinetica misurata del rilascio frazionario per ^{132}Te, ^{137}Cs e ^{99}Mo. In rosso si vede l'andamento di temperatura durante il transitorio [Pontillon and Ducros, 2010a].

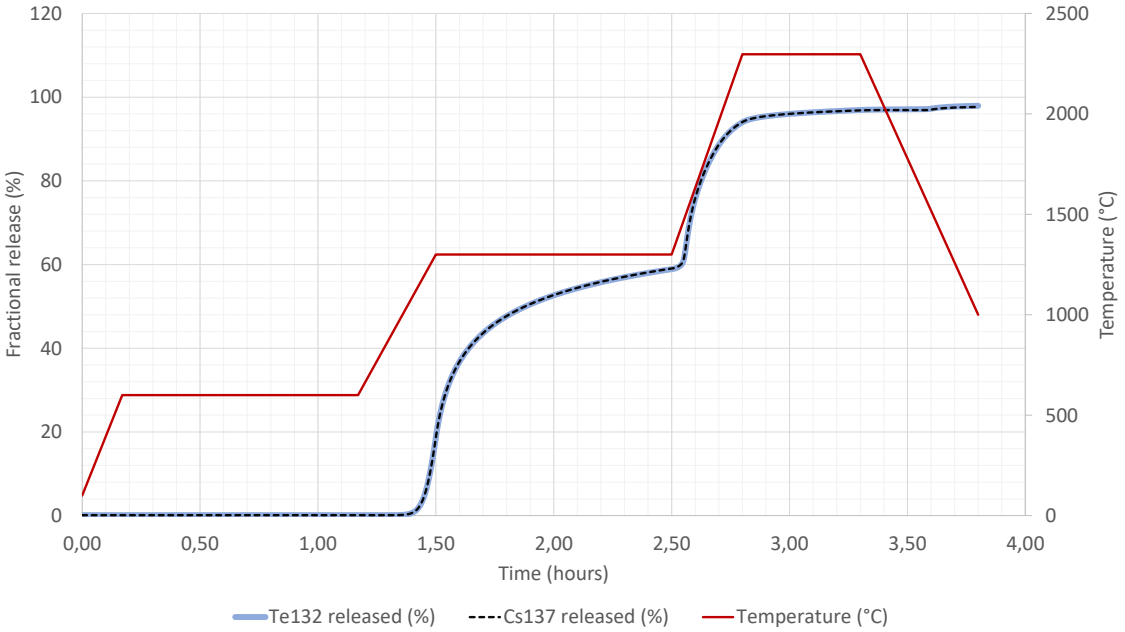

Figure 8. VERCORS 4: cinetica simulata del rilascio frazionario per ^{132}Te, ^{137}Cs, isotopi volatili descritti dal modello implementato in SCIANTIX. In rosso si vede l'interpolazione del transitorio di temperatura.

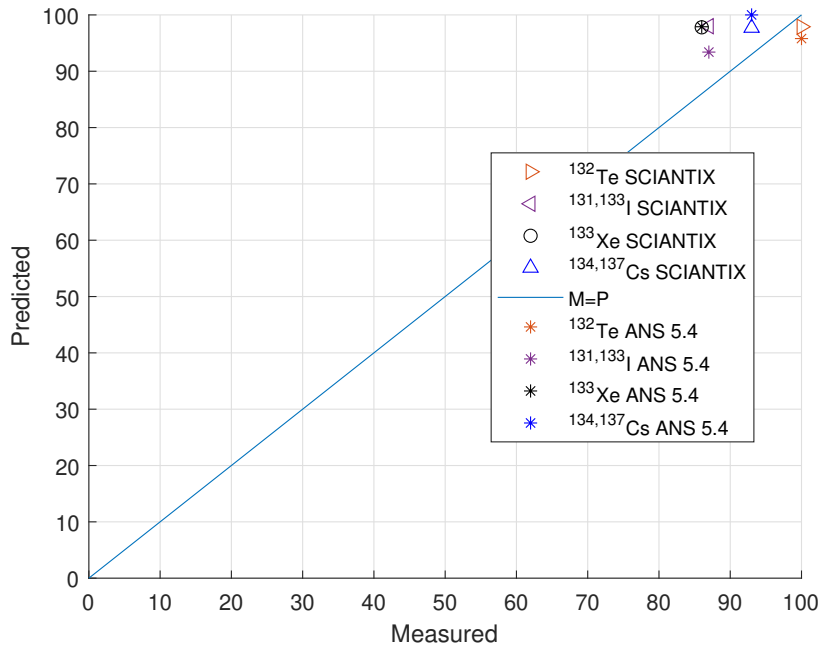

Figure 9. VERCORS 4: grafico dei valori predetti contro quelli misurati del rilascio frazionario a fine transitorio. Il grafico riguarda gli isotopi per cui sono disponibili i risultati delle misurazioni. I valori sotto la bisettrice sottostimano il rilascio, quelli sopra lo sovrastimano.

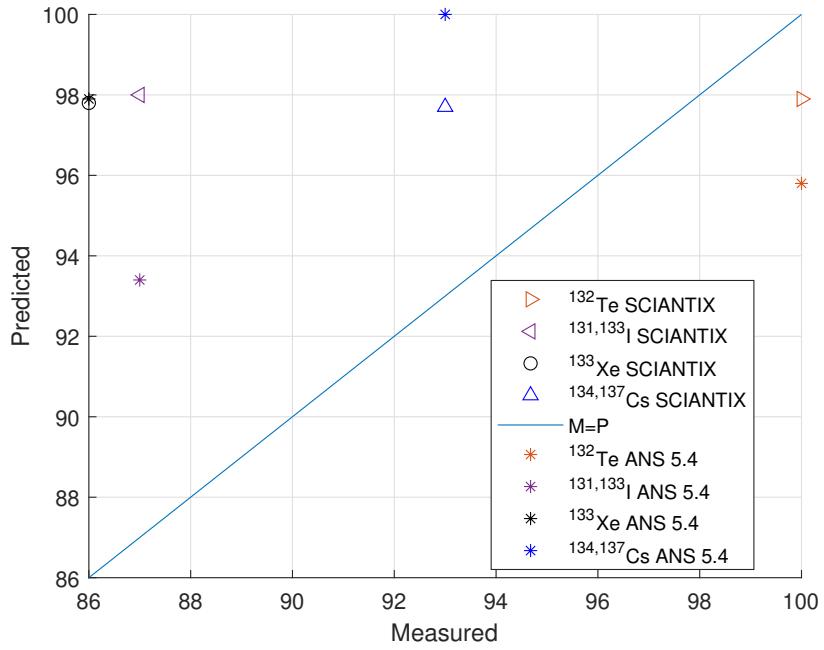

Figure 10. VERCORS 4: ingrandimento del grafico precedente. Si apprezza in maniera migliore la bontà della predizione numerica. Riguardo SCIANTIX, l'errore maggiore è commesso per gli isotopi del cesio, in cui il rilascio è sovrastimato del 13%. L'unica sottostima avviene per il tellurio con un errore del 2%.

Conclusioni

Il modello sviluppato ed implementato nel codice SCIANTIX presenta vantaggi rispetto alla metologia ANS 5.4, per valutare il rilascio frazionario radioattivo di isotopi gassosi e volatili. La base fisica del modello rende possibile simulare sia condizioni stazionarie che transitorie. I risultati delle simulazioni VERCORS confermano che i valori di rilascio a fine transitorio sono in linea con quanto predetto dal modello attuale ANS 5.4, commettendo un errore inferiore all'1%. La descrizione della cinetica del rilascio è uno strumento utile che non veniva fornito dalla metologia precedente. Grazie a questa descrizione temporale si riescono ad apprezzare i fenomeni di rilascio repentino provocati dagli sbalzi di temperatura. La descrizione della cinetica, per temperature inferiore a 1500 °C, descrive in maniera conservativa il fenomeno del rilascio. Principalmente a causa di interazioni chimiche con i materiali strutturali del campione e della strumenzione. Per temperature superiori invece il rilascio quasi totale degli isotopi è modellizzato più accuramente, a causa della prevalenza della diffusione termica rispetto ad altri fenomeni.

Il vantaggio di utilizzare SCIANTIX per la valutazione del rilascio radioattivo degli isotopi gassosi e volatili, al posto di ANS 5.4, ha due ragioni di fondo. Grazie alla base fisica del modello si possono elaborare transitori rapidi, oltre condizioni stazionarie. Ad esempio, condizioni incidentali severe come quelle che si vengono a creare durante LOCA o SGTR. Infine SCIANTIX non è un modello parassitico come ANS 5.4. Il primo descrive diversi fenomeni che possono influenzarsi a vicenda. Da una simulazione si ottengono informazioni non solo riguardo al rilascio frazionario degli isotopi radioattivi ma anche dei gas di fissione stabili e inerti. Al contrario, ANS 5.4 richiede altri modelli per la descrizione di prodotti di fissione con emivita lunga (maggiore di unanno) o stabili. Infine non è un modello adatto a descrivere reattori che impiegano combustibili ad ossidi misti (MOX), come alcuni reattori di quarta generazione.

Infine, il modello presente in SCIANTIX offre la possibilità di essere perfezionato includendo diversi miglioramenti. Ad esempio, sarà possibile includere l'accoppiamento tra isotopi radioattivi di tipo padre-figlio attraverso una matrice di decadimento non diagonale. Sarà possibili effettuare analisi di sensitività sui parametri fisici più interessanti, come il coefficiente di diffusione o la dimensione del grano, attraverso il problema di diffusione-decadimento aggiunto. Per ultimo, sarà possibile estendere il database di validazione del modello accoppiando SCIANTIX a codici di performance integrali, e.g. TRANSURANUS o BISON. Questo permetterà l'esecuzione di test integrali su campioni di barrette IFA ed il confronto con il database di validazione di ANS 5.4.

List of Acronyms

ANS	American Nuclear Society
AP	Activation Product
EDF	Électricité de France
FCLT	Fuel Centerline Temperature
FG	Fission Gas
FGR	Fission Gas Release
FP	Fission Product
FPC	Fuel Performance Code
HN	Heavy Nuclei
IFA	Instrumented Fuel Assembly
IGB	Inert Gas Behaviour
LAMA	Laboratory for Active Materials
LOCA	Loss-of-Coolant Accident
LWR	Light Water Reactor
NPP	Nuclear Power Plant
MMS	Method of Manufactured Solutions
MOX	Mixed Oxides
MTR	Material Testing Reactor
ODE	Ordinary Differential Equation
SA	Severe Accident
SEM	Scanning Electron Microscope
PIE	Post Irradiation Examination
PDE	Partial Differential Equation
PWR	Pressurized Water Reactor
R2CA	Reduction of Radiological Consequences of design basis and extension Accidents
SGTR	Steam Generator Tube Rupture

List of Symbols

a	(m)	spherical grain radius
A_{gf}	(m^2)	inter-granular bubble average area
b	(s^{-1})	resolution rate
B	($\text{at}\,\text{m}^{-3}\,\text{s}^{-1}$)	isotope production rate
c_v	(/)	cation vacancy concentration
C	($\text{at}\,\text{m}^{-3}$)	intra-granular isotope concentration
$\bar{C}$	($\text{at}\,\text{m}^{-3}$)	integral average of intra-granular isotope concentration
C_∞	($\text{at}\,\text{m}^{-3}$)	equilibrium integral average of intra-granular isotope concentration
C_∞^K	($\text{at}\,\text{m}^{-3}$)	numerical approximation of equilibrium integral average of intra-granular isotope concentration
C_b	($\text{at}\,\text{m}^{-3}$)	in-bubble intra-granular isotope concentration
C_s	($\text{at}\,\text{m}^{-3}$)	in-solution intra-granular isotope concentration
d	(m)	atomic jump distance
D	($\text{m}^2\,\text{s}^{-1}$)	single gas atom diffusion coefficient in UO_2 lattice
D_{eff}	($\text{m}^2\,\text{s}^{-1}$)	effective gas atom diffusion coefficient in UO_2 lattice
D_0	($\text{m}^2\,\text{s}^{-1}$)	Arrhenius law pre-exponential constant
$\dot{F}$	($\text{fiss}\,\text{m}^{-3}\,\text{s}^{-1}$)	fission rate density
F_c	(/)	fractional coverage
g	(s^{-1})	trapping rate
H	(J)	activation energy
j_v	(s^{-1})	thermally activated vacancy jump rate
k_B	(J/K)	Boltzmann constant
K	(/)	number of modes of the finite spectral decomposition
L	($\text{at}\,\text{m}^{-3}$)	decayed isotope concentration
m	(/)	trapped atoms per bubbles
N_{gf}	($\text{bub}\,\text{m}^{-2}$)	inter-granular bubble density
N_{ig}	($\text{bub}\,\text{m}^{-3}$)	intra-granular bubble density
p	(/)	convergence error of a numerical method

P	$(\mathrm{at\,m^{-3}})$	produced isotope concentration
r	(m)	radial coordinate
R	$(\mathrm{at\,m^{-3}\,s^{-1}})$	isotope release rate
R_{gf}	(m)	inter-granular bubble radius of curvature
R_{ig}	(m)	intra-granular bubble mean radius
R/B	(/)	instantaneous fractional release
$(R/B)_\infty$	(/)	equilibrium fractional release
$(R/B)_\infty^K$	(/)	numerical approximation of equilibrium fractional release
S/V	$(\mathrm{m^{-1}})$	surface-to-volume ratio
t	(s)	time
T	(K)	temperature
T_{IC}	(K)	bubble interconnection temperature
T_e	(s)	equilibrium time
X	$(\mathrm{at\,m^{-3}})$	released isotope concentration from grain boundary
y	(at/fiss)	cumulative thermal fission yield in ^{235}U
u_C	(/)	relative error on numerical intra-granular concentration
$u_{R/B}$	(/)	relative error on numerical fractional release
U	$(\mathrm{at\,m^{-3}})$	grain-boundary isotope concentration
Z_0	(m)	mean influence radius of a fission fragment
α	(/)	precursor enhancement factor
β	$(\mathrm{GWd/tUO_2})$	nuclear fuel burnup
λ	$(\mathrm{s^{-1}})$	decay rate
Λ_k	$(\mathrm{s^{-1}})$	spectral diffusion-decay rate
γ	$(\mathrm{J/m^2})$	$\mathrm{UO_2}$-bubble surface tension
η	(/)	average number of nucleated bubbles per fission fragment
μ	(/)	dimensionless group for diffusion-decay problem
ν	$(\mathrm{bub\,m^{-3}\,s^{-1}})$	bubble nucleation rate
ρ	$(\mathrm{kgm^{-3}})$	nuclear fuel density
σ_h	$(\mathrm{J/m^{-3}})$	fuel matrix hydrostatic stress
τ	(/)	dimensionless time
Ω	$(\mathrm{m^3})$	Xenon covolume

List of Figures

List of Tables

Introduction

Under nominal conditions, in Light Water Reactor (LWR), radioactive FPs are generated from fission events in UO_2 grains. Their low solubility make them diffuse toward grain boundaries or precipitate into intra-granular bubbles. The majority of FPs reaches the grain boundary and is absorbed into inter-granular bubbles. With irradiation, the latter accumulate FPs. Through coalescence mechanisms, larger bubbles form until they connect the rod free volume within fuel interior, offering a diffusive path for FPs with higher volatility [White and Tucker, 1983, White, 2004, Pastore et al., 2013].

The notion of source term is generally related to the amount of dangerous material released from a nuclear power plant to the environment, after an accident [Housiadas et al., 2012]. It is used in radiological risk assessment and NPP licensing process [Soffer et al., 1995]. The ANS Glossary of Definition and Terminology defines the source term as the timing, quantity, physical and chemical form of, and thermal energy associated with, a release of radioactive material from a plant during an accident [American Nuclear Society, 2016]. Within a nuclear reactor, radioactive material includes FPs, generated during nominal operation within the irradiated fuel rods, Activation Products (APs) from core structural elements and Heavy Nuclei (HN), such as uranium and transuranium isotopes. Therefore, the source term can be deduced from the gap activity, i.e. the inventory of gaseous and volatile FPs that are accumulated in the rod free volume and that, if the cladding breaks, are released and can leakage towards the primary circuit [Soffer et al., 1995, Housiadas et al., 2012].

The gap activity include long-lived (with half-live longer than one year) FPs and short-lived (with half-live shorter than one year) FPs. Short-lived FPs, though negligible in mass, are responsible for most of the radioactivity that can be released to the environment [Housiadas et al., 2012]. The radiological impact of short-lived FPs is represented by the dose transferred to environment and individuals, and it depends on their volatility and half-life. For example, radiological impact of ^{131}I, the isotope that provides the larger equivalent dose to individuals [Turnbull and Beyer, 2009], lasts less than one month, while the impact of ^{134}Cs covers a period of about 2 years,

To date, thanks to several experimental programs [Kleykamp, 1985, Ducros et al., 2013], it is possible to identify schematically four groups of FPs with decreasing volatility:

1. Gaseous (FG) (Xe, Kr) and volatile FPs (I, Cs, Sb, Te, Cd, Rb, Ag).
2. Semivolatile FPs (Mo, Rh, Ba, Pd, Tc).
3. Low-volatile FPs (Sr, Y, Nb, Ru, La, Eu, Ce).

4. Nonvolatile FPs (Zr, Nd, Pr).

Fission gases are inert gases with a low solubility that exist as in-solution atoms in the UO_2 matrix, or within intra- and inter-granular bubbles. Gas in inter-granular bubbles is most likely to be released under accident conditions. Volatile FPs chemical state has not been fully explained today. Most are probably in the form of dissolved atoms and above a certain temperature they are found in a gaseous form and can migrate radially to condense in cooler areas, such as in contact with the cladding. In addition, it has been often hypothesized that compounds, as CsI, are formed [Olander, 1976, Kleykamp, 1985, Housiadas et al., 2012].

As previously highlighted, it is of fundamental importance to evaluate source term and gap activity in a nuclear reactor. In order to model the behaviour of radioactive isotopes and to evaluate the source term, two different approach are available [Housiadas et al., 2012, Pizzocri et al., 2020]

1. Physics-based approach. Through mechanistic models, the known physical phenomena coming into play are taken into consideration. They result flexible and powerful in the description of transient condition, despite the generally substantial computational effort.

2. Correlation-based approach. Mechanistic models are replaced with simplified empirical descriptions. They are easily implementable in numerical codes and are matched to low computational costs. This approach is preferred when the physics description of the involved phenomena appears difficult and together it is possible to exploit a large number of experimental data to build the desired correlation.

Physics-based modelling of FPs release must include intra-granular diffusion of gas atoms to grain boundary, intra-granular bubble behaviour, nucleation, growth, trapping and resolution phenomena, coalescence, interconnection and subsequent release. In addition, the chemical and transport properties of the FPs, within the fuel matrix, are of fundamental importance. Firstly, their behaviour is influenced by the oxygen potential of the fuel pin. Secondly, the physical properties of the fuel (e.g. thermal conductivity, swelling, creep, melting point) are influenced by the chemical state of the fission products [Kleykamp, 1985].

The state-of-the-art methodology available to evaluate the radioactive FPs release and the gap activity is the ANS *Method for Calculating the Fractional Release of Volatile Fission Products from Oxide Fuel*, ANS 5.4 [Turnbull and Beyer, 2009]. ANS 5.4 has been developed for stationary conditions of the reactor and to evaluate the fractional release of short-lived volatile and gaseous FPs. It should not be applied to accidents which involve abrupt temperature variations and to determine the release of stable or long-lived FPs.

ANS 5.4 methodology exploits a correlation-based model to evaluate the fractional release of radioactive isotopes of interest. The correlation adopted by ANS 5.4 describes the inter-granular bubble interconnection through an empirical criterion function of the fuel burnup and temperature, the Vitanza (or Halden) threshold. In addition, chemical phenomenon of fuel oxidation and transport of FPs after release from fuel rod void are neglected.

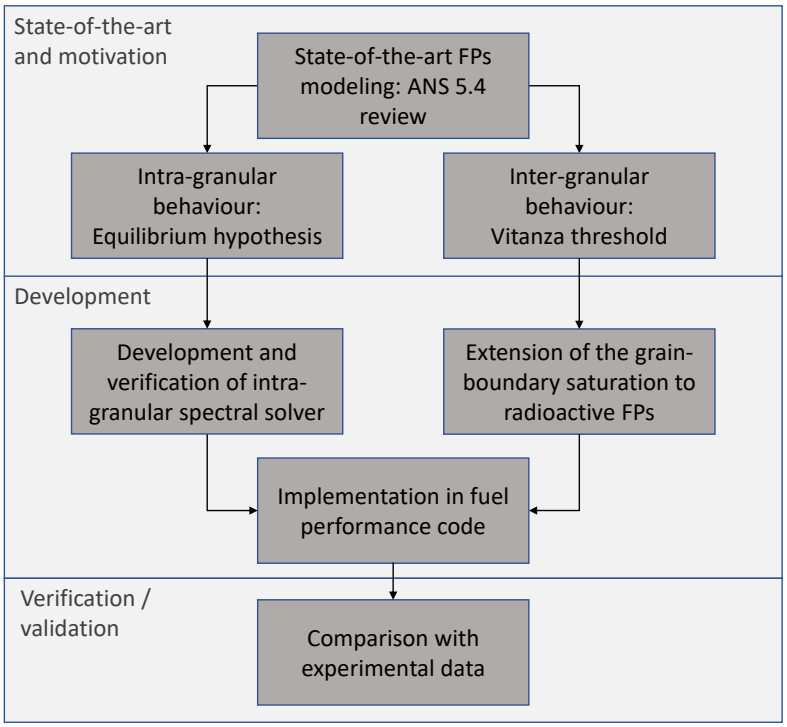

Figure 11. The structure of the present work consist of a preliminary state-of-the-art description, which highlights the possible developments. Once the latter have been introduced, they must be compared to a set of existing experimental data, to confirm the model reliability.

To review the ANS 5.4 methodology, an analytic derivation of the equilibrium fractional release is provided in Chap. 1. In Chap. 2 the spectral decomposition of of the intra-granular concentration allows another analytic derivation, equivalent to the precedent, of the intra-granular problem and, more importantly, the development of an algorithm to be implemented in SCIANTIX, a 0D meso-scale Fuel Performance Code (FPC) [Pizzocri et al., 2020]. The consistency of the newly implemented algorithm is tested via MMS [Oberkampf et al., 2004]. A physics-based model for grain-boundary behaviour is described in Chap. 3, based on existent works about bubble evolution [White, 2004, Veshchunov, 2008, Pastore et al., 2013]. The description is extended to radioactive FPs and similarly SCIANTIX routines is modified to include radioactive FPs in the grain-boundary development. Eventually, the intra- and inter-granular model for the evaluation of radioactive gaseous and volatile FPs release is compared against the experimental VERCORS results, representative out-of-pile simulations of LOCA accidents [Ducros et al., 2013].

This work is situated within the Reduction of Radiological Consequences of design basis and extension Accidents (R2CA) European project. The goal of R2CA project is the development of improved computational methodologies for the realistic evaluation of source term during LOCAs concerning LWRs and improving the iodine release evaluation during a Steam Generator Tube Rupture (SGTR) sequences. R2CA aims at improving accident management and proposing new reactor systems instrumentation, thereby upgrading facility safety [R2CA, 2019].

Chapter 1

State-of-the-art model: ANS 5.4

Abstract. Radioactive Fission Products (FPs) release is of fundamental importance for fuel rod and NPP design and licensing. The current methodology available to evaluate the radioactive release is the ANS 5.4 methodology, *Method for Calculating the Fractional Release of Volatile Fission Products from Oxide Fuel*. This methodology is tailored to Light Water Reactors (LWRs), in operative conditions that do not involve abrupt temperature transients. If coupled with isotopic yields, it provides the *gap activity*, which is the inventory of volatile FPs that are released from the fuel rod if the cladding is breached.

The current ANS 5.4 methodology applies to short-lived (with half-live shorter than one year) volatile and gaseous FPs of radiological interest, namely krypton, xenon, iodine and tellurium. Other models are needed to determine the release of stable or long-lived nuclides. The description behind the methodology consists in a stationary correlation-based model. The mechanistic description of the thermal release is replaced with an empirical criterion, function only of the fuel burnup and temperature. As a consequence, some limitations arise. Predicted release fraction values are often strongly conservative. Even with respect to the validation database, the predicted releases are at least one order of magnitude above the measured data. Moreover, burst releases caused by sudden temperature variations, e.g. during a severe accident, are not reproducible.

The aim of the present chapter is to review the ANS 5.4 methodology and the model basic assumption. The intra-granular diffusion problem for radioactive isotopes is tackled from scratch. The analytic formula for the release is derived from the concentration equation and it is underlined how the asymptotic behaviour is the one adopted in the ANS 5.4 model.

1.1 Introduction

The present chapter focuses on the ANS 5.4 methodology. Sec 1.2 reviews the basic assumptions of the model. The methodology defines the fractional release R/B of unstable gas atoms during irradiation starting from the equivalent sphere model of UO_2 [Booth, 1957]. In Sec. 1.3 the intra-granular model is developed, beginning from the following Partial Differential Equation (PDE)

$$\frac{\partial C}{\partial t} = \alpha D \nabla^2 C - \lambda C + B$$

where $C(r,t)$ $(\mathrm{at\,m^{-3}\,s^{-1}})$ is the isotope concentration, D $(\mathrm{m^2\,s^{-1}})$ is the diffusion coefficient of the isotope in the fuel matrix, α is a corrective factor depending on the isotope precursor, λ $(\mathrm{s^{-1}})$ is the decay rate and B $(\mathrm{at\,m^{-3}\,s^{-1}})$ is the source term. The equilibrium fractional release, written as $(R/B)_\infty$ is shown to be

$$\left(\frac{R}{B}\right)_\infty = \frac{3}{\sqrt{\mu}}\left(\coth\sqrt{\mu} - \frac{1}{\sqrt{\mu}}\right)$$

which depends on $\mu = \lambda a^2/D$. The thermal Fission Gas Release (FGR) model is described in Sec. 1.4. The release process is usually considered to be controlled by atomic diffusion to the fuel grain boundaries [White and Tucker, 1983] and it follows a two-step simplified description [Barnes, 1964, Whapham, 1966].

1. Gas atoms are uniformly produced in the grain bulk and diffuse towards the grain boundaries, where they accumulate in grain boundaries bubbles, until grain boundary saturation.

2. When the saturation threshold is reached, instant release begins. Gas is brought from the grain boundaries to the fuel rod free volume, neglecting all the mechanisms that bring the fission products from grain boundary to the fuel rod void, like tunnel formation, percolation, grain faces diffusion, etc. The neglected phenomena does not considerably affect the gap activity but only the FGR kinetics [Bernard et al., 2002].

The chosen empirical correlation for the incubation period is based on the Halden threshold [Vitanza et al., 1979], reflecting the strong dependence between fuel temperature T (K) and burnup β ($\mathrm{GWd/tUO_2}$). The correlation has been calibrated over the results obtained at the Halden Reactor Project about radioactive releases. The set of volatile and gaseous FPs to which ANS 5.4 is applied is shown in Tab. 1.1. It consists of short-lived isotopes, i.e. their half-lives are shorter then one year. The ANS 5.4 methodology has been applied to an example case described in Sec. 1.6.

Eventually, the model is tailored on fuel densities between 95 % to 98 % of theoretical density, grain size between 6 μm to 15 μm and open porosity between 0.1 % to 3.0 %. The available data in Tab. 1.1 come from the ANS 5.4 report [Turnbull and Beyer, 2009]. The only exception is the cumulative yield y of thermal fission in ^{235}U, taken from the IAEA online database [IAEA, 2020].

Table 1.1. Decay constants, precursor enhancement factors and fission yields for radioactive fission products [Turnbull and Beyer, 2009,IAEA, 2020].

Nuclide	Decay rate (s^{-1})	Half-life	α (/)	Fission yield (%)
^{85m}Kr	4.30×10^{-5}	4.48 h	1.31	1.303
^{87}Kr	1.52×10^{-4}	1.27 h	1.25	-
^{88}Kr	6.78×10^{-5}	2.84 h	1.03	-
^{89}Kr	3.35×10^{-3}	3.15 min	1.21	-
^{90}Kr	2.15×10^{-2}	32.3 s	1.11	-
^{131}I	9.98×10^{-7}	8.04 d	1.0	2.878
^{132}I	8.44×10^{-5}	2.28 h	137	4.276
^{133}I	9.26×10^{-6}	20.8 h	1.21	6.59
^{134}I	2.20×10^{-4}	52.6 min	4.4	-
^{133}Xe	1.53×10^{-6}	5.243 d	1.25	6.6
^{135m}Xe	7.55×10^{-4}	15.3 min	23.5	1.22
^{135}Xe	2.12×10^{-5}	9.10 h	1.85	6.61
^{137}Xe	3.03×10^{-3}	3.82 min	1.07	-
^{138}Xe	8.19×10^{-4}	14.1 min	1.00	-
^{139}Xe	1.75×10^{-2}	39.7 s	1.00	-

1.2 Model assumptions

The basic hypothesis for the diffusion model employed in the ANS 5.4 methodology are the following ones:

1. Fission gas atoms are born in the fuel grains. The diffusion along the concentration gradient, from where the atoms are produced, is main mechanism for diffusion to the grain boundaries (trapping and irradiation-induced resolution from nanometre-size intra-granular gas bubbles are neglected). Once the grain-boundaries have been reached, the gas atoms precipitates in inter-granular bubbles.

2. Inter-granular bubbles are held on the grain boundaries and continuously absorb gas atoms from the grain interiors. When the bubbles reach a saturation condition, they interconnect, forming a pathway that connect the fuel interior with the pellet surface, and allowing the gas release to the fuel rod void volume.

3. The criterion for grain boundary interconnection is an empirical function of only temperature and burnup [Vitanza et al., 1979].

4. Once the grain boundary interconnection has occurred, the grain boundary remains linked to the rod internal void volume for the rest of the irradiation (i.e. no resintering of the grain boundary is experienced).

5. The intra-granular diffusive process of each radionuclide depends both on the single-atom diffusion coefficient in the uranium dioxide and on its radioactive precursor. The derivation of the precursor enhancement factor α is valid if one of two conditions is met:

(a) The precursor is immobile after release. This is believed to be the case with the xenon precursor, iodine,

(b) The precursor is mobile but has a half-life much less than the transit time from the fuel to the detector. This is the case for the krypton precursor, bromine.

6. The nuclides are in radioactive equilibrium in terms of release and decay, i.e. secular equilibrium holds. This assumption is approximately correct, for a single radionuclide, if fuel temperatures remain constant for at least three half-lives of the nuclide at issue.

7. The diffusion coefficients for the nuclides of interest are assumed to be the same as xenon or a multiple of that for xenon, i.e., $D(\mathrm{Xe}) = D(\mathrm{Kr}) = D(\mathrm{I}) = D(\mathrm{Br})/20 = D(\mathrm{Te})/4$.

8. Fuel densification, which tends to increase fuel temperature, and reduction in the porosity volume fraction, which tends to decrease fuel temperature, are neglected.

9. Athermal release mechanisms, such as recoil or knockout, λ-independent, are neglected.

10. Sweeping mechanism, i.e. the accumulation of intra-granular gas at moving grain boundaries, is neglected.

Following hypothesis (1), the mass balance within the fuel grain for a single isotope is

$$\frac{\partial C(r,t)}{\partial t} = \alpha D \nabla^2 C(r,t) - \lambda C(r,t) + B \tag{1.1}$$

This partial differential equation describes the evolution of $C(r,t)$, fission product concentration ($\mathrm{at\,m^{-3}}$), which results at time t from direct production by fission B ($\mathrm{at\,m^{-3}\,s^{-1}}$), loss by diffusion $\alpha D \nabla^2 C$ and radioactive decay[1] $-\lambda C$. Every radioactive fission product is characterized by a decay constant λ ($\mathrm{s^{-1}}$) and a source term $B = y\dot{F}$, where y is its cumulative fission yield and $\dot{F}$ is the fission rate density ($\mathrm{fiss\,m^{-3}\,s^{-1}}$). From hypothesis (7), the adopted diffusion coefficients are proportional to the Xe-diffusion coefficient. The Xe-diffusion coefficient, D ($\mathrm{m^2\,s^{-1}}$), in irradiated UO_2 fuels is made up of three terms, each one describes a distinct physical process that influences different temperature ranges [Turnbull et al., 1982].

$$D(T,\dot{F}) = D_1(T) + D_2(T,\dot{F}) + D_3(\dot{F}) \tag{1.2}$$

1. $D_1(T)$ is the intrinsic diffusion coefficient. It predominates at $T > 1200$ °C and, since it describes a thermally activated volume diffusion, is written in the usual Arrhenius form

$$D_1(T) = D_0 e^{-\Delta H/k_B T} \tag{1.3}$$

ΔH is an activation energy, D_0 is a diffusion pre-exponential constant and k_B is the Boltzmann constant. During irradiation the insoluble fission products, such

[1] Transmutation effects are neglected.

as xenon and krypton, occupy lattice vacancy positions. It exists a similarity between gas atoms diffusion and cation self-diffusion, but it depends on the gas concentrations and on the number of radiation-induced defects. Matrix self-diffusion is the slowest mass transport mechanism occurring in the fuel [Rest, 2003].

2. $D_2(T, \dot{F})$ represents a diffusion controlled by both temperature and fission rate. For temperatures between 800 and 1200 °C the vacancy concentration is partly controlled by the fission rate. Based on random walk model

$$D_2(T, \dot{F}) = d^2 j_v c_v \tag{1.4}$$

where d is the atomic jump distance, j_v is the termally activated vacancy jump rate and c_v is the cation vacancy concentration [Turnbull et al., 1982, Turnbull and Beyer, 2009].

3. $D_3(\dot{F})$ is the athermal diffusion coefficient. When $T < 800$°C the vacancy jump rate is negligible and diffusion occurs by atomic collision cascades. This athermal contribution is empirically written as

$$D_3(\dot{F}) = A\dot{F} \tag{1.5}$$

In the end the diffusion coefficient is [Turnbull et al., 1982]

$$D = 7.6 \times 10^{-10} e^{-35000/T} + 4 \times 1.41 \times 10^{-25} \sqrt{\dot{F}} e^{-13800/T} + 2 \times 10^{-40} \dot{F} \tag{1.6}$$

where T (K) and F (fiss $\mathrm{m}^{-3}\,\mathrm{s}^{-1}$).

In the ANS 5.4 methodology the diffusion coefficient has been revised to provide a better fit with the Haldon Reactor Project gas release data. Nevertheless the variations remain within the scatter of the Turnbull's DIDO release data, data upon which the coefficients of the diffusion model were based during the 1970s. The revised diffusion coefficient, adopted in ANS 5.4, is [Turnbull and Beyer, 2009]

$$D = 7.6 \times 10^{-11} e^{-35000/T} + 1.41 \times 10^{-25} \sqrt{\dot{F}} e^{-13800/T} + 2 \times 10^{-40} \dot{F} \tag{1.7}$$

The precursor enhancement factor α reproduces empirically the precursor (p) effect on the diffusing isotope (n). It was ignored in the first 1982 methodology for all the isotopes with the exception of the ^{133}Xe and ^{135}Xe. The relationship used in the current ANS5.4 is given by [Friskney and Speight, 1976]

$$\alpha = \left(\frac{1 - (y_0/x_0)^3}{1 - (y_0/x_0)^2} \right)^2 \tag{1.8}$$

where $y_0 = \sqrt{D_\mathrm{p}/\lambda_\mathrm{p}}$ and $x_0 = \sqrt{D_\mathrm{n}/\lambda_\mathrm{n}}$. The fractional release of an isotope significantly increases when its diffusion rate is slow relative to its precursor, especially when these have half-lives comparable with the irradiation time [Friskney and Speight, 1976]. Intuitively, α reflects that the fractional release of a daughter isotope is not exclusively determined by its own diffusivity. The fact that the precursor diffuses before the

decay increases the fractional release of the daughter. Precursors with relatively high diffusivities and half-lifes comparable to the irradiation time experiences a significant increase in fractional release. This argument has been used to explain the different fractional releases observed for ^{134}Cs and ^{137}Cs even though they should exhibit the same diffusivity [Brown and Faircloth, 1976]. Similarly the variation in the observed fractional releases of ^{131}Xe and ^{132}Xe has been attributed to the diffusion of their longest lived precursors ^{131}I and ^{131}Te.

1.3 Intra-granular gas behaviour

The dominant mechanism of release is generally supposed to be the diffusional release, namely the diffusion of radioactive isotopes through the fuel open porosity [Friskney and Speight, 1976]. Other minor release mechanisms are knockout, recoil and evaporation. However, since their relative contribution is negligible and their behaviour is not well established, it is possible to ignore them [Beck, 1960, Olander, 1976]. The current ANS 5.4 methodology, as most of the mechanistic FGR models for LWR fuel [Rest, 2003], exploits the equivalent sphere model [Booth, 1957] to describe the diffusional release. Booth modeled the polycrystalline UO_2 sinter as a collection of uniform spheres with an equivalent radius a. The equivalent radius a is related to the *surface-to-volume ratio* S/V by the following

$$\frac{S}{V} = \frac{4\pi a^2}{4/3\pi a^3} = \frac{3}{a} \tag{1.9}$$

The fuel is made up of fissile material and it is initially free of a given radionuclide. It is irradiated at constant fission rate $\dot{F}$ (fiss m^{-3} s^{-1}) and the isotope is homogeneously produced at a constant rate B. The gas atom produced diffuses through the sphere according to Fick's law, decays, if radioactive, according to the natural decay law and escapes from the sphere once reached the boundary.

The equivalent sphere model alone neglects the effects of the initial closed porosity, the kinetic aspects and the time required to traverse the interconnected porosity to the surface of the fuel element. The ANS 5.4 methodology, by exploiting the hypothesis (3), considers the initial closed porosity.

The intra-granular problem (Eq. 1.1) is written by taking advantage of the spherical symmetry of the problem and initial and boundary conditions are highlighted. The isotopes concentration $C(r,t)$ satisfy the following well-posed problem.

$$\begin{cases} \dfrac{\partial C(r,t)}{\partial t} = \dfrac{\alpha D}{r^2}\dfrac{\partial}{\partial r}\left(r^2\dfrac{\partial C(r,t)}{\partial r}\right) - \lambda C(r,t) + B & \\ C(r,0) = 0 & 0 < r < a \\ C(a,t) = 0 & t > 0 \\ C(0,t) = C_0 & t > 0 \end{cases} \tag{1.10}$$

where C_0 must be finite. The solution is obtained by substitution. By defining $U(r,t)$ such that

$$C(r,t) = \frac{1}{r}\left[U(r,t)e^{-\lambda t} + \frac{B}{\lambda}\left(r - \frac{a\sinh r\sqrt{\lambda/\alpha D}}{\sinh a\sqrt{\lambda/\alpha D}}\right)\right] \tag{1.11}$$

it is achieved a simple diffusion problem for $U(r,t)$

$$\begin{cases} \dfrac{\partial U(r,t)}{\partial t} = \alpha D \dfrac{\partial^2 U(r,t)}{\partial r^2} & \\ U(0,t) = U(a,t) = 0 & t > 0 \\ U(r,0) = U_0 & 0 < r < a \end{cases} \tag{1.12}$$

with

$$U_0 = \frac{B}{\lambda}\left(\frac{a \sinh r\sqrt{\lambda/\alpha D}}{\sinh a\sqrt{\lambda/\alpha D}} - r\right) \tag{1.13}$$

The time-dependent solution is easily found using Fourier series

$$C(r,t) = \\ \frac{B}{\lambda r}\left(r - \frac{a \sinh\sqrt{\lambda r^2/\alpha D}}{\sinh\sqrt{\lambda a^2/\alpha D}} + \frac{2\lambda a^3}{\alpha D \pi}\sum_{n=1}^{\infty}\frac{(-1)^n \sin(n\pi r/a) e^{-(\lambda + n^2\pi^2\alpha D/a^2)t}}{n(n^2\pi^2 + \lambda a^2/\alpha D)}\right) \tag{1.14}$$

The time dependence of $C(r,t)$ is entirely contained in the exponential term. The characteristic time needed for equilibrium depends then on the exponent $\lambda + n^2\pi^2\alpha D/a^2$. The first modal component, for $n = 1$, is the slowest, since if n increases the exponential decreases. Then, once the first mode has reached the equilibrium, the concentration has done the same thing. It is commonly said that an exponential transient finishes after 5 characteristic times, with $e^{-5} \approx 0.0076$. As a consequence, a reasonable characteristic time for our problem is

$$T_e = \frac{5}{\lambda + \alpha D\pi^2/a^2} \tag{1.15}$$

The release rate R ($\mathrm{at\,m^{-3}\,s^{-1}}$) is obtained from the concentration gradient at the boundary of the sphere $r = a$. According to first Fick's law, the flux density $\vec{J}$ of a diffusing concentration ϕ is proportional to its concentration gradient

$$\vec{J} = -D\nabla\phi \tag{1.16}$$

The release rate of gas atoms that reach the spherical grain boundary then is

$$R = -\alpha D \frac{3}{a}\left.\frac{\partial C(r,t)}{\partial r}\right|_{r=a} \tag{1.17}$$

The release rate R is a function of the time t, in line of principle it can be evaluated instantaneously. A helpful quantity is the release fraction, defined as the ratio R/B. It is the ratio of the rate at which atoms are being released to the rate at which they are being produced.

$$\frac{R}{B} = \frac{3}{\sqrt{\mu}}\left(\coth\sqrt{\mu} - \frac{1}{\sqrt{\mu}}\right) - \frac{6}{\pi^2}\sum_{n=1}^{\infty}\frac{e^{-(n^2\pi^2/\mu + 1)\tau}}{n^2 + \mu/\pi^2} \tag{1.18}$$

where $\mu = \lambda a^2/\alpha D$ is a dimensionless parameter and $\tau = \lambda t$ is dimensionless characteristic time. The parameter μ is an important control parameter for the diffusion-decay

problem. It weights the decay over the diffusion mechanism and one may expects that it influences the equilibrium value.

As initially specified, ANS 5.4 is valid under the secular equilibrium hypothesis. The previous formula for R/B (Eq. 1.18) could be labeled as *instantaneous release fraction*, since it depends on t, while the *equilibrium release fraction* is

$$\left(\frac{R}{B}\right)_\infty = \frac{3}{\sqrt{\mu}}\left(\coth\sqrt{\mu} - \frac{1}{\sqrt{\mu}}\right) \tag{1.19}$$

which is the same formula adopted in the ANS 5.4 methodology [Turnbull and Beyer, 2009]. In particular, the current ANS 5.4 methodology uses Eq. 1.19 as release fraction, but defines the control parameter μ in terms of the surface area to volume ratio S/V

$$\mu = \frac{9\lambda}{(S/V)^2\alpha D} \tag{1.20}$$

Eq. 1.19 can be further simplified, if the release fraction is small enough, i.e. $(R/B)_\infty < 2$ %. Indeed, whenever $\mu > 22000$

$$\left(\frac{R}{B}\right)_\infty \approx \frac{3}{\sqrt{\mu}} = \frac{S}{V}\sqrt{\frac{\alpha D}{\lambda}} \tag{1.21}$$

the approximation is valid with a small excess relative error, less than 1×10^{-2}.

As an application, to test the validity of the Fourier approach and to observe the functional form of the solution, it is possible to consider the case of a single isotope and numerically implement the exact equations in MATLAB. Let's consider the isotope $^{135\mathrm{m}}$Xe, $\lambda = 7.55 \times 10^{-4}$ s^{-1} and $\alpha = 23.5$ [Turnbull and Beyer, 2009]. For a real UO_2 grain $a = 5$ μm. The diffusion coefficient is computed by Eq.(1.2) at $T = 1000$ K and $\dot{F} = 1 \times 10^{19}$ fiss m^{-3} s^{-1}. The case just described could represent the nominal steady-state operation of a Gen. III PWR. The characteristic time of the isotope $T_e \approx 6.62 \times 10^3$ s is a bit less of 2 hours. The cumulative fission yield in ^{235}U due to thermal fission is $y = 0.0122$. It is possible to evaluate $\mu \approx 1.39 \times 10^4$. Firstly, it is considered the solution $C(r,t)$ made up of the superposition of 500 modes. The discrete time axis is defined from 0 to the equilibrium time with 150 discretization points, the discrete space axis is defined from $-a$ to a with 300 discretization points. In Fig. 1.1 the three dimensional plot is shown. The solution correctly respect the data on the parabolic boundary. At $r = \pm a$ the solution goes to zero but the concentration gradient has an absolute value of about 1×10^{27}, therefore the Dirichlet boundary condition is hard to appreciate. An interesting quantity is the spatial average of the concentration. The average is computed on the sphere, so one gets

$$\bar{C}(t) = \frac{3}{4\pi a^3}\int_0^a C(r,t)4\pi r^2 dr \tag{1.22}$$

The formula for $\bar{C}(t)$ can be obtained exploiting the analytic solution of $C(r,t)$

$$\bar{C}(t) = \frac{6B}{\lambda\pi^2}\left(\frac{\pi^2}{6} - \frac{\pi^2\coth\sqrt{\mu}}{2\sqrt{\mu}} + \frac{\pi^2}{2\mu} - \sum_{n=1}^{\infty}\frac{e^{-(1+n^2\pi^2/\mu)\lambda t}}{n^2(n^2\pi^2/\mu+1)}\right) \tag{1.23}$$

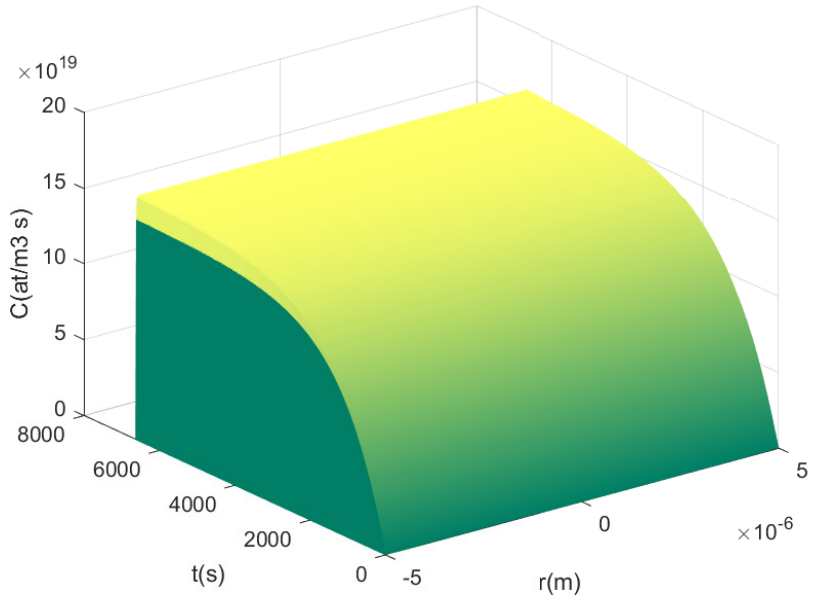

Figure 1.1. 3D plot of the concentration $C(r,t)$ obtained with Fourier decomposition.

where, for sake of clarity, $\mu = \lambda a^2/\alpha D$

$$\bar{C}(t) = \frac{6B}{\lambda\pi^2}\left(\frac{\pi^2}{6} - \frac{\pi^2}{2\mu}\left(\sqrt{\mu}\coth\sqrt{\mu} - 1\right) - \sum_{n=1}^{\infty}\frac{e^{-(1+n^2\pi^2/\mu)\lambda t}}{n^2(n^2\pi^2/\mu + 1)}\right) \tag{1.24}$$

Now two convergent mathematical series are involved [Beck, 1960]

$$\sum_{k=1}^{\infty}\frac{1}{k^2} = \frac{\pi^2}{6} \tag{1.25}$$

and

$$\sum_{k=1}^{\infty}\frac{1}{k^2 + a^2} = \frac{1}{2a^2}\left(a\pi\coth(a\pi) - 1\right) \tag{1.26}$$

By properly manipulating the equation, the final expression for $\bar{C}(t)$ is

$$\bar{C}(t) = \frac{6B}{\lambda\pi^2}\sum_{k=1}^{\infty}\frac{1}{k^2}\frac{1}{1 + \pi^2k^2/\mu}\left(1 - e^{-\left(1+\pi^2k^2/\mu\right)\lambda t}\right) \tag{1.27}$$

or replacing $\mu = \lambda a^2/\alpha D$

$$\bar{C}(t) = \frac{6B}{\pi^2}\sum_{k=1}^{\infty}\frac{1}{k^2}\frac{1}{\lambda + \alpha D\pi^2k^2/a^2}\left(1 - e^{-\left(\lambda+\alpha D\pi^2k^2/a^2\right)t}\right) \tag{1.28}$$

The equilibrium average concentration C_∞ is not reported in ANS 5.4 background paper, nevertheless it is useful to write its expression

$$C_\infty = \frac{B}{\lambda} - \frac{3B}{\lambda\sqrt{\mu}}\left(\coth\sqrt{\mu} - \frac{1}{\sqrt{\mu}}\right) \tag{1.29}$$

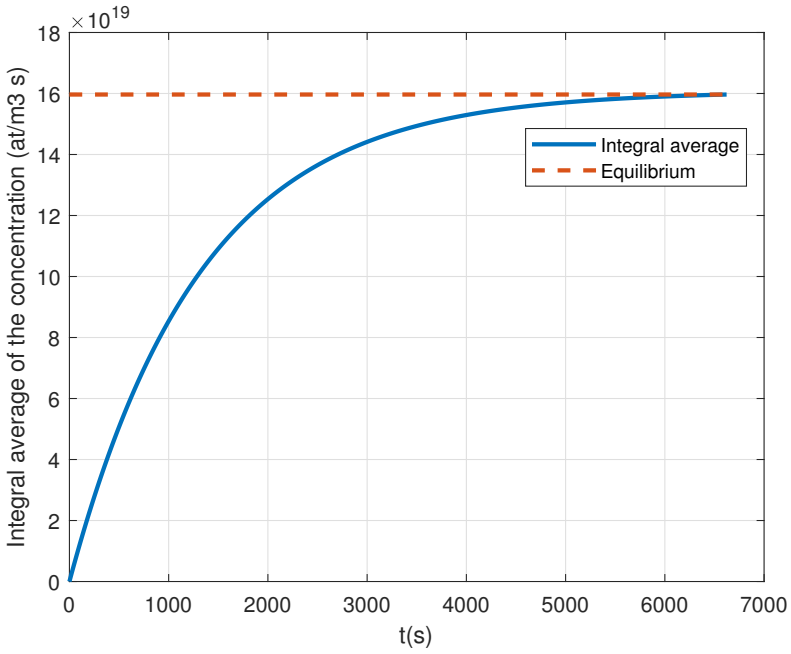

Figure 1.2. Integral average of the concentration over the sphere against its equilibrium value.

Eq. 1.28 is the analytic solution for the concentration of an isotope, averaged over the sphere of radius a. In Fig. 1.2 the average concentration $\bar{C}(t)$ is shown. It correctly starts from 0 and reaches an equilibrium value. Anyway, ANS 5.4 provides a methodology for the calculation of the equilibrium fractional release. Another manipulation can be performed. From the average concentration it is possible to obtain the release fraction Eq. (1.18). From the initial expression of $\bar{C}(t)$ one gets

$$\frac{\lambda \bar{C}(t)}{B} = 1 - \frac{3}{\sqrt{\mu}}\left(\coth\sqrt{\mu} - \frac{1}{\sqrt{\mu}}\right) - \frac{6}{\pi^2}\sum_{k=1}^{\infty}\frac{e^{-(1+n^2\pi^2/\mu)\lambda t}}{n^2(1+n^2\pi^2/\mu)} \tag{1.30}$$

and the instantaneous release fraction emerges as

$$\frac{R}{B} = 1 - \frac{\lambda \bar{C}(t)}{B} - \frac{6}{\pi^2}\sum_{k=1}^{\infty}\frac{e^{-(1+n^2\pi^2/\mu)\lambda t}}{n^2} \tag{1.31}$$

The equilibrium fractional release can be easily expressed as a function of the equilibrium concentration

$$\left(\frac{R}{B}\right)_{\infty} = 1 - \frac{\lambda C_{\infty}}{B} \tag{1.32}$$

In Fig. 1.3 the fractional release R/B is plotted with the equilibrium value (Eq. 1.19) adopted in ANS 5.4. It is possible to note that, again, the curve correctly starts from 0. As time passes, the release rate R increases until the transient finishes, and the transient phase is governed by the exponential terms.

ANS 5.4 applies to release of short-lived FPs by assuming a period of constant power operation, generally over three half-lives of the described nuclides [Turnbull and Beyer, 2009]. Under this work hypothesis it is possible to evaluate the fractional

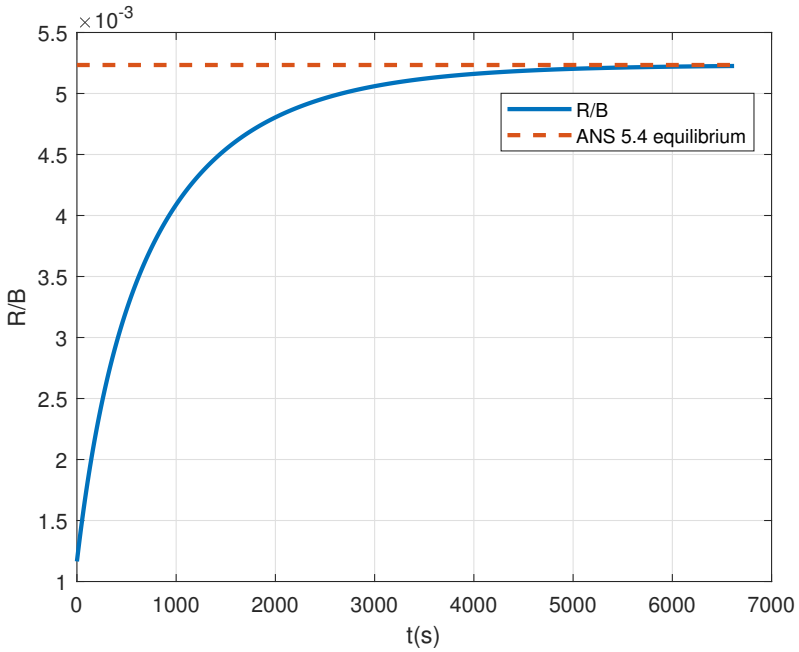

Figure 1.3. Temporal evolution of the release fraction against its equilibrium value.

release of a specified nuclide through the equilibrium value (Eq. 1.19). It is useful to consider when this assumption makes the ANS 5.4 approach valid and the entailed limitations.

- The model is reasonably relevant when the nuclides are in radioactive equilibrium in terms of release and decay. If the maximum half-live of the considered isotopes (Tab 1.1) is about eight days, it is clear that one or two months of constant temperature operation may be required.

- In the background report [Turnbull and Beyer, 2009] it is specified that the model is shaped on postulated accidents which do not involve sudden temperature variations. In addition burst releases due to temperature variations grater than 300 K are not described. Therefore, representative scenarios are releases during in-pile operation, shortly after reactor operation or fuel-handling accident. The prediction of a release associated to an abrupt transient can be performed in a conservative way by assuming a temperature equal to the maximum one.

- The release associated to the mentioned scenario is computed by considering only the equilibrium value (Eqs. 1.19, 1.32). In Fig. 1.3 the comparison between the neglected transient and the conservative ANS equilibrium solution is highlighted. Asymptotically the solutions are identical but a time-dependent approach would permit a more accurate description of the FPs release.

- As a consequence of the model assumptions, it is not possible to describe severe accidents, where large temperature increases appear, or out-of-pile experiments, e.g. annealing experiments, useful in the FPs release evaluation. In general, it is not possible to follow the temporal evolution of the release.

- If the isotopic yields are not supplied, one may evaluate the fractional release $(R/B)_\infty$, where $B = y\dot{F}$ (1.19). The output of the simulation is normalized with respect to the source term and the yield is not needed. The only useful parameter is $\mu = \lambda a^2/\alpha D$. If the isotopic yields are supplied, the model predicts the gap activity, namely the FPs inventory.
- Alternatively, if the original diffusion-decay equation coupled with the suitable initial and boundary conditions (Eq. 1.10), is solved through an appropriate numerical scheme, one can obtain a numerical solution C_N and use its equilibrium value to obtain the fractional release (Eq. 1.32). in this case the fission yields knowledge becomes mandatory, in order to obtain the time-dependent concentration (Eq. 1.28).

1.4 Inter-granular gas behaviour

With FPs inter-granular behaviour it is roughly intended the behaviour of the gas atoms once they have reached the inter-granular bubbles. Indeed experimental observations of fractured surfaces of UO_2 have shown that the grain boundaries are populated by large, micron-sized, lenticular bubbles. When the bubble density on the grain boundaries is sufficiently high and the bubbles are large enough, their extensive interconnection can occur (Fig. 1.4). A network of interconnected bubbles is formed, all the gas is stored in the open porosity and, if a point of the network gets in touch with an easy escape route, e.g. a crack, the gas is vented out of the fuel pellet. The onset of FPs release occurs generally after the grain-boundary porosity has attained a certain value. In general the porosity P of a ceramic material is a property representative of the quantity of existing pores (bubbles) and it is defined as [Olander, 1976]

$$P = \frac{\text{volume of pores}}{\text{volume of pores + volume of solid}} \tag{1.33}$$

and, although it reduces the fuel thermal conductivity, an amount of pores appear desirable to accommodate the FPs produced during irradiation. In reality the grain boundaries saturation constitutes an incubation time for the onset of FPs release. The delay imposed by the closed porosity, in the case of radioactive atoms, is significant, and the delay can be a consequence of the closed lenticular boundary porosity or of the progressive development and collapse of grain-edge porosity, where grain-edge indicates the region where three grains meet. The incubation time defines a threshold for thermal release and experimentally the duration of such period is observed to be strongly dependent on fuel temperature T (°C) and burnup β (GWd/tUO_2) [Vitanza et al., 1979, Bernard and Bonnaud, 1997]. A simple empirical correlation for the incubation threshold is based on the Halden, or Vitanza, threshold

$$\beta = \beta_0 \exp\left(\frac{T_0}{T}\right) \tag{1.34}$$

In the original paper the empirical parameters T_0 and β_0 were adjusted on FGR measured from Halden Reactor Project Post Irradiation Examination (PIE) puncturing

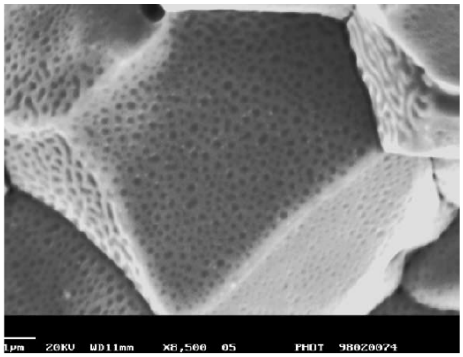

(a) Early stage of grain-boundary porosity development. The burnup of the fuel sample was ≈ 13 GWd/t, the mean projected bubble radius is 85 nm and there are approximately 9 bubbles per μm^2.

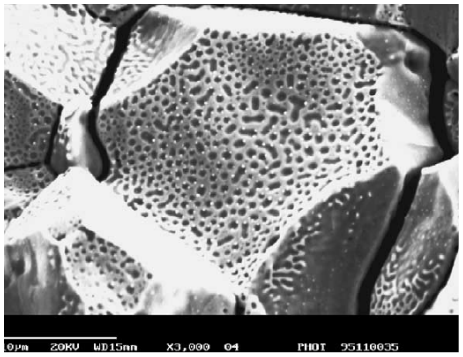

(b) Moderate grain-boundary porosity development. The burnup of the sample was ≈ 21 GWd/t, the mean projected radius is 220 nm and there are approximately 1.3 bubbles per μm^2.

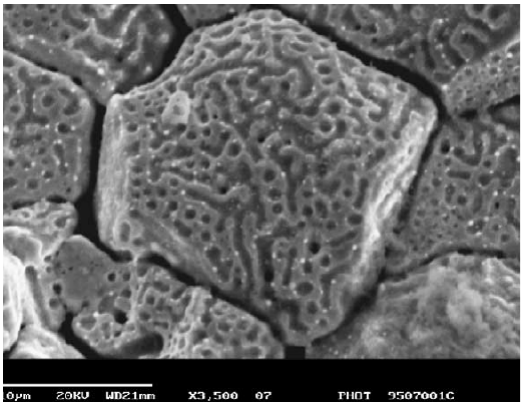

(c) Advanced grain-boundary porosity development. The mean projected bubble radius is 260 nm and there are approximately 0.43 bubbles per μm^2.

Figure 1.4. Grain-boundary porosity development in a fuel sample, from early stage of irradiation to bubble interconnection [White, 2004].

data, not on radioactive FPs measurements. Then $T_0 = 9800$ °C and $\beta_0 = 0.005$ GWd/tUO_2.

It is worth pointing out that resintering of grain boundary is neglected. Namely, when bubbles interconnection has occurred, the bubble network remains linked to the rod void volume.

ANS 5.4 methodology, which deals with radioactive gaseous and volatile FPs, adopts a slightly modified version of the Vitanza criterion. The original criterion considered the Fuel Centerline Temperature (FCLT) while ANS 5.4 considers the local fuel temperature at a given radial node (Sec. 1.5, [Turnbull and Beyer, 2009]). In addition, since the original criterion has been shown to underestimate the release threshold at high burnup, the correlation has been modified at high burnup. The modifications are conservative in the release evaluation and provide a better fit to the Halden release data of radioactive isotopes.

Despite the fact that empirical correlations are easily integrated in numerical code,

the main limitation introduced is that it can describe properly only commercial UO_2 fuel with rod burnup lower than 70 GWd/tUO_2, fuel densities between 95 % and 98 % of theoretical density, grain sizes between 6 μm and 15 μm and open porosity between 0.1 % and 0.3 % of theoretical density.

Eventually, the temperature for grain boundary bubble interconnection is

$$T_{\mathrm{IC}} = \frac{9800}{\ln(176\beta)} \ ^{\circ}\mathrm{C} \qquad \beta < 18.2 \ \mathrm{GWd/tUO_2} \tag{1.35}$$

$$T_{\mathrm{IC}} = 1434 - 12.85\beta \ ^{\circ}\mathrm{C} \qquad \beta \geq 18.2 \ \mathrm{GWd/tUO_2} \tag{1.36}$$

The release fraction R/B for a given nuclide, during an irradiation period at constant temperature T, is given by Eq. (1.19) using the following criterion

$$\left(\frac{S}{V}\right) = 120 \ \mathrm{cm^{-1}} \quad T < T_{\mathrm{IC}} \tag{1.37}$$

$$\left(\frac{S}{V}\right) = 650 \ \mathrm{cm^{-1}} \quad T \geq T_{\mathrm{IC}} \tag{1.38}$$

The two values of surface-to-volume ratio respectively correspond the equivalent radii $a = 250$ μm and $a \approx 46$ μm. The surface S of the fuel element should consider the contribution of the fuel open porosity. The S/V values have been empirically estimated from $^{85\mathrm{m}}$Kr measurements (Sec. 1.6) but it can be assessed that the increase of S/V can be reasonably justified. From the point of view of S/V, the interconnection of the results results in more surface available for diffusion, at constant volume. From the point of view of the equivalent radius, a smaller grain correspond to an increase of the release. The criterion is easily implementable but the drawbacks of the description could be too penalizing.

1. It is a step criterion, it does not consider the gradual increase of the inter-granular bubbles size, together with the decrease in their number.

2. It is a experimental criterion with a poor physical base.

3. The number values of the surface-to-volume ratio are not in line with the single grain dimension. That values have been extrapolated from the data, mirroring the release fraction experimentally measured.

1.5 Numerical implementation of the algorithm

The current ANS 5.4 methodology can be summarized as follows

1. evaluation of the interconnection temperature T_{IC}, from the fuel burnup β;

2. choice of the surface-to-volume ratio S/V, from the interconnection temperature T_{IC};

3. for every isotope the release-to-birth ratio R/B is computed, using Eqs. 1.19

As already mentioned, the approach is valid for the simulation of an stationary condition, i.e. a situation without abrupt temperature or power transients. The total release in a fuel rod can be determined with an integral numerical simulation, for example through a thermo-mechanicalFPC,where the whole rod is modeled with n radial and m axial nodes. For every node a local, equilibrium, release is computed. The total release, of a single isotope, is then determined by a weighted sum of the local releases from all the chosen nodes, each one at constant temperature and burnup

$$\left(\frac{R}{B}\right)_{\text{isotope}} = \sum_{j=1}^{m}\left(\frac{P_j^{\text{pellet}}V_j^{\text{ring}}}{P^{\text{avg}}V^{\text{rod}}}\sum_{i=1}^{n}\left(\frac{P_{i,j}^{\text{ring}}V_{i,j}^{\text{ring}}}{P_j^{\text{pellet}}V_j^{\text{node}}}\left(\frac{R}{B}\right)_{i,j}\right)\right) \tag{1.39}$$

where P^{avg} is the average rod power, P_j^{pellet} is the average power of the pellet in the axial node j, $P_{i,j}^{\text{ring}}$ is the average power of the local radial ring. The same notation holds for the volume variables.

Let's apply the ANS 5.4 methodology to evaluate the fractional release of several radionuclides, in an example case of a LWR working in steady-state conditions for four years and a half (approximately 60000 h) at a fission rate of 1.00×10^{19} fiss $\text{m}^{-3}\,\text{s}^{-1}$. Without accessing a FPC, a simplified lumped approach is preferred ($m = n = 1$). The asymptotic fractional releases (Eq. 1.19) can be evaluated for a set of radioactive isotopes (Tab. 1.2), before interconnection $(R/B)_{\infty,i}$ and after interconnection $(R/B)_{\infty,f}$. The fuel temperature is kept at 1000 K. In this fission rate and temperature conditions the diffusion coefficient (Eq. 1.7) is $D \approx 2.453 \times 10^{-21}$ $\text{m}^2\,\text{s}^{-1}$. In nuclear fuel analysis it is common to represent a quantity of interest as a function of the burn-up β (GWd/tUO_2), defined as the energy produced by fission events per unit fuel mass. If one fission event yields approximately $E_f \approx 200$ MeV and the nuclear fuel density is $\rho \approx 10970$ $\text{kg}\,\text{m}^{-3}$, then, in steady-state

$$\beta\ (\text{GWd/tUO}_2) = \int_0^t \frac{\dot{F}E_f}{\rho}dt \approx 0.001185\ t(\text{h}) \tag{1.40}$$

In order to get the temporal evolution of the fuel burnup, in the operative conditions considered above, a lumped simulation is performed with the meso-scale code SCIANTIX (Sec. 2.2, [Pizzocri et al., 2020]). According to the Halden threshold, the bubble interconnection happens after 46440 hours of steady-state functioning, when $\beta \approx 55$ GWd/tU.

Coherently with ANS 5.4 methodology, the equilibrium quantity of interest, $(R/B)_\infty$, has been evaluated, prior and after interconnection. In addition, considered $(R/B)_\infty = 1 - \lambda C_\infty/B$, also the intra-granular concentrations C_∞ have been

Table 1.2. Properties of the considered radioactive FPs.

Nuclide	Decay constant (s^{-1})	α	$(R/B)_{\infty,i}$	$(R/B)_{\infty,f}$
$^{85\text{m}}$Kr	4.30×10^{-5}	1.31	1.037×10^{-4}	5.618×10^{-4}
^{131}I	9.98×10^{-7}	1.00	5.948×10^{-4}	3.219×10^{-3}
^{133}I	9.26×10^{-6}	1.21	2.148×10^{-4}	1.163×10^{-3}
^{133}Xe	1.53×10^{-6}	1.25	5.371×10^{-4}	2.907×10^{-3}
$^{135\text{m}}$Xe	7.55×10^{-4}	23.5	1.048×10^{-4}	5.678×10^{-4}
^{135}Xe	2.12×10^{-5}	1.85	1.756×10^{-4}	9.507×10^{-4}

computed. For every isotope it has been computed that $\mu > 22000$, hence the following approximations hold

$$C_\infty \approx \frac{B}{\lambda}\left(1 - \frac{3}{\sqrt{\mu}}\right), \quad \left(\frac{R}{B}\right)_\infty \approx \frac{3}{\sqrt{\mu}}, \tag{1.41}$$

It is interesting to evaluate the relative variations, for C_∞ and $(R/B)_\infty$ in function of $\mu = \lambda a^2/\alpha D = \frac{9\lambda}{\alpha D(S/V)^2}$ by exploiting that before interconnection $S/V = 120$ cm^{-1} and after interconnection $S/V = 650$ cm^{-1}. For $(R/B)_\infty$ it is obtained the following estimation

$$\frac{(R/B)_{\infty,f} - (R/B)_{\infty,i}}{(R/B)_{\infty,i}} \approx \sqrt{\frac{\mu_i}{\mu_f}} - 1 = \frac{(S/V)_f}{(S/V)_i} - 1 \approx 4.42 \tag{1.42}$$

while for the intra-granular equilibrium concentration

$$\frac{C_{\infty,i} - C_{\infty,f}}{C_{\infty,i}} = \frac{3}{\sqrt{\mu_i} - 3}\left(\sqrt{\frac{\mu_i}{\mu_f}} - 1\right) \approx \frac{13.26}{\sqrt{\mu_i} - 3} \approx (1.33 \div 4.2) \times 10^{-3} \tag{1.43}$$

since $\mu_i \sim 10^{7\div 8}$. For this reason the variation of the intra-granular concentrations (Fig. 1.5) is reasonably imperceptible while the fractional releases of the isotopes change significantly (Fig. 1.6). Moreover, to a first approximation, the variation of the equilibrium release fraction is the same for all the isotopes and it is imposed by the change of the surface-to-volume ratio.

From Fig. 1.6 it can be noted how ANS 5.4 works. Once the bubble interconnection occurs, FPs release instantaneously begins. It is a conservative way to evaluate the FGR, the temporal dependence is totally ignored and the grain-boundary physics aspects are suppressed.

1.6 Validation database

The current ANS 5.4 methodology has been calibrated and validate on a radiological release database deriving from gas-flow type Halden Instrumented Fuel Assembly (IFA) experimental measurements. Namely, IFA-504, IFA-558 and IFA-633.

- ^{85m}Kr measurements from IFA-504 and IFA-558 were used for model fitting.
- ^{85m}Kr measurements from IFA-633 and ^{131}I measurements from IFA-504 and IFA-558 were used for model validation.

IFA-504 experiment consisted of four fuel rods irradiated from 60 to 90 GWd/tU, IFA-558 experiment consisted of six fuel rods irradiated to 40 GWd/tU. The model assumes that the rods have been in stationary conditions for a sufficient amount of time and that gas atoms are released only by diffusive mechanism. The small recoil component is significant only for very short-lived isotopes, which, if released, may decay outside the fuel, then it has been neglected.

If the ^{85m}Kr release database consists in hundreds of measurements in several operating conditions, assessment of ^{131}I release entails some difficulties. It is known

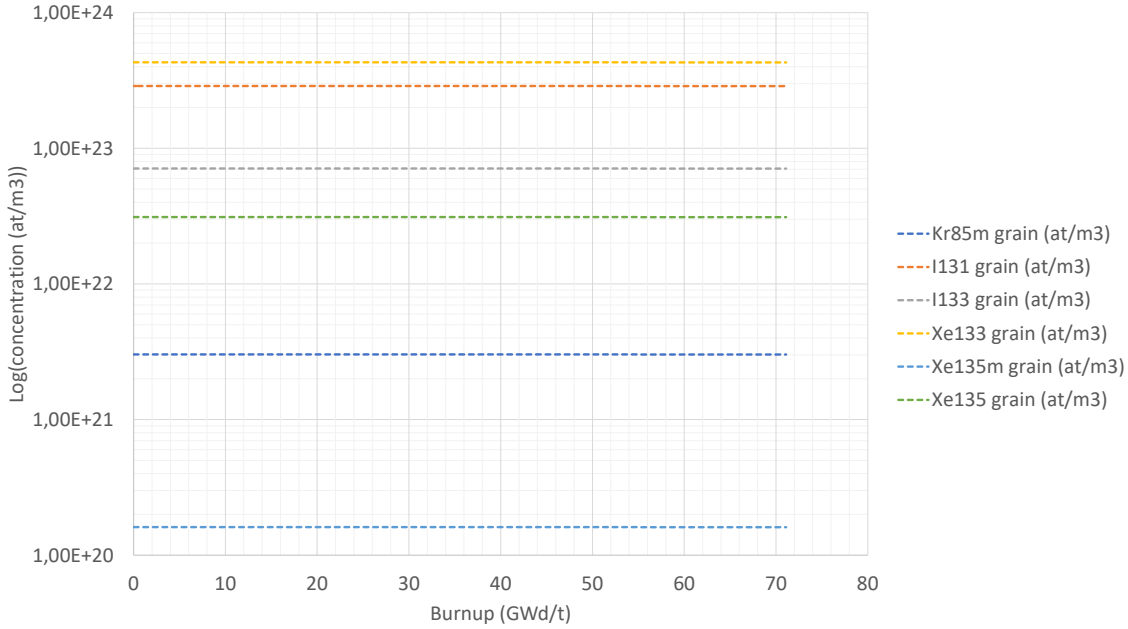

Figure 1.5. Analytic equilibrium concentrations computed according to ANS 5.4 methodology. It has been preferred a linear-logarithmic scale, for sake of clarity. Bubble interconnection happens at a burnup of about 55 GWd/t but the lowering effect is negligible.

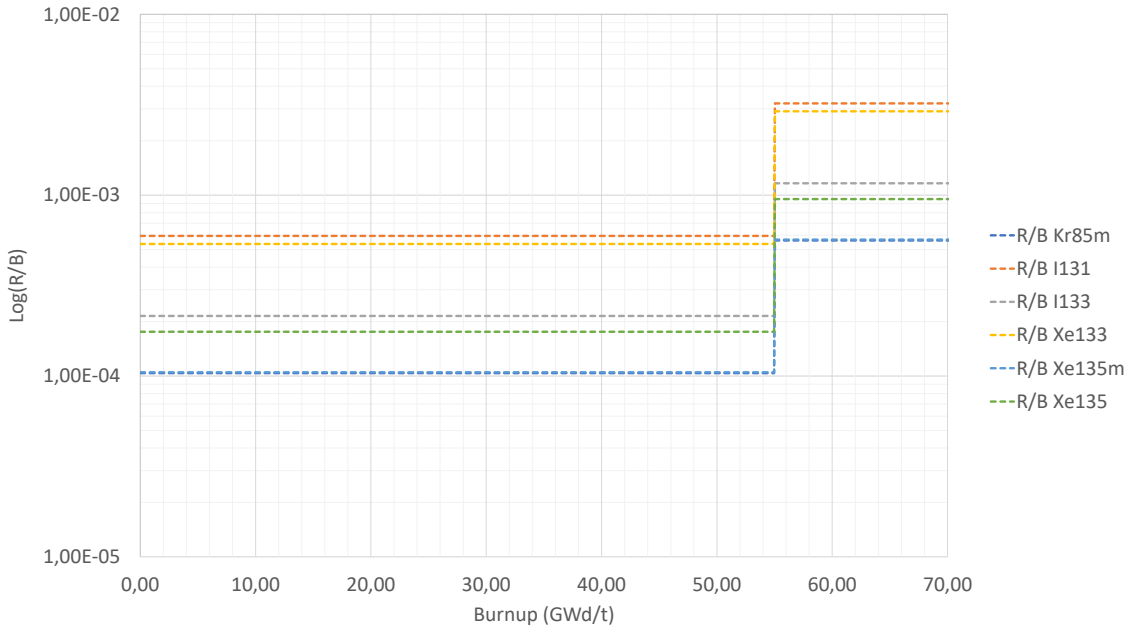

Figure 1.6. Analytic equilibrium release fractions computed according to ANS 5.4 methodology. It has been preferred a linear-logarithmic scale, for sake of clarity. Bubble interconnection happens at a burnup of about 55 GWd/t and the release fraction suddenly increase of factor approximately constant for all the isotopes.

that in standard conditions iodine is solid but it sublimates easily if heated. As a consequence iodine isotopes are not transported through the unheated gas flow lines to the gamma detector of the instrumentation. Iodine release measurements have been performed indirectly, thanks to detection of xenon daughter isotopes. Since the 99 % of the ^{131}I decay results in a stable Xe isotope, a total of 21 measurements have been obtained from the IFA considered. ANS 5.4 focused on the development of an accurate estimate of ^{131}I, because it is the radioactive isotope that provides the largest contribution to equivalent dose to individuals, due to its dose to the thyroid.

The ^{85m}Kr have been used to estimate the^{131}I release, by simply scaling the R/B [Turnbull and Beyer, 2009] or by applying the fractal mathematics [White, 2001]. Both of the approach proved inadequate to predict ^{131}I release from ^{85m}Kr release.

1.7 Closing remarks

ANS 5.4 methodology has been developed and validated with the purpose of evaluating the source term and gap activity of LWRs. The former is the fractional release of radioactive gaseous and volatile FPs, the latter is the inventory of radioactive isotopes that are released to the primary reactor system if the fuel rod cladding is breached. ANS 5.4 methodology is suitable to assess radiological consequences of postulated accidents that do not involve abrupt power transients, since it has been designed to fit reactor stationary conditions, although ANS 5.4 release predictions are often strongly conservative. Lastly, ANS 5.4 methodology does not consider the FPs transport after release from the fuel rod free volume towards the primary circuit, and neglect chemical interactions, such as significant fuel oxidation, that can substantially increase the release [Turnbull and Beyer, 2009].

In this chapter a review of the ANS 5.4 methodology has been carried out. The basic assumptions of the methodology deal with intra-granular behaviour of radioactive gaseous and volatile FPs and with grain-boundary bubble behaviour.

From the intra-granular point of view, the behaviour of a radioactive isotope which diffuses from grain interior towards grain boundary is ruled by a parabolic PDE for the isotope concentration. The counterbalance between isotope production rate, due to external irradiation, diffusion and decay phenomena physically gives rise to a transient evolution which becomes stationary after a certain equilibrium time. ANS 5.4 methodology exactly considers the latter regime, or secular equilibrium regime, to predict source term and gap activity.

Conversely, the intra-granular problem has been analytically solved for the integral average of the concentration, essential for obtaining the time-dependent expression of the fractional release, and it has been shown that, by taking advantage of the secular equilibrium hypothesis, fractional release coincides with ANS 5.4 equilibrium formula.

The mathematical proof of the ANS 5.4 equilibrium formula is of fundamental importance because it highlights the accuracy of the full derivation, being the PDE solution unique (Sec. A), and allows further and more accurate development of the problem. In particular, the next chapter is dedicated to the development and the implementation of an intra-granular solver able to describe concentration and release of radioactive gaseous and volatile FPs, in the same way obtained in this chapter and that, at equilibrium, coincide with ANS 5.4 results.

The grain-boundary description adopted by the ANS 5.4 methodology is based on an empirical correlation, the Vitanza threshold [Vitanza et al., 1979], modified at high burnup to fit better the Halden radioactive release data [Turnbull, 2001]. As many empirical correlations, the modified Vitanza threshold is easily implementable in a numerical code and requires scarce computational effort [Pizzocri et al., 2020]. On the other hand, it is not applicable during transient conditions, which well represent Severe Accidents (SAs), and it is limited by its validation database. In other words, it can deal only with commercial UO_2 fuel with rod burnup lower than 70 GWd/tU, fuel densities between 95 % and 98 % of theoretical density, grain sizes between 6 μm and 15 μm and open porosity between 0.1 % abd 0.3 % of theoretical density.

Chapter 2

Development and verification of improved numerical approach

Abstract The current ANS 5.4 methodology, described in the previous chapter, provides a methodology for the calculation of the fractional release of radioactive FPs of primary importance for the radiological risk analysis. It is usable during postulated accidents which do not involve sudden temperature transients and burst releases. In the previous pages, the intra-granular problem for the concentration of a radioactive isotope has been tackled from scratch. Starting from the Booth model, the ANS equilibrium fractional release formula has been derived, together with an expression for the average, equilibrium, intra-granular concentration of a radioactive isotope. The grain boundary behaviour has been described with a simple empirical correlation, the Vitanza threshold, function of fuel temperature and burnup. The limitations of the methodology, mainly its conservativeness and the asymptotic approach, have been instantiated. For this reasons, in the present chapter, the same intra-granular problem, considered by ANS model, is solved with an equivalent approach, which analytically takes advantage of the spectral decomposition of the concentration. This method have been integrated into an existing 0D meso-scale FPC through an intra-granular spectral solver, verified via MMS. The latter is a technique for developing a special type of analytical solution to be used for testing numerical algorithms, fundamental in Verification and Validation (V&V) framework, in order to assess the algorithm numerical consistency. The output of the new solver is the time-dependent average concentration, from which it is possible to evaluate the fractional release that, in stationary conditions, agrees with ANS 5.4 prediction. In addition, the opportunity to describe rapid transients is given. Through an example case, the intra-granular spectral model is verified against the ANS 5.4 predictions. Eventually, it is described the implementation of the coupled decay problem, neglected in ANS 5.4.

2.1 Introduction

In the following pages, the diffusion-decay intra-granular problem is solved in an alternative way, with respect to the ANS 5.4 methodology model (Sec. 1.4, [Turnbull and Beyer, 2009]). The basic assumptions are presented in Sec. 2.2. Essentially, they resemble those of ANS 5.4 methodology, with the exception of little modifications with reference to the intra-granular bubble behaviour [Speight, 1969, White and Tucker, 1983]. The leading advantage of the alternative solution lies in the spectral decomposition of the concentration, ideally

$$C(r,t) = \sum_{k=1}^{\infty} x_k(t)\psi_k(r)$$

where $x_k(t)$ is the k-th temporal coefficient, to be computed, and ψ_k is the known eigenfunction of the Laplace operator in spherical symmetry, the sinc function. By resorting this hypothesis, the radioactive diffusion problem (Eq. 1.10) is transformed from a single PDE to an infinite set of Ordinary Differential Equations (ODEs) (Sec. 2.3).

The consistency with ANS 5.4 methodology, first of all, is analytically proofed, because the same time-dependent formulas for the integral average of the concentration (Eq. 1.28) and release fraction (Eq. 1.18) are obtained, which at equilibrium regime reduce to

$$C_\infty = \frac{B}{\lambda} - \frac{3B}{\lambda\sqrt{\mu}}\left(\coth\sqrt{\mu} - \frac{1}{\sqrt{\mu}}\right)$$

$$\left(\frac{R}{B}\right)_\infty = \frac{3}{\sqrt{\mu}}\left(\coth\sqrt{\mu} - \frac{1}{\sqrt{\mu}}\right)$$

typical of ANS 5.4 model, where again $\mu = \lambda a^2/\alpha D$.

Another important advantage is that this model can be easily integrated in the 0D, meso-scale code SCIANTIX [Pizzocri et al., 2020], which is able to elaborate time-varying input and to compute lumped, time-depending quantities. The spatial discretization is naturally brought into the code thanks the spectral decomposition, while the time derivative is numerically discretized with the A-stable implicit Euler scheme [Quarteroni et al., 2006].

The verification of the implemented solver is carried via MMS (Sec. 2.4), a technique for developing a special type of analytical solution to be used for testing numerical algorithms, fundamental in Verification and Validation (V&V) framework, in order to assess the algorithm numerical consistency [Oberkampf et al., 2004].

The comparison with ANS 5.4 methodology results is provided in Sec. 2.5, where it has been considered a typical LWR in stationary conditions, for which the Vitanza threshold is satisfied. For a set of radioactive gaseous and volatile FPs the integral average of the concentration and the release fraction are compared to the respective equilibrium values, being the latter typical of ANS 5.4 model, and a short error analysis is carried out.

2.2 Intra-granular model assumptions

The intra-granular problem relies on the same basic assumptions listed previously in Sec. 1.2. Indeed, the identical equivalent sphere model [Booth, 1957] is the starting point for the problem setting. In summary, radioactive FPs are produced in the irradiated fuel grains, due to their low solubility they diffuse towards grain boundary where accumulate in inter-granular bubbles. The improved inter-granular description is the subject of the next chapter. Only two hypothesis of the intra-granular ANS 5.4 model are discussed:

1. Gas atoms produced in grains diffuse towards grain boundaries through repeated trapping in and irradiation-induced resolution from nanometre-size intra-granular gas bubbles [Speight, 1969, White and Tucker, 1983, Pastore et al., 2013].

2. The secular equilibrium hypothesis is not necessary. All the quantities maintain their temporal dependence.

In order to describe properly the isotopes behaviour, it is necessary to take into account that intra-granular gas can exist as in-solution or trapped gas. After a short period of irradiation, it is observed that the fuel grains become populated with small bubbles of radius $r \sim 1$ nm, which rapidly stabilizes in both size (R_{ig}) and number density (N_{ig}) [Turnbull, 1971, White and Tucker, 1983]. Bubbles behaviour is governed by three mechanisms:

1. Nucleation: bubbles are nucleated *homogeneously* as a consequence of the interactions between in-solution and re-solution gas atoms, and *heterogeneously* when the bubbles are created in the wake of energetic fission fragments [Olander and Wongsawaeng, 2006]. It is assumed that the predominant nucleation mechanism is the heterogeneous one [White and Tucker, 1983, Pizzocri et al., 2018].

2. Trapping: intra-granular bubbles act as fixed saturable traps which can absorb matrix gas [White and Tucker, 1983, Pizzocri et al., 2018].

3. Re-solution: energetic FPs can interact with trapped gas atoms, leading to the re-introduction of gas to the UO_2 matrix. Bubbles are destroyed mainly by thermal spike interactions [White and Tucker, 1983, Pizzocri et al., 2018, Setyawan et al., 2018].

Intra-granular bubbles are heterogeneously nucleated at a rate ν ($\text{bub}\,\text{m}^{-3}\,\text{s}^{-1}$)

$$\nu = 2\eta\dot{F} \tag{2.1}$$

The number of nucleated bubbles per fission fragment, η, from experimental observations [Turnbull, 1971, White and Tucker, 1983] has been estimated between 5 and 25. $\dot{F}$ is the fission rate and the factor 2 considers the number of fission fragments produced per fission.

Trapping and resolution

The diffusion process is influenced by the repeated intra-granular trapping in and irradiation-induced resolution from intra-granular bubbles [Speight, 1969, White and Tucker, 1983]. A part of gas atoms which reach the grain boundary is dissolved back to the interior of the grain due to irradiation processes, but the majority of the gas diffuses into grain-face bubbles.

A possible phenomenological model is the one outlined by Speight [Speight, 1969] who considered the diffusion of atoms from a spherical grain with a fixed number of saturable and immobile traps. The trapping rate, or absorption rate of dissolved gas into the traps, is g (s^{-1}) and the resolution, from the traps, rate is b (s^{-1}). They are calculated as [Ham, 1958, White and Tucker, 1983, Pizzocri et al., 2018]

$$g = 4\pi D N_{\text{ig}} R_{\text{ig}} \tag{2.2}$$

and

$$b = 2\pi (R_{\text{ig}} + Z_0)^2 l_f \dot{F} \tag{2.3}$$

where R_{ig} is the mean intra-granular bubbles radius, N_{ig} is the number density of the intra-granular bubbles, D is the single-atom diffusion coefficient, l_f is the mean length traveled by a fission fragment and Z_0 is the mean influence radius of a fission fragment.

The consequence of trapping and resolution phenomena is that C_s, in-solution gas concentration, may be lost by absorption at gas bubbles, becoming C_b, trapped gas concentration, or enhanced by the demolition of these bubbles. Simultaneously, decay process removes radioactive gas. The intra-granular gas behavior can be described by the following system of equations.

$$\begin{cases} \dfrac{\partial C_s}{\partial t} = \alpha D \nabla^2 C_s - \lambda C_s + b C_b - g C_s + S \\ \dfrac{\partial C_b}{\partial t} = g C_s - b C_b - \lambda C_b \end{cases} \tag{2.4}$$

If the total concentration is defined as $C = C_s + C_b$, with the quasi-stationary condition $\partial C_b / \partial t = 0$, and solving the problem for C, it is obtained

$$\frac{\partial C}{\partial t} = D_{\text{eff}} \nabla^2 C - \lambda C + S \tag{2.5}$$

With respect to the initial equation, the diffusion coefficient is multiplied by an equilibrium fraction, identifying the in-solution concentration, available to diffuse, $C_s = \frac{b+\lambda}{b+\lambda+g} C$ and, conversely, the trapped atoms concentration $C_b = \frac{g}{b+\lambda+g} C$.

In the end, the effective diffusion coefficient considered is

$$D_{\text{eff}} = \frac{b+\lambda}{b+\lambda+g} D \tag{2.6}$$

The situation is further complicated since trapping and resolution rates are not fixed quantities, they depend on time-varying variables: R_{ig} and N_{ig}. For the intra-granular bubbles, it is assumed that they are spherical, homogeneously distributed

and of equal size [Ham, 1958, White and Tucker, 1983]. Intra-granular bubble radius is calculated accordingly to [Olander and Wongsawaeng, 2006]

$$R_{\text{ig}} = \left(\frac{3\Omega m}{4\pi}\right)^{1/3} \tag{2.7}$$

where $\Omega = 4.4581 \times 10^{-29}$ m^3 is the Xenon covolume, m represents the number of trapped atoms per bubble and is given by

$$m = \frac{C_b}{N_{\text{ig}}} \tag{2.8}$$

The bubbles concentration is N_{ig} and obey to the following equation [Pizzocri et al., 2018]

$$\frac{\partial N_{\text{ig}}}{\partial t} = \nu - bN_{\text{ig}} \tag{2.9}$$

The previous evolutionary equation for N_{ig} is fundamental in the computation of the trapping rate g and the resolution rate b. It is anticipated here that the further developments are integrated in SCIANTIX, a 0D meso-scale code [Pizzocri et al., 2020] which is able to solve the equation for N_{ig} and to provide g and b.

Bubble mobility

In principle one should consider the mobility of intra-granular bubbles, in the effective diffusion theory just described. Indeed both in-solution and trapped gas atoms experience diffusional motion [Lösönen, 2000]. That means to contemplate an additional term of the form $D_b\nabla^2 C_b$. It happens that, up to now, the available diffusive models manage to describe the gas release due to both intra- and inter-granular release [Bernard et al., 2002] but do not describe the only intra-granular release [Verma et al., 2020]. Intra-granular bubbles are extremely small and numerous. Recent models, including the bubbles diffusion in a vacancy gradient and the Brownian motion, cannot explain the large fission gas release observed during out-of-pile experiments. For this reason, the simplifying assumption of fixed intra-granular bubbles has been made in this description.

2.3 Intra-granular spectral diffusion solver

The solution of Eq. 1.10 can be derived analytically by means of a spectral approach [Friskney and Speight, 1976]. The diffusion-decay well-posed problem is

$$\begin{cases} \dfrac{\partial C(r,t)}{\partial t} = \dfrac{\alpha D}{r^2}\dfrac{\partial}{\partial r}\left(r^2\dfrac{\partial C(r,t)}{\partial r}\right) - \lambda C(r,t) + B & \\ C(r,0) = C_0, & 0 < r < a \\ C(a,t) = 0, & t > 0 \\ \left.\dfrac{\partial C(r,t)}{\partial r}\right|_{r=0} = 0, & t > 0 \end{cases} \tag{2.10}$$

With respect to the system 1.10 a finite initial conditions has been introduced and the boundary condition in $r = 0$ has been modified into a symmetry boundary condition, consequence of the spherical symmetry of the problem. The change in the initial condition allows a more general treatment while the change in the boundary condition does not alter the solution. First of all, it is assumed that $C(r,t)$ can be decomposed in superposition of spatial modes and temporal coefficients [Pastore et al., 2018]

$$C(r,t) = \sum_{k=1}^{\infty} x_k(t)\psi_k(r) \tag{2.11}$$

where $\psi_k(r)$, the k-th spatial mode, is chosen as the eigenfunction of the radial part of the spherical Laplacian, satisfying both the Dirichlet boundary condition $C(0,t) = 0$ and the symmetry condition $\partial C/\partial r|_{r=0} = 0$, i.e. the normalized cardinal sine:

$$\psi_k(r) = \frac{1}{\sqrt{2\pi a}} \frac{\sin \theta_k r}{r} \tag{2.12}$$

The k-th eigenvalue is $-\theta_k^2$, the symmetry boundary condition requires that $\theta_k = k\pi/a$. The complete set of eigenfunctions benefit from the property of orthonormality with respect to the following scalar product

$$< \psi_m(r)|\psi_n(r) >= \int_0^a \psi_m(r)\psi_n(r)4\pi r^2 dr = \delta_{mn} \tag{2.13}$$

By substituting Eq. 2.11 into Eq. 2.10, and projecting it on the n-th spatial mode, the following ordinary differential equation is achieved

$$\begin{cases} \dfrac{\mathrm{d}x_n(t)}{\mathrm{d}t} =< \psi_n|B > - \left(\lambda + \alpha D \dfrac{\pi^2 n^2}{a^2}\right) x_n(t) \\ x_n(0) = g_n \end{cases} \tag{2.14}$$

The equation is now a simple decay problem with an external source. Time coefficients are evaluated with the Laplace transform

$$x_n(t) = \frac{< \psi_n|B >}{\lambda + \alpha D\pi^2 n^2/a^2} \left(1 - e^{-\left(\lambda + \alpha D\pi^2 n^2/a^2\right)t}\right) + g_n e^{-\left(\lambda + \alpha D\pi^2 n^2/a^2\right)t} \tag{2.15}$$

where

$$< \psi_n|B >= -B\sqrt{\frac{8}{\pi}} \frac{(-1)^n}{n} \sqrt{a^3} \tag{2.16}$$

and

$$x_k(0) = g_k =< \psi_k|C_0 > \tag{2.17}$$

Let's put $\Lambda_n = \lambda + \alpha D\pi^2 n^2/a^2$, as an effective decay rate of the problem.

$$C(r,t) = \sum_{k=1}^{\infty} \psi_k \frac{< \psi_k|B >}{\Lambda_k} \left(1 - e^{-\Lambda_k t}\right) + \sum_{k=1}^{\infty} \psi_k g_k e^{-\Lambda_k t} \tag{2.18}$$

The numerical implementation reveals that the solution is equivalent to the one obtained with the Fourier decomposition, for a sufficient number of modes considered.

Again, let's compute the spatial average of the concentration. Due to the spectral decomposition, it results that

$$\bar{C}(t) = \frac{3}{4\pi a^3}\int_0^a C(r,t)4\pi r^2 dr = \frac{3}{4\pi a^3}\sum_{k=1}^{\infty} x_k(t) < \psi_k|1 > \tag{2.19}$$

by substituting Eq. 2.18 into the integral average

$$\bar{C}(t) = \frac{6B}{\pi^2}\sum_{k=1}^{\infty}\frac{1}{k^2\Lambda_k}\left(1 - e^{-\Lambda_k t}\right) + \frac{6C_0}{\pi^2}\sum_{k=1}^{\infty}\frac{1}{k^2}e^{-\Lambda_k t} \tag{2.20}$$

The release rate is computed thanks to Eq. 1.17

$$R = \frac{3B}{\sqrt{\mu}}\left(\coth\sqrt{\mu} - \frac{1}{\sqrt{\mu}}\right) - \frac{6B}{\pi^2}\sum_{n=1}^{\infty}\frac{e^{-(n^2\pi^2/\mu+1)\tau}}{n^2+\mu/\pi^2} + \frac{6C_0\lambda}{\mu}\sum_{k=1}^{\infty}e^{-(n^2\pi^2/\mu+1)\tau} \tag{2.21}$$

If the initial concentration is $C_0 = 0$ the fractional release is correctly identical to Eq. 1.18. From the point of view of the temporal dependence, the two approaches are perfectly equivalent.

$$\frac{R}{B} = \frac{3}{\sqrt{\mu}}\left(\coth\sqrt{\mu} - \frac{1}{\sqrt{\mu}}\right) - \frac{6}{\pi^2}\sum_{n=1}^{\infty}\frac{e^{-(n^2\pi^2/\mu+1)\tau}}{n^2+\mu/\pi^2}$$

While, if $B = 0$ but C_0 is finite, it exists a contribution in the fractional release, expressed as $R/\lambda C_0$.

$$\frac{R}{\lambda C_0} = \frac{6}{\mu}\sum_{k=1}^{\infty}e^{-(n^2\pi^2/\mu+1)\tau} \tag{2.22}$$

The fractional release due to the initial concentration $R/\lambda C_0$ represents the fraction of gas atoms released from the spherical grain due to diffusion minus decay loss. This contribute lasts until the characteristic time of the diffusion $T_e = 5/(\lambda(1+1/\mu))$. It is possible to consider the equilibrium concentration, at finished transient

$$C_\infty = \frac{6B}{\pi^2}\sum_{k=1}^{\infty}\frac{1}{k^2(\lambda + \alpha D\pi^2 k^2/a^2)} \tag{2.23}$$

which yields the following result

$$C_\infty = \frac{B}{\lambda} - \frac{3B}{\lambda\sqrt{\mu}}\left(\coth\sqrt{\mu} - \frac{1}{\sqrt{\mu}}\right) \tag{2.24}$$

The equilibrium fractional release, the ones used by ANS 5.4, is exactly

$$\left(\frac{R}{B}\right)_\infty = 1 - \frac{\lambda}{B}C_\infty = \frac{3}{\sqrt{\mu}}\left(\coth\sqrt{\mu} - \frac{1}{\sqrt{\mu}}\right) \tag{2.25}$$

To test the consistence of the spectral decomposition, the same case of the ^{135m}Xe (Sec. 1.3) is briefly repeated. Since the expression for $\bar{C}(t)$ and R/B are identical to the ones of the previous example, only the solution $C(r,t)$, is shown in Fig.2.1 to observe the equivalence of the spectral decomposition.

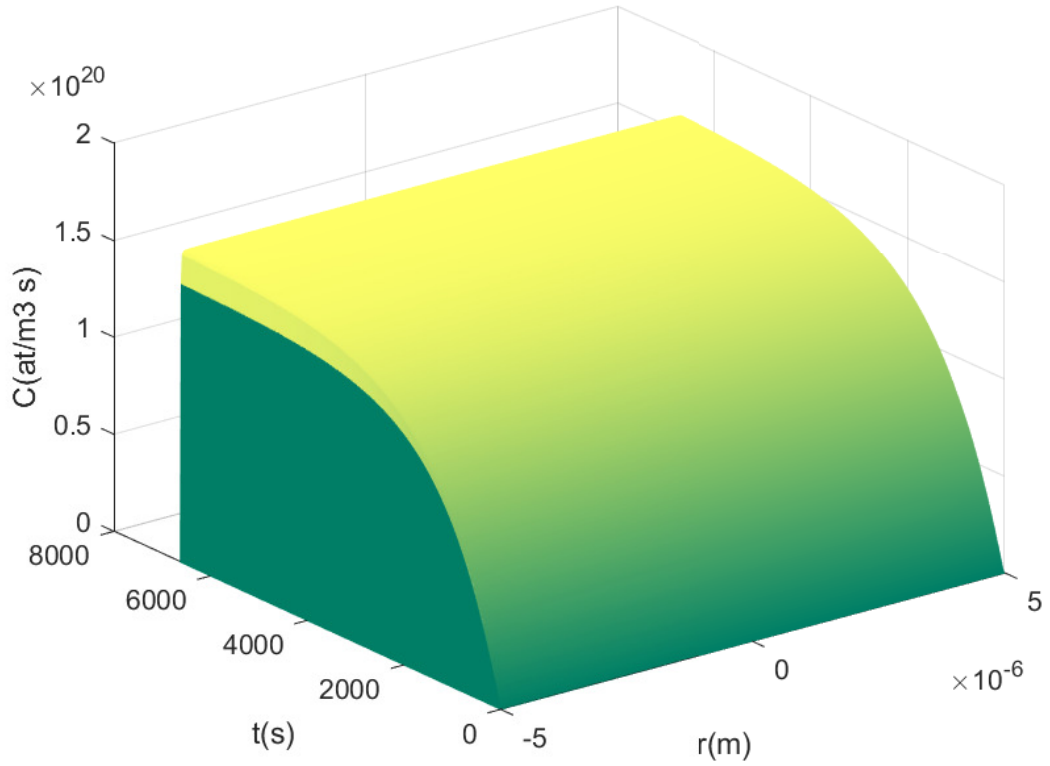

Figure 2.1. 3D plot of the concentration $C(r,t)$ obtained with spectral decomposition.

In summary, the intra-granular model which describes the behaviour of the radionuclide concentration is represented by Eq. (2.10).

$$\frac{\partial C}{\partial t} = \alpha D \nabla^2 C - \lambda C + B \tag{2.26}$$

By making the *ansatz* that the concentration can be approximated as a linear combination of spatial modes, known, and time coefficients, unknown

$$C(r,t) \approx \sum_{k=1}^{K} x_k(t)\psi_k(r) \tag{2.27}$$

we transform the problem in the determination of a set of K ordinary differential equations for the time coefficients

$$\frac{\mathrm{d}x_k}{\mathrm{d}t} = B_k - \Lambda_k x_k \tag{2.28}$$

Where $B_k =< B|\psi_k >$ and $\Lambda_k = \lambda + \alpha D\pi^2 k^2/a^2$. When the set of coefficient $x_k(t)$ has been determined, it is possible to reconstruct both the concentration $C(r,t)$ and the average $\bar{C}(t)$, given by

$$\bar{C}(t) \approx \frac{3}{4\pi a^3} \sum_{k=1}^{K} x_k \psi_k \tag{2.29}$$

The presented methodology is easy to be implemented in a numerical code. Indeed the intra-granular spectral solver has been integrated in the meso-scale code SCIANTIX [Pizzocri et al., 2020], a 0D stand-alone computer code designed at Politecnico di Milano. Currently SCIANTIX covers the description of intra- and inter-granular inert gas behaviour in UO_2. The 0D approach means that the output of the code consists in a time-dependent local computation of the quantities of interest, e.g. the isotope released concentration or the local intra- and inter-granular swelling. For the radioactive fission products, it simply means that the output of the code is the concentration $\bar{C}$, averaged on the the whole spherical grain.

The choice of such code is a key factor. The available length-scale fuel performance codes, such as TRANSURANUS [Lassmann, 1992], are thermo-mechanical codes which simulate the behaviour of s nuclear fuel rod at the macro-scale, where mechanisms like mechanical interactions or temperature rises are fundamental for the component failure. To work properly, fuel performance codes require dedicated meso-scale codes. SCIANTIX occupies this position and a valid model for the radioactive fission gas release allows evaluation of the radiological risk tied to a potential radioactive release.

Without entering the over-detailed description of the SCIANTIX code, it is worth mentioning that, up to now, the code solves a set of time-dependent ordinary differential equations with the implicit, absolutely stable, first order implicit Euler scheme [Quarteroni et al., 2006]. The input of the code is the collection of temperature, fission rate and hydrostatic stress at several time instants. The time domain $t \in (0, T)$ is divided in a sequence of discrete time instants $t_0, t_1, \ldots, t_N$ and N identical sub-intervals $t_{n+1} - t_n = h$. Each equation for x_k is solved by applying

$$x_k^{n+1} = \frac{x_k^n + B_k h}{1 + \Lambda_k h} \tag{2.30}$$

The initial value for each mode $x_k(0)$ is known. This method provides the average, 0D, concentration of a certain number of isotopes

$$\bar{C}_i(t) = \frac{3}{4\pi a^3} \sum_{k=1}^{K} x_k \psi_k \tag{2.31}$$

where the subscript i virtually stands for the i-th isotope.

It has been discussed that the current ANS 5.4 approach does not solve numerically the intra-granular diffusion-decay problem. Instead it considers the asymptotic value, in the secular equilibrium hypothesis, not of the concentration C_∞ but of the fractional release $(R/B)_\infty$

$$\left(\frac{R}{B}\right)_\infty = \frac{3}{\sqrt{\mu}} \left(\coth \sqrt{\mu} - \frac{1}{\sqrt{\mu}} \right) \tag{2.32}$$

with $\mu = \lambda a^2 / \alpha D$. Moreover it has been previously shown that, through the equilibrium concentration C_∞, it is possible to obtain the ANS 5.4 fractional release, namely

$$\left(\frac{R}{B}\right)_\infty = 1 - \frac{\lambda}{B} C_\infty \tag{2.33}$$

In the end, the advantages of the time-dependent solution are the followings

- The solution of the intra-granular problem pursued with a spectral decomposition of the spatial dependence is easy to be implemented in a numerical code.

- The SCIANTIX code is able to elaborate both stationary and time-varying input.
- In steady-state conditions, i.e. the only situation in which ANS 5.4 is applicable, the solution, in terms of fractional release, coincides with the ANS formula.
- For time-varying input, the output is an average, local value for the radionuclide concentration which continuously depends on the input data.

2.4 Solver verification via Method of Manufactured Solution

One of the improvement with respect to the ANS 5.4 methodology is the implementation of a numerical algorithm capable of describing the transient behaviour of the radionuclides. The spectral approach is preferred for a numerical implementation in a meso-scale code which already solves equations with a implicit Euler discretization of the time derivative. Mainly because the the diffusion-decay equation is lead to decay equation, easy to solve implicitly at order 1. In addition, a meso-scale code performs a lumped computation, then Eq.(1.28) acts as output quantity.

The diffusion-decay problem is implemented in SCIANTIX, a meso-scale fuel performance code [Pizzocri et al., 2020]. From a computational point of view, Verification and Validation (V&V) of a numerical code is of primary importance, within a reliability framework [Oberkampf et al., 2004]. The numerical algorithm verification affects the numerical consistency and the efficiency of the code. It lies upon the comparison between a highly accurate solution, if available, and the computational one. There is a hierarchy of confidence in highly accurate solutions. When the analytical solution is not available, it is possible to develop a special type of analytical solution to be used as benchmark. The Method of Manufactured Solutions (MMS) is a technique for developing a special type of analytical solution to be used for testing numerical algorithms. Briefly, it is structured as follows.

1. A specific solution is assumed to satisfy the PDE of interest.
2. The solution is replaced in the PDE and the equation is rearranged such that a forcing source term appears.
3. The PDE is numerically solved with the forcing source term and the two solutions are compared.

Let's suppose that a solution of the form $C(r,t) = R(r)T(t)$, which satisfies Eq. (1.10). Boundary conditions for $R(r)$ are $R(a) = 0$ and $R'(0) = 0$, while the initial condition is modeled by $T(0) = 0$. The problem becomes

$$RT' = B_M - \lambda_M RT + D_M T \nabla^2 R \tag{2.34}$$

where the subscript M stands for Manufactured. Indeed the manufactured source is written as

$$B_M = R(\lambda_M T - T') - D_M \nabla^2 R \tag{2.35}$$

If $a = 1$, $D_M = 1$ and $R = 15/6(1 - r^2)$, then $\nabla^2 R = -15$. The manufactured decay rate is chosen as $\lambda_M = -T'/T$, so that $B_M = 15 D_M T = 15T$. A possible expression for T is $T = \sin(t)e^t t$. The numerical solution, evaluated by the code with an implicit time scheme of order 1, has to be compared to the manufactured average concentration

$$C_M = 3 \int_0^1 r^2 (RT) dr = T \tag{2.36}$$

By defining the error between the manufactured average concentration $C_M(t_k)$ and the computational solution $C_N(t_k)$, at time t_k and with a constant time step Δt, as

$$e(\Delta t) = |C_M(t_k) - C_N(t_k)| \tag{2.37}$$

the numerical solution C_N converges to the exact manufactured solution C_M, with order p if

$$e(\Delta t) < C \Delta t^p \tag{2.38}$$

To give an estimate of p, two numerical solutions are computed, respectively with time step Δt and $2\Delta t$. S

Since roughly $e(\Delta t) \approx \Delta t^p$

$$\frac{2e(\Delta t)}{e(2\Delta t)} = 2^{1-p} \tag{2.39}$$

and an estimate of p may be given by

$$p = 1 - \log_2 \left(\frac{2e(\Delta t)}{e(2\Delta t)} \right) \tag{2.40}$$

The MMS is carried from $t = 0$ to $t = 1$. In Fig. 2.2 the manufactured average solution C_M and the numerical solutions C_N, computed with a time step one the double of the other, are shown. It is worth noting that the numerical solution less accurate is the one obtained with the double time step $2\Delta t$. In Fig. 2.3 the estimate of the convergence order p of the method is shown. As expected, it asymptotically approaches to one, since the time derivative is discretized with implicit Euler method of order one.

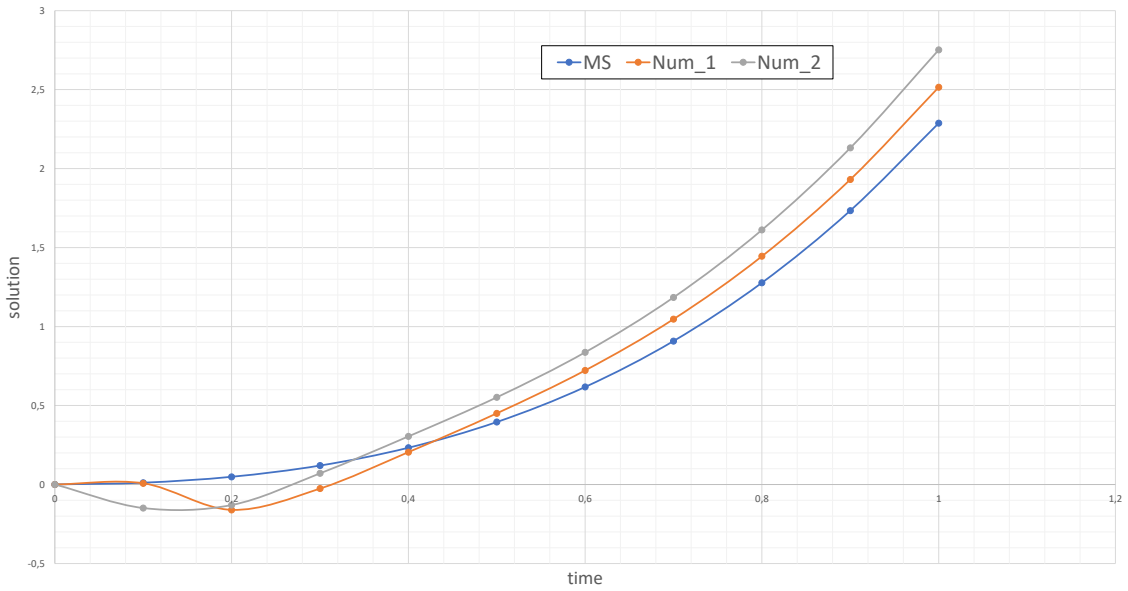

Figure 2.2. Comparison between the manufactured solution and the computational solutions at different time steps.

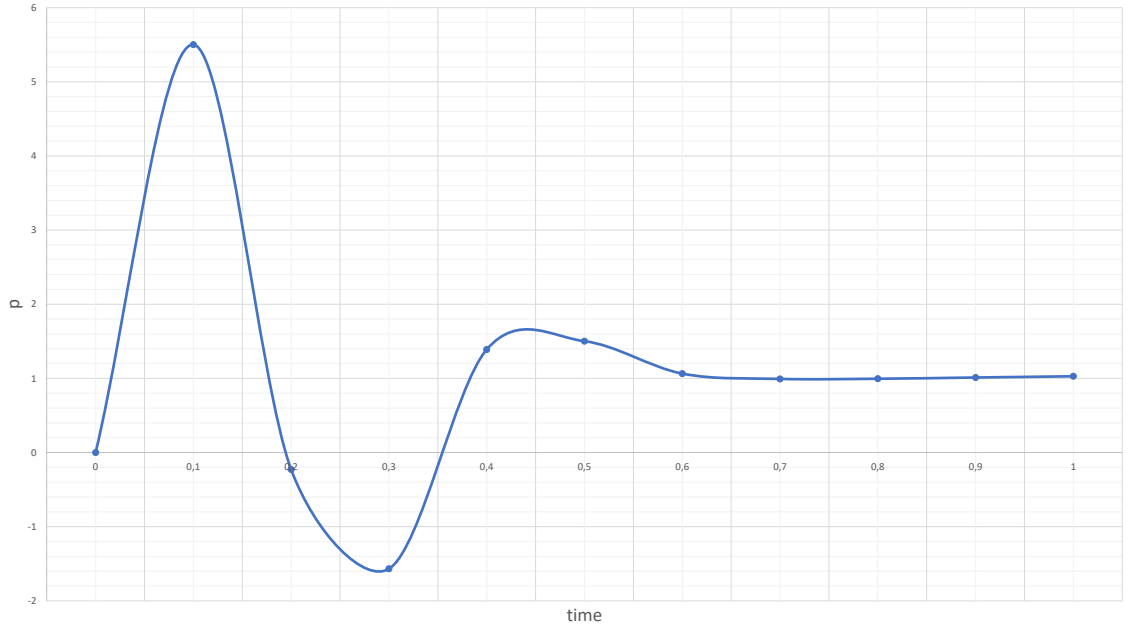

Figure 2.3. Behaviour of the estimated order of convergence p. Despite the initial oscillations, the method shows an order of convergence equal to one. As expected since it depends on the implicit Euler discretization.

2.5 Comparison with ANS 5.4 results

Now that the intra-granular problem has been analyzed, it is instructive to test whether, in stationary conditions, the results coincide with the ANS 5.4 predictions. For sake of simplicity, it is repeated the example already stated in Sec. 1.5 of a LWR working in stationary conditions for four years and a half (approximately 60000 h) at a fission rate $\dot{F} = 1 \times 10^{19}$ fiss m^{-3} s^{-1} and at a temperature $T = 1000$ K. The radioactive gaseous and volatile FPs of interest are ^{85m}Kr, ^{131}I, ^{133}I, ^{133}Xe, ^{135m}Xe, ^{135}Xe. They belong to the short-lived FPs category and are kept decoupled, i.e. the matrix $\overline{\overline{\Lambda}}$ is diagonal. Their equilibrium release fractions has been already evaluated prior and after bubble interconnection (Tab. 1.2), according to ANS 5.4 methodology (Sec. 1.3, Eq. 1.19).

In order to get the temporal evolution of fuel burnup and the integral average of the listed isotopes, in the operative conditions mentioned above, a lumped simulation have been performed with the meso-scale code SCIANTIX [Pizzocri et al., 2020]. The intra-granular spectral solver considers the superposition of the first $K = 1000$ modes, in order to be sufficiently accurate. Indeed, the implemented spectral solver returns the integral average of the concentration (Eq. (2.20)), approximated to a finite number K of modes

$$\bar{C}(t) \approx C^K = \frac{6B}{\pi^2} \sum_{k=1}^{K} \frac{1}{k^2 \Lambda_k} \left(1 - e^{-\Lambda_k t}\right) + \frac{6C_0}{\pi^2} \sum_{k=1}^{K} \frac{1}{k^2} e^{-\Lambda_k t} \tag{2.41}$$

where $\Lambda_k = \lambda + \alpha D \pi^2 k^2 / a^2$. Note that for the example described, $C_0 = 0$, that means to consider fresh fuel condition and that, roughly speaking, the error can be estimated to be proportional to K^{-2}.

In the current SCIANTIX version it has been added the option to resort to Vitanza threshold, namely to modify the grain radius $a = \frac{3}{S/V}$ during the simulation. According to the Vitanza threshold, the bubble interconnection happens after 30920 hours of steady-state functioning, when $\beta \approx 55$ GWd/tU.

Firstly, SCIANTIX computes the integral average concentration C^K of the several FPs and the result is compared to the analytic equilibrium values C_∞. Secondly, the equilibrium release fraction is evaluated from C^K and compared to the analytic equilibrium value $(R/B)^K_\infty = 1 - \lambda C^K_\infty / B$, where C^K_∞ represent the equilibrium value of C^K (Fig. 2.4)

The plot of the C^K for the complete set of FPs considered is shown in Fig. 2.5. The ANS 5.4 equilibrium results C_∞ appear as dashed lines, SCIANTIX ones C^K as solid lines. It has been preferred a semi-logarithmic plot, with logarithmic scale on the x-axis and linear scale on the y-axis, for sake of clarity. Indeed the transient phase of all the isotopes is not greater then 2000 h, it is much shorter than the simulated time (60000 h) and a linear-linear scale is not suitable to graphically notice the transient phase. Similarly, the bubble interconnection effect is little noticeable. In Sec. 1.5 it has been justified that the relative variation on the equilibrium concentration is of the order of magnitude of 10^{-3} (Eq. 1.43) while the respective variation of the equilibrium release fraction is of the order of magnitude of the unity (Eq. 1.42). For this reason, the bubble interconnection effect mainly affects the release fraction than the concentration.

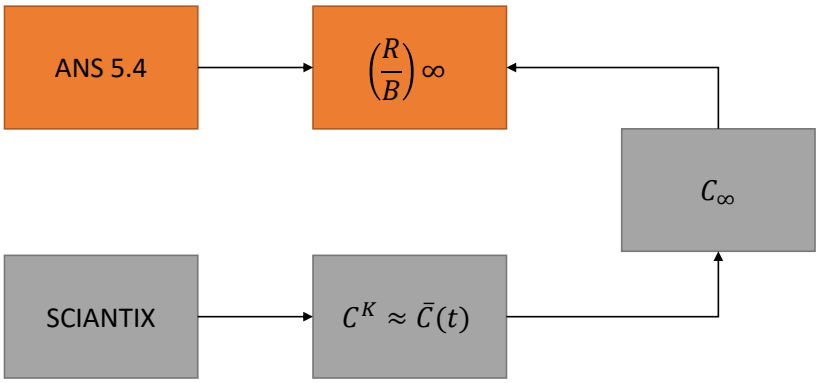

Figure 2.4. The comparison with ANS 5.4 results is carried out following the steps highlighted in the picture. SCIANTIX numerical results are used to obtain the analytic results of ANS 5.4 methodology.

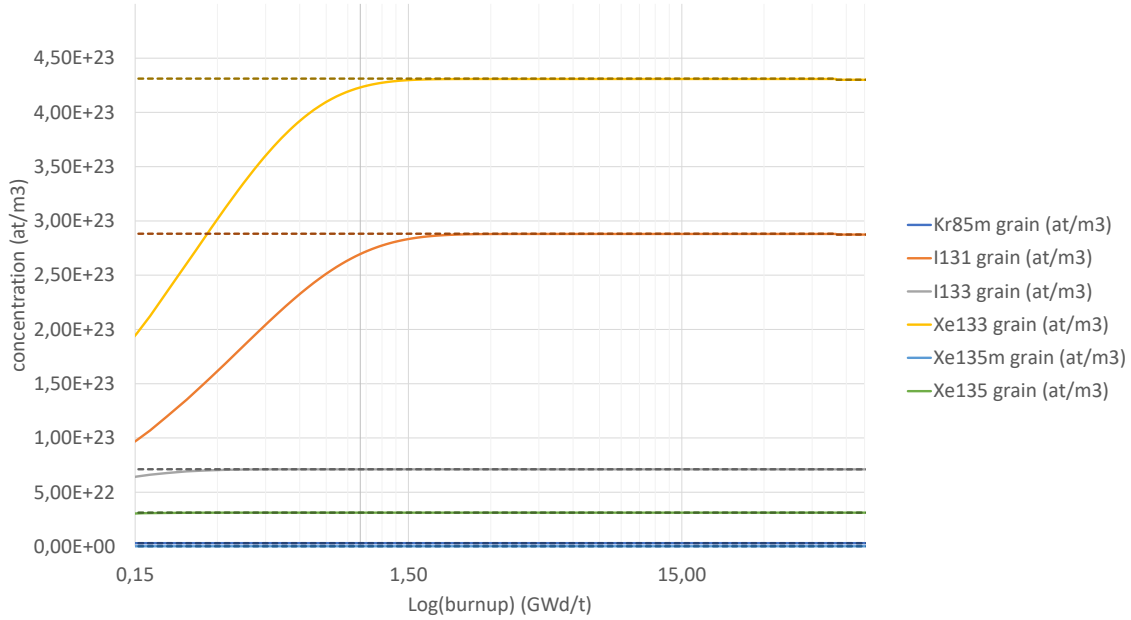

Figure 2.5. Integral average of the concentrations computed by SCIANTIX. The dashed lines represent the analytic equilibrium values that are reached at the end of the transient phase, represented with solid lines. It has been preferred a logarithmic-linear scale, for sake of clarity. The bubble interconnection effect is little noticeable since it scarcely affects the intra-granular concentration.

To notice the concentration drop after the bubble interconnection, an enlargement of the ^{133}Xe has been provided in Fig. 2.6, where it is more evident that the integral average concentration computed with SCIANTIX, C^K, reaches the the correct analytic asymptotic values C_∞ by committing a small relative error u_C, briefly discussed at the end of this section.

Roughly speaking, the bubble interconnection, or grain-boundary saturation, represents the onset of the gaseous and volatile FPs release [White and Tucker,

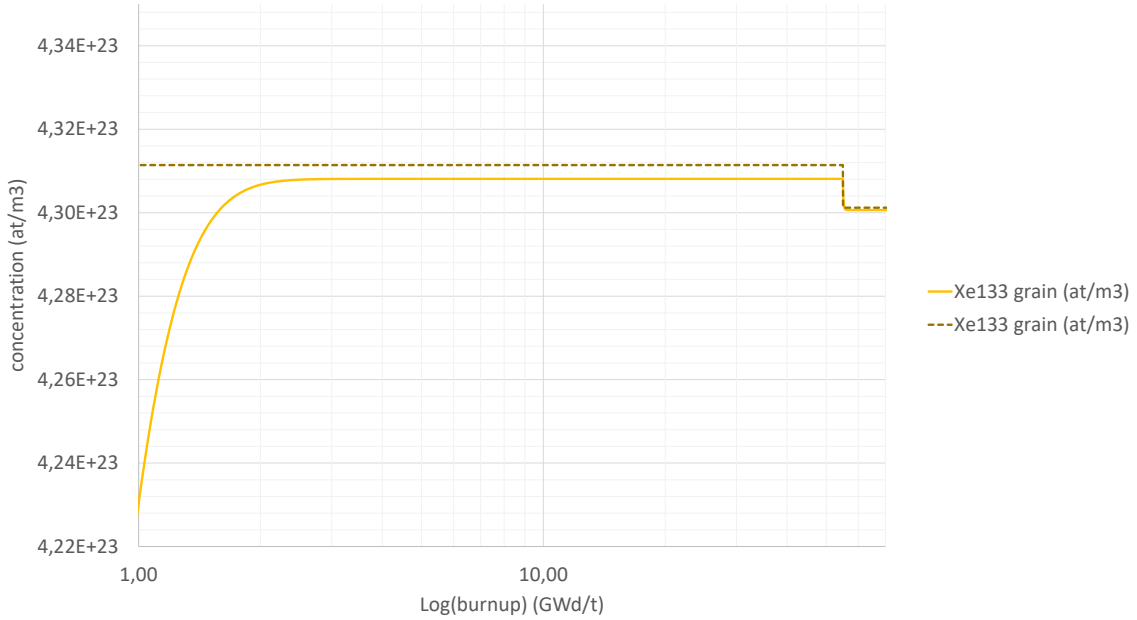

Figure 2.6. Enlargement of the ^{133}Xe intra-granular behaviour. The integral average of the concentration computed with SCIANTIX (solid line) correctly starts from zero and approaches to its equilibrium value (dashed line). In addition, it is able to follow the variation imposed by the Vitanza threshold by committing a small relative error.

1983, White, 2004, Pastore et al., 2013]. Similarly, within the model employed by ANS 5.4 methodology, the equilibrium release fraction increases at the threshold, as an effect of the increment of the surface-to-volume ratio (Sec. 1.4) to the detriment of the decrease of the intra-granular concentration.

Coherently with the outlined procedure (Fig. 2.4), it is possible to obtain, from C^K, the numerical equilibrium release fraction $(R/B)^K_\infty$. Anyway, one must pay attention to a misleading feature. In Sec. 1.3 the exact relation (Eqs. 1.31) between instantaneous release fraction and integral average of the concentration has been derived

$$\frac{R}{B} = 1 - \frac{\lambda \bar{C}(t)}{B} - \frac{6}{\pi^2} \sum_{k=1}^{\infty} \frac{e^{-(1+n^2\pi^2/\mu)\lambda t}}{n^2}$$

while SCIANTIX allows the computation of an inaccurate instantaneous release fraction $(R/B)^K$

$$\left(\frac{R}{B}\right)^K = 1 - \frac{\lambda C^K}{B} \tag{2.42}$$

which, due to the lack of the summation term, gives back accurate[1] results only if the exponential functions are null, i.e. at equilibrium regime

$$\left(\frac{R}{B}\right)^K_\infty = 1 - \frac{\lambda C^K_\infty}{B} \tag{2.43}$$

[1]The error with respect to the analytic formula decreases as K increases, i.e. if the modal superposition is carried out with an adequate number of modes.

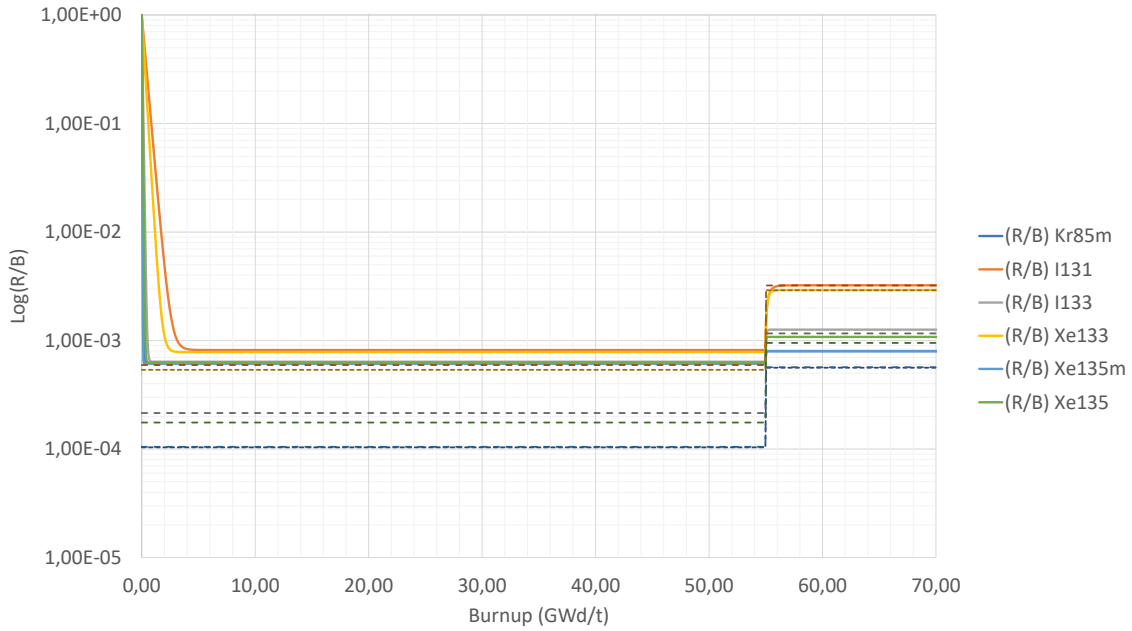

Figure 2.7. The solid lines represent the instantaneous release fractions computed through SCIANTIX and the dashed lines represent the analytic ANS 5.4 solutions. It has been preferred a logarithmic-linear scale, for sake of clarity. The relative error between the two quantities is significant but it decreases after bubble interconnection.

This is noticeable in Fig. 2.7, where the quantity $(R/B)^K = 1-\lambda C^K B$ has been plotted for the several isotopes of interest (solid line), and, though it starts from 1 instead of 0, it reaches the equilibrium value (dashed line) by committing a determined relative error. The relative error between $(R/B)^K_\infty$ and $(R/B)_\infty$ is predictably higher with respect to the relative error for the equilibrium integral average of the concentration. It is remarkable that the relative error between $(R/B)^K_\infty$ and $(R/B)_\infty$ decreases after the bubble interconnection, i.e. with increasing surface-to-volume ratio.

To notice the behaviour of the relative error between $(R/B)^K_\infty$ and $(R/B)_\infty$, before and after bubble interconnection, an enlargement of the ^{85m}Kr and ^{131}I cases have been provided in Fig. 2.8. The dashed lines represent the analytic ANS 5.4 solution for the equilibrium release fraction, namely the Vitanza threshold effect, while the solid lines represent the numerical solution obtained with SCIANTIX simulations. As noted before, the relative error between predicted and numerical values decreases after interconnection.

It is possible to obtain a relation between the dimensionless parameter $\mu = \lambda a^2/\alpha D$, which characterizes the diffusion-decay problem, and the relative error about the equilibrium integral average of the concentration and the release fraction. Let's define the relative errors u_C and $u_{R/B}$ as

$$u_C = \frac{C^K_\infty}{C_\infty} - 1, \quad u_{R/B} = \frac{(R/B)^K_\infty}{(R/B)_\infty} - 1 \tag{2.44}$$

such as

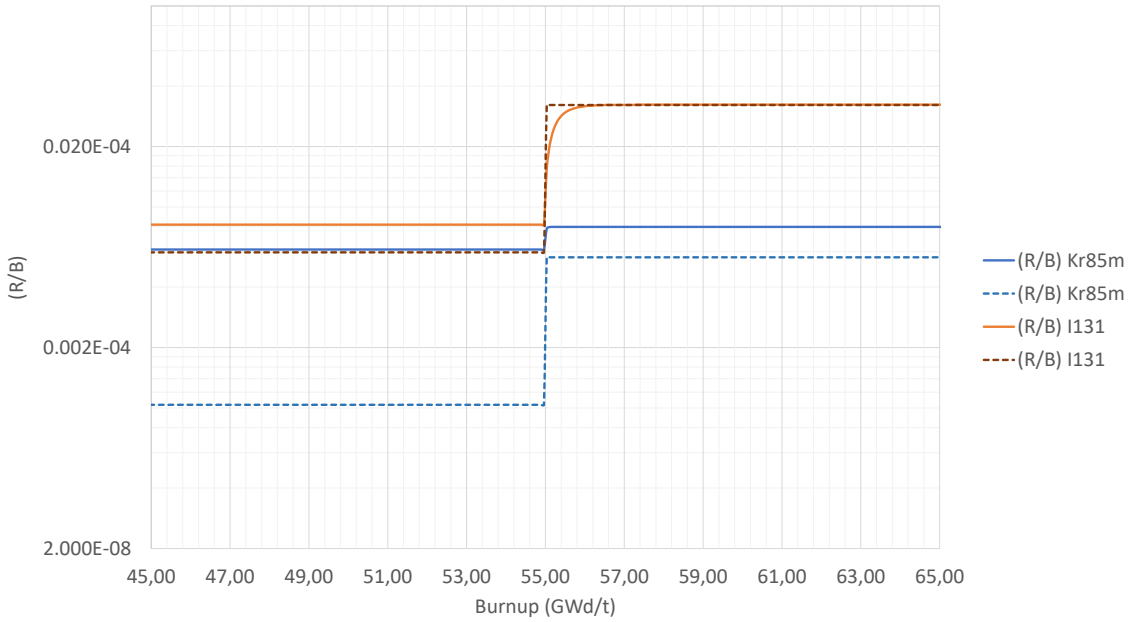

Figure 2.8. Enlargement of Fig. 2.7 for ^{85m}Kr and $_{131}$I. The solid lines represent the instantaneous release fractions computed through SCIANTIX and the dashed lines represent the analytic ANS 5.4 solutions. It has been preferred a logarithmic-linear scale, for sake of clarity. The relative error between the two quantities is significant before interconnection and it decreases after the latter phenomenon.

- $u_C > 0$, $u_{R/B} > 0$: the numerical equilibrium result overestimate the analytic equilibrium one.
- $u_C < 0$, $u_{R/B} < 0$: the numerical equilibrium result underestimate the analytic equilibrium one.

Since for the case of interest $(R/B)_\infty < 0.02$, and conversely, $\lambda C_\infty/B > 0.98$, the following approximation holds (Eq. 1.21)

$$C_\infty \approx \frac{B}{\lambda}\left(1 - \frac{3}{\sqrt{\mu}}\right), \quad \left(\frac{R}{B}\right)_\infty \approx \frac{3}{\sqrt{\mu}}, \tag{2.45}$$

therefore a first-order approximation gives back

$$u_{R/B} \approx (R/B)^K_\infty \frac{\sqrt{\mu}}{3} - 1, \quad u_C \approx -u_{R/B}\frac{3}{\sqrt{\mu}} \tag{2.46}$$

In Tab. (2.1) there have been compared the numerical outputs of SCIANTX simulation, the parameter $\mu = \lambda a^2/\alpha D$ for the considered isotopes and the relative errors (Eq. 2.46. One can make some observations exploiting the fact that the diffusion coefficient αD of the several FPs is similar (Tab. 1.1).

- At equilibrium regime, low-μ radioactive isotopes are characterized by a high C_∞ value. Since it is possible to read μ as a dimensionless decay rate λ, a low-μ regime corresponds to a low decay rate which physically keeps the number of available atoms elevated.

Table 2.1. Numerical results and relative uncertainties.

Nuclide	$\mu = \lambda a^2/\alpha D$	C_∞^K (at m^{-3})	$u_C \approx u_{R/B}3/\sqrt{\mu}$	R/B_∞^K	$u_{R/B} \approx 1-(R/B)_\infty^K\sqrt{\mu}/3$
Before interconnection	$S/V = 3/a = 120$ cm^{-1}				
^{85m}Kr	8.36×10^8	3.0284×10^{21}	-5.110×10^{-4}	6.147×10^{-4}	4.926
^{131}I	2.54×10^7	2.8814×10^{23}	-2.228×10^{-4}	8.175×10^{-4}	0.374
^{133}I	1.95×10^8	7.1121×10^{22}	-4.230×10^{-4}	6.377×10^{-4}	1.968
^{133}Xe	3.12×10^7	4.3104×10^{23}	-2.449×10^{-4}	7.819×10^{-4}	0.455
^{135m}Xe	8.19×10^8	1.6149×10^{20}	-5.101×10^{-4}	6.149×10^{-4}	4.864
^{135}Xe	2.92×10^8	3.1160×10^{22}	-4.523×10^{-4}	6.278×10^{-4}	2.576
After interconnection	$S/V = 3/a = 650$ cm^{-1}				
^{85m}Kr	2.85×10^7	3.0278×10^{21}	-2.349×10^{-4}	7.968×10^{-4}	0.418
^{131}I	8.67×10^5	2.8745×10^{23}	-3.793×10^{-4}	3.226×10^{-3}	0.001
^{133}I	6.65×10^6	7.1077×10^{22}	-9.516×10^{-4}	1.259×10^{-3}	0.082
^{133}Xe	1.06×10^6	4.3011×10^{23}	-8.986×10^{-6}	2.919×10^{-3}	0.003
^{135m}Xe	2.79×10^7	1.6146×10^{20}	-2.325×10^{-4}	8.005×10^{-4}	0.410
^{135}Xe	9.95×10^6	3.1146×10^{22}	-1.283×10^{-4}	1.079×10^{-3}	0.135

- Similarly, low-μ radioactive isotopes are characterized by a high $(R/B)_\infty$ value. Together with the previous argument, one can say that the diffusion coefficient intensifies the release and $\mu \propto D^{-1}$.
- It can be verified that $(R/B)_\infty^K \propto \sqrt{\mu} \propto \sqrt{\lambda}$, a well-known result of the intra-granular diffusion theory [Friskney and Turnbull, 1979].

2.6 Closing remarks

Among the basic assumptions of the ANS 5.4 methodology, the secular equilibrium hypothesis justifies the use of the equilibrium fractional release. In this chapter the ANS 5.4 intra-granular diffusion-decay problem for a radioactive isotope is newly solved with a different approach, based on the spectral decomposition of the concentration. The latter approach is proofed to be consistent with ANS 5.4 methodology.

It is developed an intra-granular spectral solver that provides a time-dependent solution of the problem. The spectral solver is implemented in SCIANTIX, a 0D meso-scale FPC, and the algorithm is verified via MMS. The output of the code is the integral average of the concentration, introduced during the ANS 5.4 review (Sec. 1.3).

With respect to ANS 5.4,SCIANTIX is able to manage sudden temperature variations, representative of SA conditions. The spectral solver provides the time-depending behaviour of the integral average concentration. From the latter quantity, it is possible to obtain the ANS 5.4 equilibrium fractional release. Therefore, the intra-granular spectral solver developed in this chapter is a valid alternative with respect to ANS 5.4 methodology.

In conclusion, the spectral solver offers the possibility to be coupled with a physics-based description of the grain-boundary phenomena. The inter-granular bubble behaviour and the coupling, in SCIANTIX, with the developed spectral solver are the object of the next chapter.

Chapter 3

Development and validation of physics-based model

Abstract The ANS 5.4 methodology provides the determination of the radioactive FPs release from oxide fuels, in assessing radiological consequences of accidents that do not involve sudden temperature variations. In the methodology, the description of the grain-boundary physics has been substituted with an empirical correlation between fuel burnup and temperature, namely the Vitanza threshold. The phenomenon which is modeled through the Vitanza threshold is the inter-granular bubble interconnection and subsequent FPs release.

It is known that, in the irradiated uranium dioxide, grain boundaries are populated with micron-size inter-granular bubbles. These bubble are able to accommodate the intra-granular FPs produced that have diffuse from the grain interior through the grain boundary. The mechanistic description of this phenomenon takes into account that these over-pressurized bubbles tend to return to their equilibrium state by vacancy absorption. Inter-granular bubble average area grows until coalescence phenomenon creates a network which, if connects the pellet surface with its bulk, causes the FPs to be released outside of the pellet.

Such physics-based description of inter-granular bubbles interconnection and grain-boundary saturation is a valid approach to model the onset of radioactive FPs release. The model available in the meso-scale code SCIANTIX has been coupled the intra-granular spectral solver previously developed. In particular, the Inert Gas Behaviour (IGB) routines, has been extended to radioactive gaseous and volatile ones, by assuming that the latter concentration are not determining in grain-boundary saturation phenomena.

Eventually the complete intra- and inter-granular solver for radioactive gaseous and volatile FPs has been validated against VERCORS experimental tests, representative of LOCA conditions. The results obtained confirm that the developed solver predicts FPs fractional release at the end of the transient with a relative error lower than 1%. In addition, the solver provide a conservative description of the release kinetics throughout the transient.

3.1 Introduction

The inter-granular bubble behaviour lies on the hypotheses described in Sec. 3.2. The development of the model (Sec. 3.3) starts from bubble growth, due to gas atoms and vacancies absorption, which brings them in a non-equilibrium state. Consequently bubbles size increases, coalescence takes place and, at grain-boundary saturation, interconnection occurs [White and Tucker, 1983, White, 2004, Pastore et al., 2013]. The period of time until interconnection is identified as incubation period, where the release is negligible [White et al., 2006]. When grain-boundary saturation is achieved, instant release is assumed to begin [Bernard et al., 2002].

The model implementation in SCIANTIX (Sec. 3.4), of inter-granular FPs concentrations, is based on a mass conservation law among produced, intra-granular, decayed, inter-granular and released isotopes. This approach provide a new definition of fractional release, suitable to use in transient conditions.

The validation of the model is carried out against the results of VERCORS experimental tests (Sec. 3.5). Eventually, the model predictions area also discussed in comparison to ANS 5.4 methodology results.

3.2 Model assumptions

It is known, from Scanning Electron Microscope (SEM) observations of fractured irradiated UO_2 pellet, that the grain boundaries are populated by micron-size bubbles. These bubbles evolve throughout irradiation period, under the effects of fission rate, temperature, FPs and vacancies absorption. Fission Gas (FG) and FPs are retained on the grain boundaries and the onset of their release is delayed until inter-granular bubble interconnection takes place [Vitanza et al., 1979, White and Tucker, 1983].

The inter-granular description considered in ANS 5.4 methodology is based on an empirical correlation between fuel temperature and burnup, the Vitanza threshold [Vitanza et al., 1979], summarized as follows (Sec. 1.4). According to the fuel burnup β, a threshold temperature for bubble interconnection T_{IC} is established as

$$T_{\mathrm{IC}} = \frac{9800}{\ln(176\beta)} \ ^{\circ}\mathrm{C} \qquad \beta < 18.2 \text{ GWd/tU}$$
$$T_{\mathrm{IC}} = 1434 - 12.85\beta \ ^{\circ}\mathrm{C} \qquad \beta \geq 18.2 \text{ GWd/tU}$$

The surface-to-volume ratio $S/V = 3/a$ varies depending on

$$\left(\frac{S}{V}\right) = 120 \text{ cm}^{-1} \quad T < T_{\mathrm{IC}}$$
$$\left(\frac{S}{V}\right) = 650 \text{ cm}^{-1} \quad T \geq T_{\mathrm{IC}}$$

and the equilibrium fractional release $(R/B)_\infty$ increases as soon as bubble interconnection occurs. Indeed, for the equilibrium fractional release of ANS 5.4, it holds that (Eq. 1.19)

$$\left(\frac{R}{B}\right)_\infty \approx \frac{S}{V}\sqrt{\frac{\alpha D}{\lambda}}$$

With respect to the ANS 5.4 methodology, it is possible to describe the mechanical state of the inter-granular bubbles relying on earlier models [Speight and Beeré, 1975, White and Tucker, 1983, White, 2004, Veshchunov, 2008, Pastore et al., 2013] that analyzed the mechanisms of interest for the next developments.

The majority of produced intra-granular FPs diffuses along the concentration gradient towards the grain boundaries[1], where it is absorbed by inter-granular bubbles. The internal pressure of these bubbles increases and a non-equilibrium state is achieved. Over-pressurized bubbles tend to absorb vacancies beyond gas atoms, growing in size until coalescence and inter-connection take place [White and Tucker, 1983, Pastore et al., 2013]. When the saturation threshold is reached, instant release is assumed to begin. Gas is brought from the grain boundaries to the fuel rod free volume, neglecting all the mechanisms that bring the FPs from grain boundary to the fuel rod void, like tunnel formation, percolation, grain faces diffusion, etc. The neglected phenomena does not considerably affect the amount of released isotopes but only the kinetics aspects [Bernard et al., 2002]. This argument holds both for stable FG and radioactive FPs, taking into account that the number of radioactive FPs decreases throughout the whole process.

For a suitable description of inter-granular bubble growth and coalescence phenomena, the following hypotheses are made:

- Grain-edges (the region where three grains meet) phenomena are neglected [Kogai, 1997].
- It is considered an initial number density of inter-granular bubbles N_{gf} and further nucleation is neglected (one-off nucleation) [White, 2004].
- It is assumed that the absorption rate of inter-granular gas is equal to the arrival rate of gas at grain boundaries [White, 2004].
- The inter-granular bubble population shares the same size and lenticular shape of circular projection, at any instant. In other words, a uniform, average bubble size A_{gf} is considered [Veshchunov, 2008].
- The flux of gas that is dissolved back from grain boundary to grain interior, by irradiation induced-resolution, is negligible [Rest, 2003].
- Bubble growth relates the coalescence rate together with the increase rate of the average inter-granular projected area on the grain boundary, A_{gf} [White, 2004].

In this development both radioactive and stable gas atoms must be considered. it is assumed that the phenomena of inter-granular bubble growth and coalescence, which depend on the number of gas atoms absorbed, are mainly driven by stable FG. This argument is reasonable if one considers that

- Fission gases, such as xenon and krypton stable isotopes, constitute the primary product of fission reactions, with a fission yield $y \approx 0.3$ [Olander, 1976].

[1] The diffusion of radioactive isotopes from the grain interior towards the grain boundaries includes the repeated trapping in and irradiation-induced resolution from intra-granular bubbles, hinted in Sec. 2.2 and neglected in ANS 5.4 methodology.

- Radioactive gaseous and volatile FPs of interest, mainly short-lived FPs, are characterized by lower cumulative thermal fission yields. Of about one or two orders of magnitude lower than the previous one ([IAEA, 2020], Tab. 1.1)

In conclusion, it is assumed that radioactive gaseous and volatile FPs are negligible in determining inter-granular bubble interconnection and release.

3.3 Inter-granular bubble behaviour

A physics-based description of the inter-granular bubble mechanical interactions requires the computation of their number density N_{gf} and average size A_{gf}. To sum up, inter-granular bubble behaviour is considered as the outcome of the following processes [Pastore et al., 2013]

1. Bubbles growth, as a consequence of the absorption of fission gas atoms and vacancies.

2. Coalescence, namely the reciprocal interaction between bubbles, that leads to the formation of larger (and fewer) bubbles.

3. Interconnection of coalesced bubbles, between the fuel interior and its surface, and subsequent instant release of isotopes towards the fuel rod plenum.

Bubble growth

Grain-face bubbles absorb fission gas atoms that have diffused from grain interior. It is here assumed that gas retention capability of grain boundary is mainly a consequence of these bubbles [White, 2004]. Mechanical equilibrium between the pressure of the gas atoms in the bubbles and the bubble capillarity is required. The latter term is the Laplace pressure which, for a sphere, reads $p = 2\gamma/R_{\text{gf}}$, with γ surface tension of the bubble and R_{gf} curvature radius. Mechanical equilibrium pressure is given by [Pastore et al., 2013]

$$p_{eq} = \frac{2\gamma}{R_{\text{gf}}} - \sigma_h \tag{3.1}$$

σ_h is the hydrostatic stress, negative if the medium is under compression.

Since pressure is an energy density, γ is the energy specific to the surface existing between gas atoms and UO_2. It differs from the UO_2/UO_2 interface value. This result influences the geometrical form of the lenticular bubbles, setting the semi-dihedral angle $\theta \approx 50°$.

Absorption of vacancies has been proofed [Speight, 1969] to be the cause of grain boundary bubbles growth and shrinkage. Vacancy absorption/emission rate is given by

$$\frac{\mathrm{d}\, n_v}{\mathrm{d}\, t} = \frac{2\pi D_v \delta_g}{k_B T S}(p - p_{eq}) \tag{3.2}$$

where S is calculated as

$$S = \frac{-((3 - F_c)(1 - F_c) + 2\ln F_c)}{4} \tag{3.3}$$

The previous parameters are D_v, vacancy diffusion coefficient, δ_g, thickness of the diffusion layer at grain boundary, k_B, Boltzmann constant, T, absolute temperature, F_c, fractional coverage. The latter represents the fraction of grain boundary covered by bubbles and its value determine the onset for gas release. From the rate equation for the vacancy number, n_v is used to determine bubble evolution. The pressure p of a Van der Waal's gas in a bubble is

$$p = \frac{kTn_g}{\Omega n_v} \tag{3.4}$$

where Ω is the vacancy volume in a grain-face bubble n_g is the number of gas atoms within the grain, that generate the bubble pressure and influences the growth rate. The volume of a bubble is calculated as

$$V = n_g\omega + n_v\Omega \tag{3.5}$$

with ω gas atom volume. Since the volume of a lenticular pore with semi-dihedral angle θ is given by

$$V = \frac{4\pi R_{\mathrm{gf}}^3}{3}\frac{f(\theta)}{\sin^3\theta} \tag{3.6}$$

with $f(\theta) = 1 - 1.5\cos\theta + 0.5\cos^3\theta$, the curvature radius of a lenticular bubble of circular projection is

$$R_{\mathrm{gf}} = \left(\frac{3V}{4\pi f(\theta)}\right)^{1/3} \tag{3.7}$$

Bubble coalescence

The coalescence process is a mechanism that reduces the number of grain-face bubbles and increases their average projected size. Bubbles increase by the absorption of vacancies and gas atoms and can intersect among themselves. For equal circular bubbles in a regular square lattice, the loss rate due to bubble growth is [White, 2004, Veshchunov, 2008]

$$\frac{\mathrm{d}\,N_{\mathrm{gf}}}{\mathrm{d}\,A_{\mathrm{gf}}} = -2N_{\mathrm{gf}}^2 \tag{3.8}$$

Preceding equation yields

$$N_{\mathrm{gf}} = \frac{N_0}{1 + 2N_0(A_{\mathrm{gf}} - A_0)} \tag{3.9}$$

where N_0 and A_0 are the initial conditions of the problem and the projected area of the inter-granular bubble is $A_{\mathrm{gf}} = \pi(R_{\mathrm{gf}}\sin\theta)^2$.

Bubble interconnection

Fission gas release, from grain face bubbles to fuel rod free volume, is a consequence of the grain-boundary saturation [Bernard et al., 2002, Pastore et al., 2013]. The fraction of grain boundary surface covered with bubbles is equal to $F_c = N_{\mathrm{gf}}A_{\mathrm{gf}}$. When the coverage reaches the saturation value $F_{\mathrm{c,sat}} = 0.5$ [Veshchunov, 2008] a fraction of gas within grain face bubbles is released, to compensate for further bubbles growth and maintain $\mathrm{d}\,F_c/\,\mathrm{d}\,t = 0$.

3.4 Numerical approach

Now that the intra-granular model has been developed, numerically implemented and verified (Sec. 2.3), and the grain-boundary physics has been explained, it is possible to integrate them in SCIANTIX. For every isotope, the following concentrations are defined

1. The produced isotope concentration P ($\mathrm{at\,m^{-3}}$) obeys to

$$\frac{\partial P}{\partial t} = y\dot{F} \tag{3.10}$$

   where y is the fission yield of the considered element.

2. The intra-granular isotope concentration C ($\mathrm{at\,m^{-3}}$) is described by

$$\frac{\partial C}{\partial t} = \alpha D_{\mathrm{eff}} \nabla^2 C - \lambda C + y\dot{F} \tag{3.11}$$

   D_{eff} takes into account trapping and resolution mechanisms (Eq. 2.6) and C is divided between an in-solution fraction C_s and an in-bubble fraction C_b, such that $C = C_s + C_b$.

3. The decayed isotope concentration L ($\mathrm{at\,m^{-3}}$) is described by

$$\frac{\partial L}{\partial t} = \lambda P - \lambda L \tag{3.12}$$

As it has been already sketched, SCIANTIX employs the backward Euler method to discretize the time-derivative. If the time domain $t \in (0, T)$ is divided in a sequence of discrete time instants $t_0, t_1, \ldots, t_N$ and N identical sub-intervals $t_{n+1} - t_n = \Delta t$, then

1. The production term is discretized as

$$P_n = P_{n-1} + y\dot{F}\Delta t \tag{3.13}$$

2. The integral average of the intra-granular concentration $\bar{C}(t)$, at every time-step, is given by the application of the spectral solver (Sec. 2.3).

3. The decayed isotope concentration L is given by

$$L_n = \frac{L_{n-1} + \lambda P_{n-1}\Delta t}{1 + \lambda \Delta t} \tag{3.14}$$

If the grain-boundary saturation is not achieved, i.e. $F_c = N_{\mathrm{gf}} A_{\mathrm{gf}} < F_{\mathrm{c,sat}}$, the following mass balance must be always satisfied, at every time step

$$U = P - C - L \tag{3.15}$$

It has been introduced the isotope concentration in the inter-granular bubbles U ($\mathrm{at\,m^{-3}}$). When the grain-boundary saturation occurs, the released isotope concentration X ($\mathrm{at\,m^{-3}}$) is introduced through the following equation

$$X = P - C - L - U \tag{3.16}$$

The computation of X is a consequence of the constraint on the fractional coverage

$$\frac{\mathrm{d}\, F_c}{\mathrm{d}\, t} = 0 \tag{3.17}$$

that holds as soon as the grain boundary saturation takes place. Indeed, the progressive variation of N_{gf} and A_{gf} would result in $F_c > 0.5$, while keeping $\mathrm{d}\, F_c / \mathrm{d}\, t = 0$ (after interconnection) gives rise to a reduction of U, that causes an increase of X.

The exploited balance represents a simplified behaviour of the intra- and inter-granular radioactive isotopes. The isotopes are uniformly produced within all the spherical grain (P), where the distribution is modified by the decay (L) and diffusive (C) processes. Eventually, the isotopes that flow out of the grain are collected in U and X, depending whether the saturation has occurred.

A similar algorithm was exploited in SCIANTIX for IGB routines. These regarded only the behaviour of stable Kr and Xe isotopes, the two most important inert gases studied in the irradiated UO_2 analysis. As stated previously, it is assumed that the grain-boundary saturation is mainly determined by the inert gases and that radioactive gaseous and volatile FPs of interest, mainly short-lived FPs, are negligible in mass. As a consequence, it has been possible to extend the grain-boundary saturation routine to the evaluation of radioactive release. This approximate description has been tested against experimental results.

The comparison of the model results with the measured fractional releases is based on the definition of a suitable fractional release for all the isotopes considered. The time-dependent fractional release can be defined as

$$\frac{R}{B} = \frac{X}{P - C - L} = \frac{X}{X + U} \tag{3.18}$$

This definition can be taken as valid since the denominator represents the fraction of produced isotopes that are available to be released. Indeed, intra-granular isotopes C during out-of-pile tests are assumed to become all trapped in intra-granular bubbles. The only contribution in the fractional release is provided by the gas at grain boundary U, which produces the increase of X.

3.5 Validation against experimental data

The new model for intra- and inter-granular radioactive isotopes behaviour has been fully implemented in SCIANTIX [Pizzocri et al., 2020], a 0D meso-scale FPC. SCIANTIX receives as input temperature history, fission rate, fuel hydrostatic stress and fabrication data, then performs a 0D simulation of the fuel behaviour. This update version of the code has been employed for a comparison phase against the experimental results of fractional release available from the VERCORS irradiation programme [Ducros et al., 2001, Ducros et al., 2013]. The comparison of the predicted fractional releases with the experimental results is crucial to assess the accuracy of the model, and ultimately to evaluate the consequences of a severe accident, e.g. a LOCA, in terms of radioactivity released [Pontillon et al., 2005].

Experimental database

VERCORS experimental programme includes a set of tests aimed at the determination of the radioactive release from irradiated fuel rod samples, of about 30 g, under conditions representative of a Pressurized Water Reactor (PWR) severe accident. The programme counts 17 experiments performed on sections of different fuel rods. The fuel samples were obtained from PWR rods, from which three pellets in their original cladding were used. In addition, the majority of the samples were re-irradiated for seven days at low linear power ($\sim$ 15 W/cm) [Pontillon et al., 2005] in a Material Testing Reactor (MTR), to rebuild the inventory of short-lived FPs, at a detectable level by gamma spectrometers. The father rods were taken from EDF's power reactors and the tests provided experimental data of interest on the fractional release of FPs and actinides from uranium dioxide.

After the fuel samples has been prepared, re-irradiated, and that the inventory of all FP has been measured, the experimental sequence was carried out in the high-activity cell at the Laboratory for Active Materials (LAMA), typically 2 or 3 days after the re-irradiation. An induction furnace heated the fuel according to a particular temperature history. The key parameters common to the different tests are the high temperature plateau and its duration, the temperature ramps, the sample initial burnup, the gaseous atmosphere (steam and/or hydrogen) of the furnace and its flow rate.

VERCORS was composed of 17 tests conducted over 14 years, from 1989 to 2002, in accordance with 3 experimental phases [Ducros et al., 2013]

VERCORS 1 - 6 The first series of tests has been conducted between 1989 and 1994, with UO_2 fuel in high temperature room. The plateau maximum temperature reached in VERCORS 1 and VERCORS 2 experiments was about 2100 K, from VERCORS 3 onward it was of about 2600 K. The plateau temperature applied to the fuel sample is an important parameter. With increasing temperature the amount of FPs released, during the plateau, increases and fuel degradation phenomena are observed. In addition, VERCORS 6 was the first test leading to early fuel collapse and partial liquid corium formation [Ducros et al., 2001].

VERCORS HT (High Temperature) The second series, conducted between 1996 and 2002, consisted in three experiments aiming to study FPs transport in the

PWR primary system and potential chemical interactions. Mixed Oxides (MOX) and UO_2 were subjected to temperature up to 2900 K or even higher, up to 3138 K, the UO_2 melting point.

VERCORS RT (Release of Transuranic) The last series, conducted alternatively to the HT configuration, included eight tests mainly focused on the release of low volatile FPs and transuranium elements.

The experimental results provided by VERCORS tests were used to assess the reference source terms for all French PWRs and to validate the semi-empirical or physics-based models concerning stable FPs release and transport. It was observed the total release of volatile species, Cs, I, Te and Sb, and the release of low volatile species. Only the gaseous and volatile species that do not chemically interact are representative for the current comparison. For example, among the chosen isotopes, Te interacts with Sn contained in the Zircaloy cladding and then it may be retained in the cladding [Pontillon and Ducros, 2010a], as it is observed in VERCORS 4 and 5.

Not all the VERCORS tests have been considered suitable to the comparison with the model developed. Only a few tests, involving UO_2 fuel and for which temperature history was available, have been chosen, namely VERCORS 4 [Pontillon and Ducros, 2010a], VERCORS 5 [Ducros et al., 2013], VERCORS 6 [Ducros et al., 2001], VERCORS RT1 [Ducros et al., 2013], VERCORS RT3 [Ducros et al., 2013], VERCORS RT6 [Ducros et al., 2013]. Similarly, it has been possible to compare the results for ^{85}Kr, ^{132}Te, ^{131}I, ^{133}I, ^{133}Xe, ^{134}Cs and ^{137}Cs. In Tab. 3.1 there have been reported the available fuel data, the measurements of fractional releases at the end of the test and the respective numerical results. Before describing the comparison between VERCORS measurements and SCIANTIX results, the radioactive isotopes traced throughout the simulations are briefly summarized and detailed.

Gaseous FG (Xe, Kr) Krypton and xenon isotopes belong to the category of the fission gases. The radiological impact of these isotopes range from the short term (half-life of about 5.24 days), for ^{133}Xe, to the long term (half-life of about 10.71 years) for ^{85}Kr.

Volatile FPs (Te, I, Cs) With respect to the radiological consequences of a severe accident in a LWR, iodine and caesium are two volatile FPs of fundamental importance. ^{131}I are ^{133}I are short-lived FP with half-life respectively of about 8 days and 20.8 hours. Their radiological impact is substantial in the first few days following a SA and becomes negligible after 1 month[2]. ^{134}Cs and ^{137}Cs are long-lived FPs, with half-life respectively of about 2 and 30 years, then, in case of SA, their radiological impact stretches over several years. The radioactive short-lived $_{132}$Te, which decays into ^{132}I, has a half-life of about 3 days and its radiological impact exhaust in less then 1 month.

The behaviour of the isotopes of interest detected during VERCORS tests is in line with the current knowledge of release mechanisms [Pontillon et al., 2010, Pontillon and Ducros, 2010a] under temperature transient conditions and it is useful to highlight some key aspects.

[2]In addition, iodine produces the 15% of the decay heat of the core 1 day after an emergency shutdown [Ducros et al., 2013].

- For temperatures lower than 1200 °C and for high burn-up fuel it is known that release is largely due to the gas retained at the grain boundaries and accumulated at this level throughout the base-irradiation.
- For temperatures lower than 1000 °C the release is activated by the micro-cracking of the grain boundaries.
- For temperatures between 1000 °C and 1200 °C the release is activated by interconnection of inter-granular bubbles
- For temperatures higher than 1200 °C the release is activated by thermal diffusion of the remaining intra- and inter-granular gases.

During VERCORS 4 and 5 tests the release of xenon, was not complete, thus suggesting a partial trapping of the gas atoms in bubbles still contained in the fuel grains. It can be stated that the release depends both on the final temperature of the test and on the high temperature plateau duration [Pontillon and Ducros, 2010a]. In addition, from VERCORS 6 onward, the release of iodine and caesium was almost complete, despite a low fraction of caesium retained in the corium. This was attributed to the formation of uranate, zirconate or oxides, not considered in the SCIANTIX model. Generally the global release of iodine and caesium was homogeneous under SA conditions. It depended very little on the test conditions if a sufficiently high temperature was attained, more or less higher than 2300 °C [Ducros et al., 2013].

Calculations

The simulation of the selected VERCORS tests has been carried out in SCIANTIX, coherently with the details of the base irradiation histories, re-irradiation details and fuel fabrication data provided in scientific literature [Ducros et al., 2001,Pontillon et al., 2005, Ducros et al., 2013]. In addition, it has been assumed that the release of FPs during the base-irradiation is negligible, consistently with experimental observation [White et al., 2006]. A single VERCORS test simulation consisted of three different steps

1. **Base-irradiation**. Base-irradiation lasts until burnup indicated in Tab. 3.1 is attained. Fission rate and temperature have been estimated from the available details about the PWR indicated in 3.1, $\dot{F} = 2.7 \times 10^{18}$ fiss m^{-3} s^{-1} and $T =$ 1000 K. During the base irradiation FG, long-lived FPs and short-lived FPs are produced. Inter-granular bubbles evolve, according to the behaviour previously hinted (Sec. 3.3) and the fractional coverage F_c slowly increases.
2. **Storage**. It seemed reasonable that between the in-pile phase and the re-irradiation phase, it exists a period of time of fuel storage, where the radioactive short-lived FPs decay. The existence of this phase also justifies the need of the next re-irradiation phase, since it is the period in which the inventory of short-lived FPs decay. In addition, during storage simulation long-lived FPs (^{85}Kr, ^{134}Cs and ^{137}Cs) slowly continue to decay.

Table 3.1. Test conditions and summary of the fractional releases at the end of the tests [Ducros et al., 2013].

	VERCORS 4	VERCORS 5	VERCORS 6	VERCORS RT1	VERCORS RT3	VERCORS RT6
PWR irradiation	Bugey	Bugey	Grave lines	Grave lines	BR3	Grave lines
Fuel burnup (GWd/tU)	38.3	38.3	60	47.3	39	71.8
Re-irradiation	Siloe	Siloe	Siloe	No	Yes (partly)	Yes
Max fuel temperature (°C)	2300	2300	2350	2300	2700	2200
Atmosphere (end of test)	Hydrogen	Steam	$H_2O + H_2$	$H_2O + H_2$	Mixed "reducing"	$H_2O + H_2$
Last plateau duration (min)	30	30	30	*c*	*c*	*c*
VERCORS fractional releases (%)						
Kr (via ^{85}Kr)				100	100	100
Te (via ^{132}Te)	100	98-100	98-100		100	99.5
I (via ^{131}I and ^{133}I)	87	93	98-100		100	100
Xe (via ^{133}Xe)	86	87	100		100	100
Cs (via ^{134}Cs and ^{137}Cs)	93	93	97	100	99.8	100
SCIANTIX fractional releases (%)						
Kr (via ^{85}Kr)				98.8	98.7	97
Te (via ^{132}Te)	97.9	97.9	99		99.1	97.3
I (via ^{131}I and ^{133}I)	98	98	98.5		99.2	97
Xe (via ^{133}Xe)	97.8	97.8	98		98.9	97.2
Cs (via ^{134}Cs and ^{137}Cs)	97.7	97.7	98	98.8	98.7	97.2
ANS 5.4 fractional releases (%)						
Kr (via ^{85}Kr)				100	100	100
Te (via ^{132}Te)	95.8	95.8	96.7		99.3	93
I (via ^{131}I and ^{133}I)	93.4	93.4	94.8		98.8	89.7
Xe (via ^{133}Xe)	97.9	97.9	98.4		99.7	96.4
Cs (via ^{134}Cs and ^{137}Cs)	100	100	100	100	100	100

c = max fuel temperature was achieved with a succession of plateaux of 10 minutes every 100 °C, from 2000 °C.

3. **Re-irradiation**. The re-irradiation simulation allows the reconstruction of the FPs inventory. This phase lasts about 7 days [Pontillon et al., 2005]. Fission rate and temperature have been estimated from the available details about the PWR indicated in 3.1, $\dot{F} = 1.7 \times 10^{18}\ \mathrm{fiss\,m^{-3}\,s^{-1}}$ and $T = 450$ K. During re-irradiation the several short-lived FPs are produced again but due to the low temperature of irradiation their diffusion is seriously reduced (Eq. 1.6).

4. **Out-of-pile**. The out-of-pile test is the most important step of the simulation because the high-temperature effect causes the burst release of FPs. Indeed, while the intra-granular isotopes in-solution become trapped in the latter bubbles, the inter-granular bubbles interconnect and the isotopes retained in inter-granular bubbles are released to the pellet outside. Out-of-pile simulation is carried out knowing that fission rate is null while the temperature transient is interpolated from the available data (Fig. 3.18).

Thanks to the previous fractional release definition it is possible to compare the experimental results of the VERCORS test against SCIANTIX and ANS 5.4 predictions (Tab. 3.1). Despite ANS 5.4 methodology is not tailored to reproduce abrupt transient conditions, it has been carried an extension of the ANS 5.4 validation database. The fractional release of the radioactive isotopes of interest has been computed (Eq. 1.19) by using the maximum fuel temperature attained during the transient. A measured vs. predicted plot of the fractional release (Figs. 3.1 and 3.2) shows that the physics-based model developed is in agreement with ANS 5.4 predictions and the error with respect to the VERCORS measurements is lower than 1%.

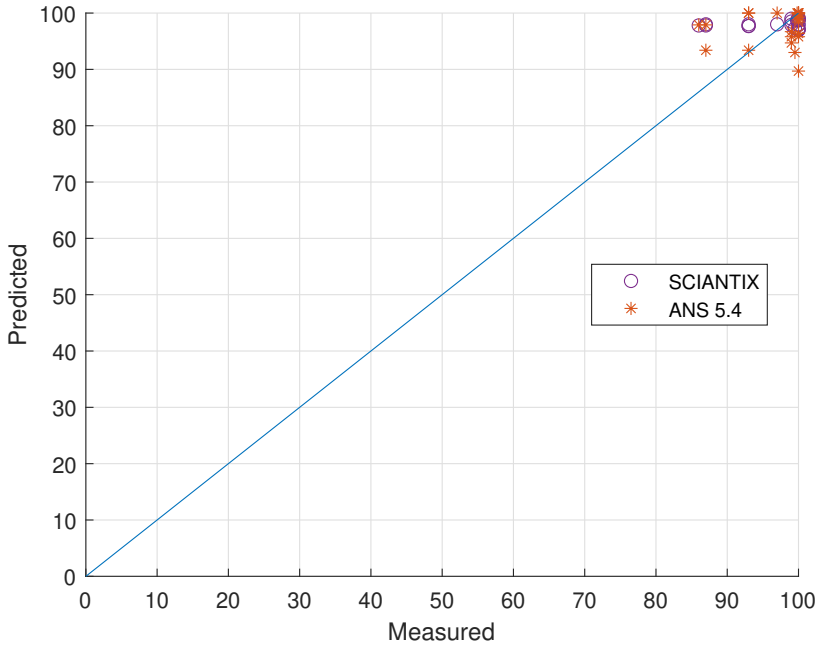

Figure 3.1. VERCORS: measured vs. predicted plot for the set of tests considered. The results above the reference bisector line overestimate the experimental fractional releases, the results below underestimate it.

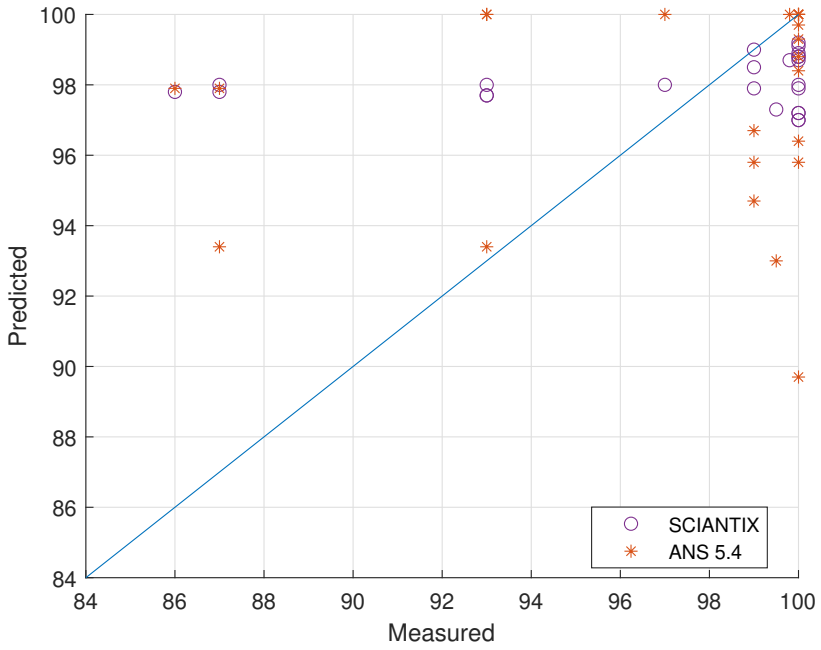

Figure 3.2. VERCORS: enlargement of the measured vs. predicted plot for the set of tests considered. The results above the reference bisector line overestimate the experimental fractional releases, the results below underestimate it.

VERCORS 4

During VERCORS 4 test, the fractional releases for ^{132}Te, ^{131}I, ^{133}I, ^{133}Xe, ^{134}Cs and ^{137}Cs have been controlled. Their numerical values, at the end of the test, are available in Tab. 3.1. In addition, it can be observed (Fig. 3.3) the emission kinetics for ^{132}Te, a short-lived FP and ^{137}Cs, a long-lived FP, and it can be compared with the predicted emission kinetics, computed with SCIANTIX, for the same two isotopes (Fig. 3.4).

With reference to the measured FPs inventory, the global release of gaseous and volatile FPs is not complete, except for ^{132}Te. This is mainly determined from the high temperature plateau ($\approx$ 2300 °C for 30 minutes). As previously suggested, it is supposed that Xe isotopes, generally located in the intra-granular region [Pontillon and Ducros, 2010a], remains partially trapped in fuel grains if temperature does not exceed 2300 $\div$ 2350 °C. A similar argument holds for iodine and caesium fractional releases.

An important improvement of the current implemented model with respect to ANS 5.4 methodology is the possibility of predict, although approximately, the emission kinetics of the isotopes describe. Concerning ^{132}Te and ^{137}Cs (Figs. 3.3 and 3.4), one can make a few remarks

- It is evident that the isotopes, in terms of fractional release and within the model framework, behave the same way. Indeed, because of the basic assumptions of the model, chemical and experimental interactions[3] cannot be described. This argument holds for all the next VERCORS simulation.

- The experimental emission kinetics is composed by two different burst releases. The first, at the end of the intermediate plateau ($\approx$ 1300 °C) and the second is activated by the subsequent temperature ramp.

- SCIANTIX emission kinetics also predicts two subsequent burst releases. The first burst release is activated in advance, during the intermediate temperature ramp ($\approx$ 1200 °C), while the second release is activated by the second high-temperature ramp, in line with the experimental observation.

- The experimental fractional release at the end of the intermediate plateau is about 40% for ^{137}Cs and 10% for ^{132}Te while the predicted ones are both conservatively about 60%. The relative error is not negligible but, with reference to ANS 5.4 methodology, it is reasonably feasible to integrate the missing interactions and improve the results.

- During the high-temperature plateau the fractional release of caesium attain its maximum value, coherently with the experimental measurements.

The retaining of ^{132}Te until intermediate plateau end is likely due to tellurium trapping in unoxidized cladding, but its release quickly saturates during the last temperature ramp. [Johnson and Johnson, 1988, Ducros et al., 2001, Pontillon et al., 2010, Ducros et al., 2013]. Indeed, that intermediate plateau has been carried out in oxidising conditions, under mixed H_2O + H_2.

[3] Initial fuel geometry, test atmosphere, etc.

In Figs. 3.5 and 3.6 the measured vs. predicted plot has been reported. As already stated, the final fractional release predicted by the model is substantially similar for the isotopes described, due to the fact that the behaviour of the isotopes at the grain-boundary level is mainly dependent from the temperature transient.

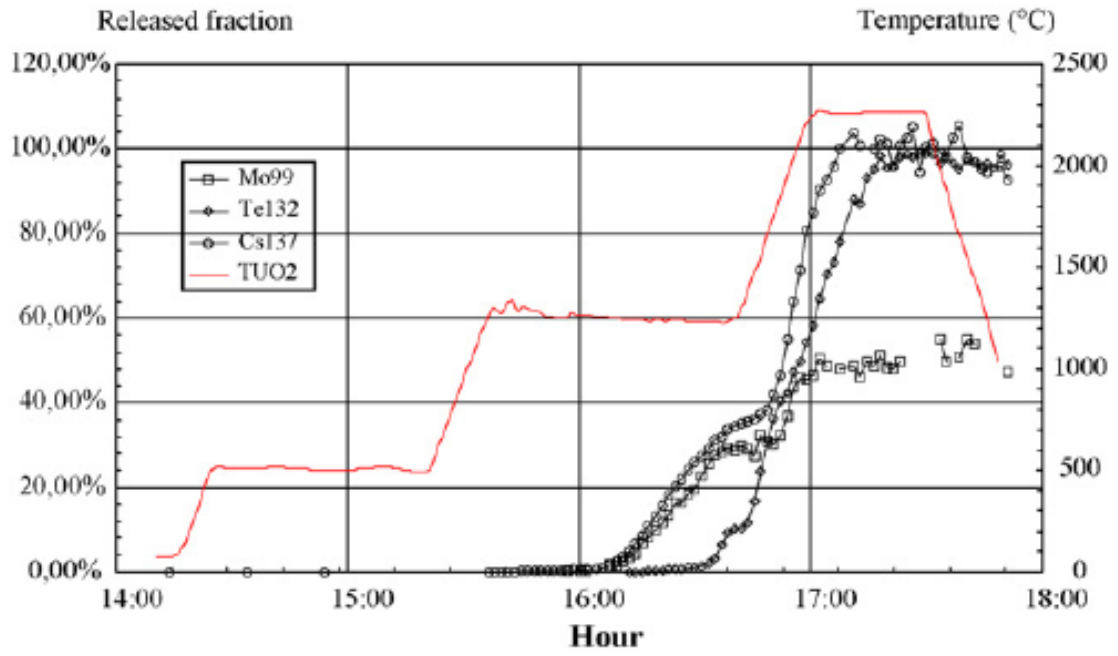

Figure 3.3. VERCORS 4: release kinetics for Te, Cs and Mo during out-of-pile test and transient temperature history [Pontillon and Ducros, 2010a].

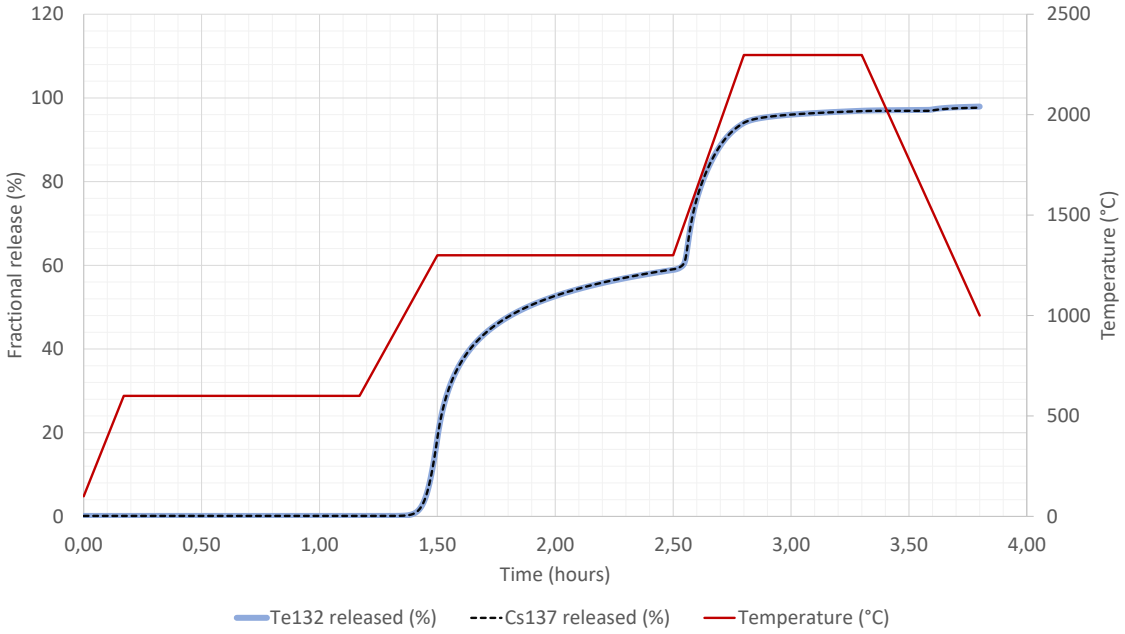

Figure 3.4. VERCORS 4: SCIANTIX numerical prediction of the emission kinetics for ^{132}Te and ^{137}Cs, superimposed with the transient temperature interpolation.

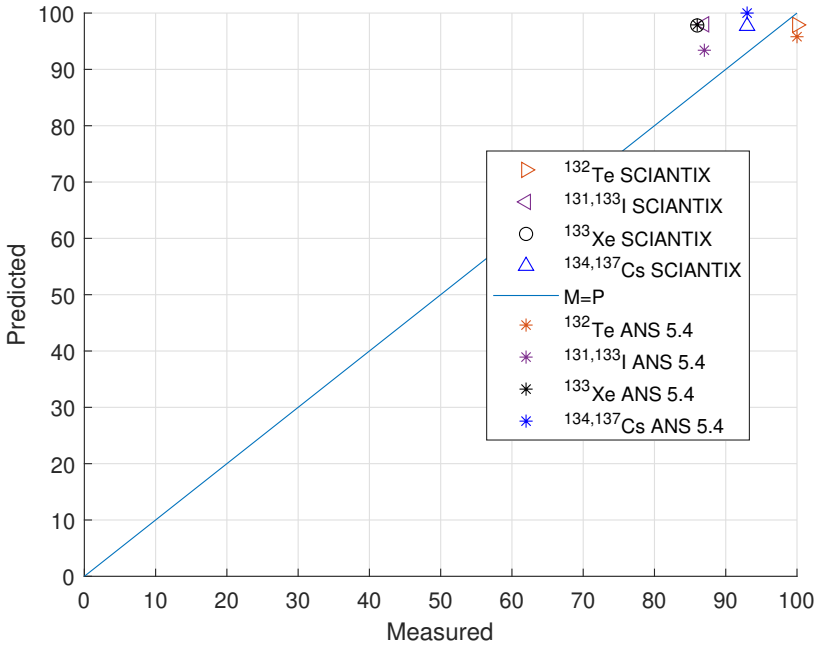

Figure 3.5. VERCORS 4: measured vs. predicted plot for the final fractional releases of the radioactive gaseous and volatile FPs of interest. The results above the reference bisector line overestimate the experimental data, the results below underestimate the experimental data.

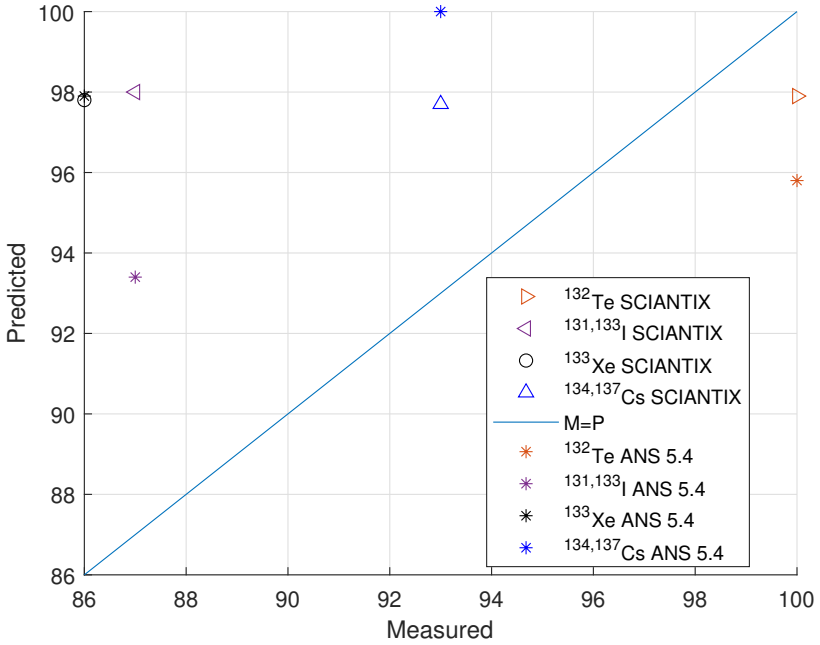

Figure 3.6. VERCORS 4: enlargement of the measured vs. predicted plot for the final fractional releases of the radioactive gaseous and volatile FPs of interest.

VERCORS 5

VERCORS 5 test is similar to the previous VERCORS 4 test. The fractional release measurements of ^{132}Te, ^{131}I, ^{133}I, ^{133}Xe, ^{134}Cs and ^{137}Cs have been controlled and their final fractional releases are available in Tab. 3.1. It can be observed the measured emission kinetics for the long-lived ^{137}Cs (Fig. 3.3) and it can be compared with the predicted one, computed with SCIANTIX (Fig. 3.4).

With respect to the measured FPs inventory, the global release of gaseous and volatile FPs is not complete and it mainly depends from the high temperature plateau ($\approx$ 2300 °C for 30 minutes). Despite VERCORS 4 test, ^{132}Te is high but not complete, probably due to the pure steam atmosphere of the test, i.e. the absence of an oxidising conditions [Johnson and Johnson, 1988, Pontillon and Ducros, 2010a, Ducros et al., 2013]. The high-temperature plateau has the same characteristics of the VERCORS 4 one, namely a 30 minutes plateau at 2300 °C. Therefore it is reasonable to observe again a partial trapping of iodine, xenon and caesium isotopes.

VERCORS 5 results provide the emission kinetics of ^{137}Cs (Fig. 3.7. Compared to the SCIANTIX simulated one (Fig. 3.8)

- The experimental emission kinetics is roughly composed by three different burst releases. The first is activated during the temperature raise from 1000 °C to 1300 °C, the second release appears at the end of the 1300 °C plateau and the third burst release is activated by the last temperature ramp towards 2300 °C.

- SCIANTIX emission kinetics also predicts three subsequent burst releases. The first burst release is weakly activated in advance, during the 1000 °C plateau, the second release is caused by the temperature ramp towards 1300 °C and the subsequent plateau, similarly to the experimental result, and the last release is reactivated by the high-temperature ramp, as observed in the experimental measures.

- The experimental fractional release during the transient is still overestimated. At the end of the 1300 °C plateau the caesium measured fractional release is abound 45% while the predicted fraction is approximately 70%.

- During the high-temperature plateau the fractional release of caesium attain its maximum value, coherently with the experimental measurements.

In Figs. 3.9 and 3.10 the measured vs. predicted plot for the fractional release at the end of the VERCORS test is shown. It is similar to the VERCORS 4 test since the temperature history is similar and they share the last to plateau ($\approx$ 1300 °C and 2300 °C), which are decisive in determining the release behaviour.

Throughout VERCORS 4 and VERCORS 5 tests, high-temperature plateau was close to fuel relocation [Ducros et al., 2001], but fuel collapse was not attained. For this reason it is reasonable to detect a partial trapping of the isotopes.

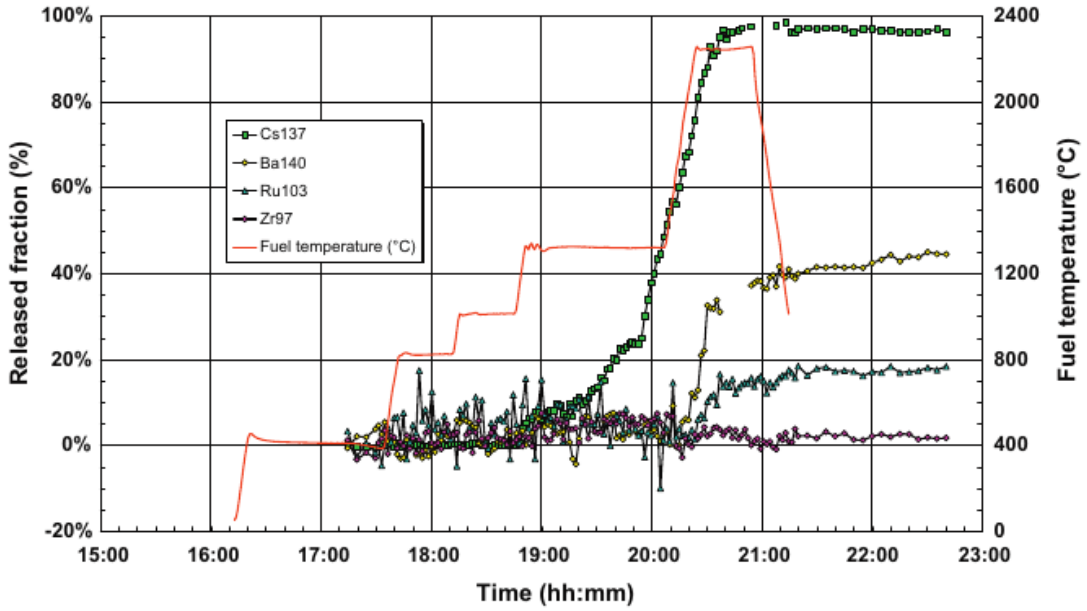

Figure 3.7. VERCORS 5: release kinetics for ^{137}Cs during out-of-pile test and transient temperature history [Ducros et al., 2013]

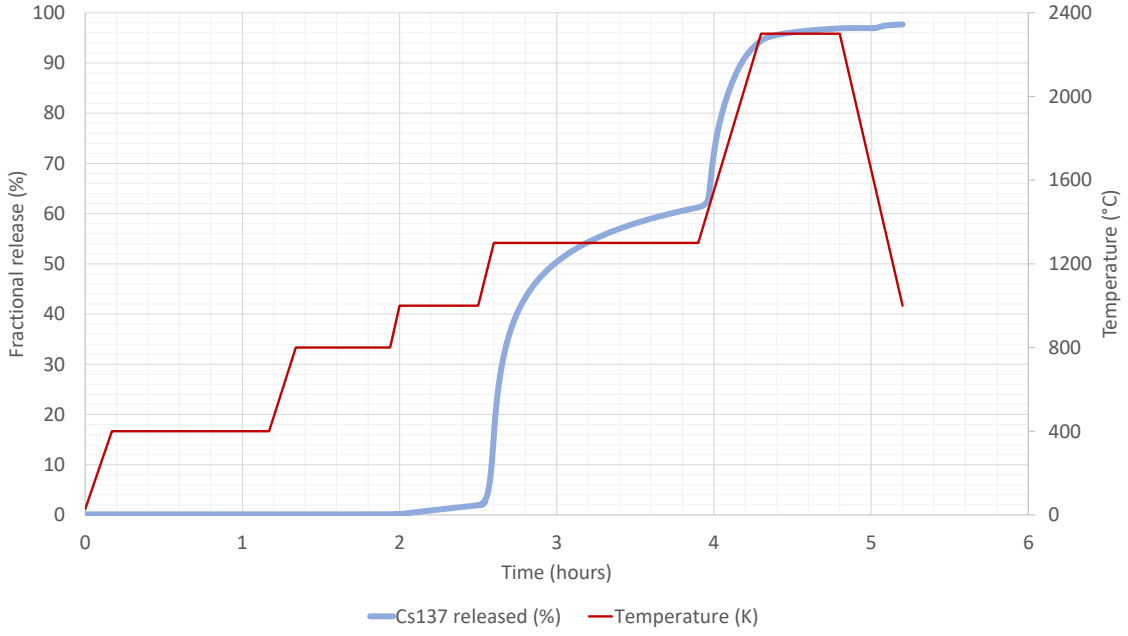

Figure 3.8. VERCORS 5: SCIANTIX numerical prediction of the emission kinetics for ^{137}Cs, superimposed with interpolated temperature history.

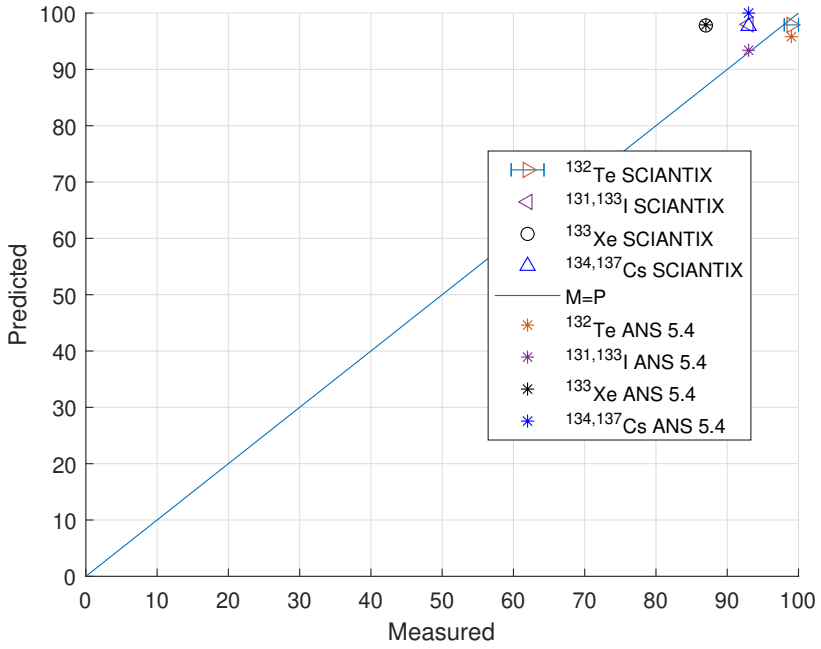

Figure 3.9. VERCORS 5: measured vs. predicted plot for the final fractional releases of the radioactive gaseous and volatile FPs of interest. The results above the reference bisector line overestimate the experimental data, the results below underestimate the experimental data.

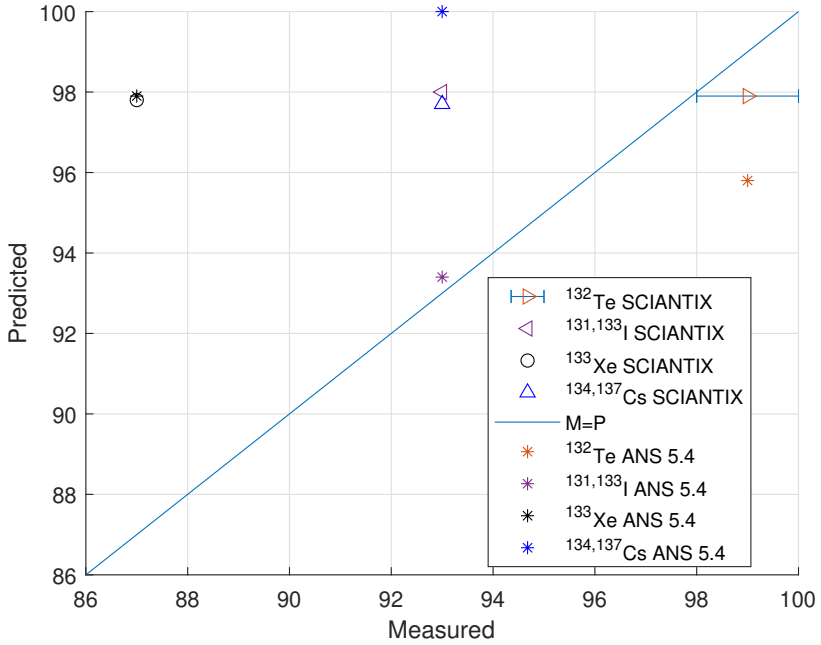

Figure 3.10. VERCORS 5: enlargement of the measured vs. predicted plot for the final fractional releases of the radioactive gaseous and volatile FPs of interest.

VERCORS 6

VERCORS 6 is a test performed in conditions comparable to the one of VERCORS 4 and 5. The main difference lies in the high-temperature plateau, which brougth to fuel collapse and consequently to a boosted fractional release measured for ^{132}Te, ^{131}I, ^{133}I, ^{133}Xe, ^{134}Cs and ^{137}Cs (Tab. 3.1). Consequently, the measured global release of gaseous and volatile FPs was almost complete, despite a fraction of caesium which remained in the corium because of the formation of chemical compound such as uranate or zirconate [Pontillon and Ducros, 2010a].

The emission kinetics is not available for any of the isotopes of interest, only the temperature history and the measured gamma activity (Fig. 3.11) can give information about the release during the transient. With reference to the numerical prediction of the emission kinetics (Fig. 3.12) one can observe that

- The experimental emission kinetics is roughly composed by three different burst releases. The first is activated during the temperature ramp from 800 °C to 2100 °C. The release is noticeable from the gamma activities since the radioactivity in the fuel decreases, the radioactivity in the zone adjacent to the fuel setup [Ducros et al., 2001] increases (Fig. 3.11) and the numerical prediction of SCIANTIX of the fractional release is around 80% for all the isotopes.

- The second release appears during the temperature ramp from 1300 °C to the 2327 °C, together with a large increases of radioactivity detected in the impactor. This burst release is also predicted by SCIANTIX simulation.

- The last release appears after fuel collapse but it is not described by the numerical model.

In Figs. 3.13 and 3.14 the measured vs. predicted plot for the fractional release at the end of the VERCORS 6 test is shown. The agreement in the global fractional releases prediction is considerably better. As already stated, the high temperature achieved during the test led to the fuel collapse, namely sample liquefaction, and the majority of retained FPs is released. Therefore, it is possible to say that the implemented intra- and inter-granular model is able to describe the UO_2 behaviour under transient conditions, for example those representative of a LOCA, where abrupt temperature variations appear.

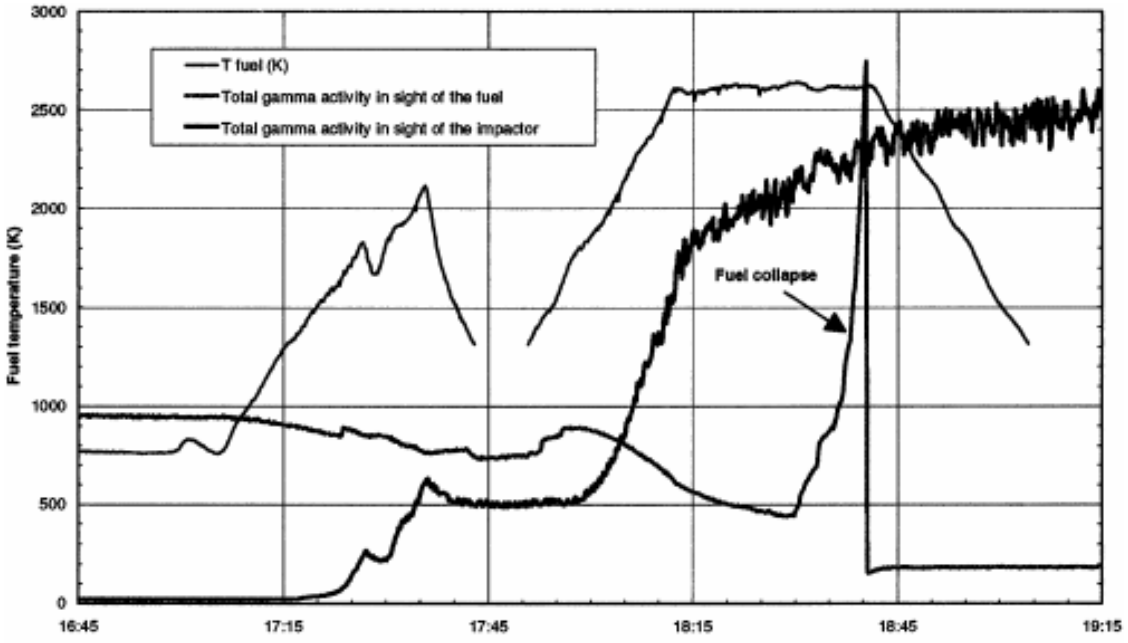

Figure 3.11. VERCORS 6: gamma activities measured during the temperature transient. The gamma activity that slowly increases during the test is the one referring to the *impactor*, which detected the most volatile FPs (probably Xe and Kr) while the other spectrometer measured the FPs leaving the fuel and detected the fuel collapse [Ducros et al., 2001].

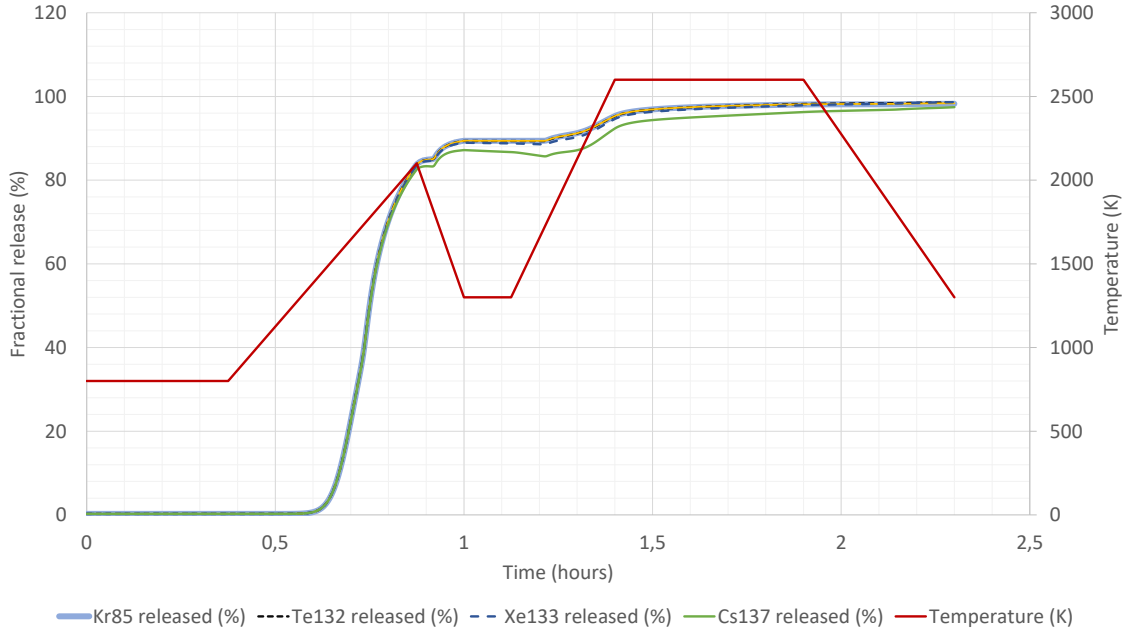

Figure 3.12. VERCORS 6: SCIANTIX numerical prediction of the emission kinetics for ^{85}Kr ^{132}Te, ^{133}Xe and ^{137}Cs, superimposed with the transient temperature history.

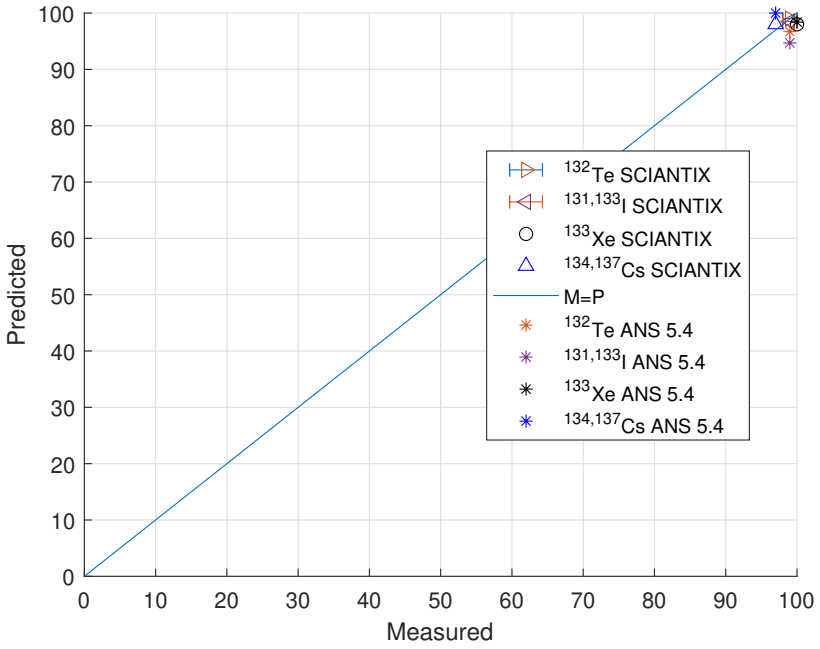

Figure 3.13. VERCORS 6: measured vs. predicted plot for the final fractional releases of the radioactive gaseous and volatile FPs of interest. The results above the reference bisector line overestimate the experimental data, the results below underestimate the experimental data.

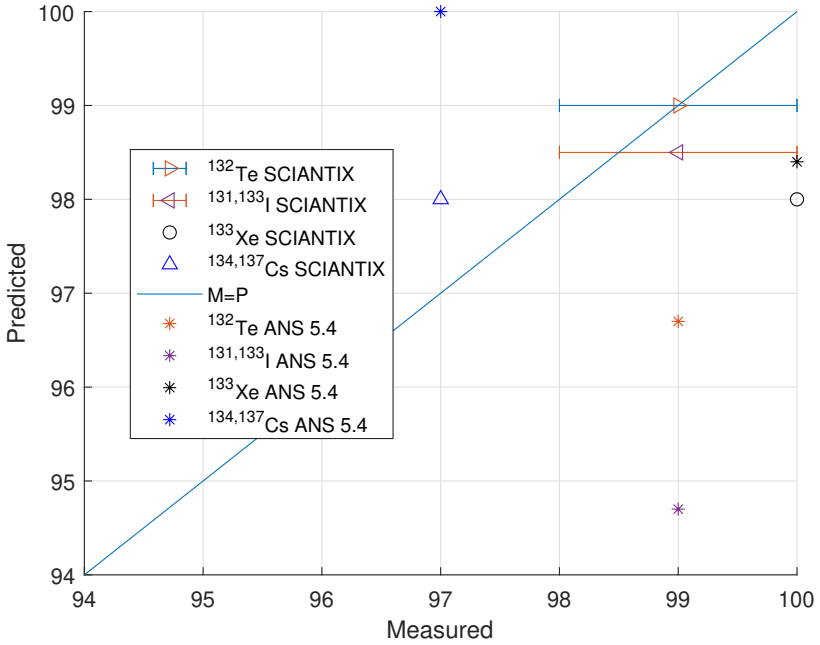

Figure 3.14. VERCORS 6: enlargement of the measured vs. predicted plot for the final fractional releases of the radioactive gaseous and volatile FPs of interest.

VERCORS RT3

During all VERCORS RT tests the fuel melting point became the target temperature. As a consequence the observed fractional releases were almost complete. With respect to VERCORS tests, the high temperature plateau was substituted by a sequence of successive plateau of 10 minutes every 100 °C, from 2000 °C to the maximum temperature. In this case of about 2700 °C. In the numerical simulation this sequence has been interpolated with a single ramp which showed anyway able to predict the global fractional release (Figs. 3.15 and 3.16).

The controlled isotopes are ^{85}Kr, ^{132}Te, ^{131}I, ^{133}I, ^{133}Xe, ^{134}Cs and ^{137}Cs. Their global fractional releases are reported in Tab. 3.1. It can be highlighted that, consistently with the phenomenon of fuel melting, the releases was almost complete for all the considered species. The only exception was caesium isotopes. The storage of caesium in the melted corium is possibly caused by the formation of compounds such as uranates or zirconates [Ducros et al., 2013].

The predicted releases are about 98% because of the intra-granular concentration C. The latter, in the model description, remains within the intra-granular bubbles, as G_b. Nevertheless, the predictions underestimate the observations by a factor of about 1.5 % (Fig. 3.18). This is remarkable, remembering that the simulations are carried out in a 0D approach and that the existing ANS 5.4 methodology used to overestimate the fractional releases at least of one or two orders of magnitude [Turnbull and Beyer, 2009].

The emission kinetics for ^{137}Cs are available in Figs. 3.15 and 3.16.

- The observed fractional release is composed by three successive burst releases.
- The first burst release is activated at about 1200 °C, in conjunction with the end of the temperature ramp from 400 °C to 1500 °C. This type release is governed by classic thermal diffusion [Pontillon and Ducros, 2010a]. The numerical model predict a faster release, with respect to the measurements. At the end of the first temperature ramp the observed fractional release is about 15% while the predicted one is about 70%.
- The second observed release is activated from 1500 °C to 2000 °C and the third is activated from 2200 °C to 2700 °C. The second and the third releases are not distinguished by the model but they are considered as a unique release.
- At the end of the whole transient, the fractional release value is almost complete, both for measured and predicted release.

With respect to the numerical values of the global fractional releases, the model is able to predict them. The underestimation is about 1.5 %, a remarkable result with reference to ANS 5.4 predictions.

Regarding the release kinetics, the intermediate transients are constantly overestimated, with a conservative approach. As a consequence, it seems that the model reasonably predict the fractional release until fuel melting. The phenomenon which causes the almost complete release of all volatile and gaseous FPs.

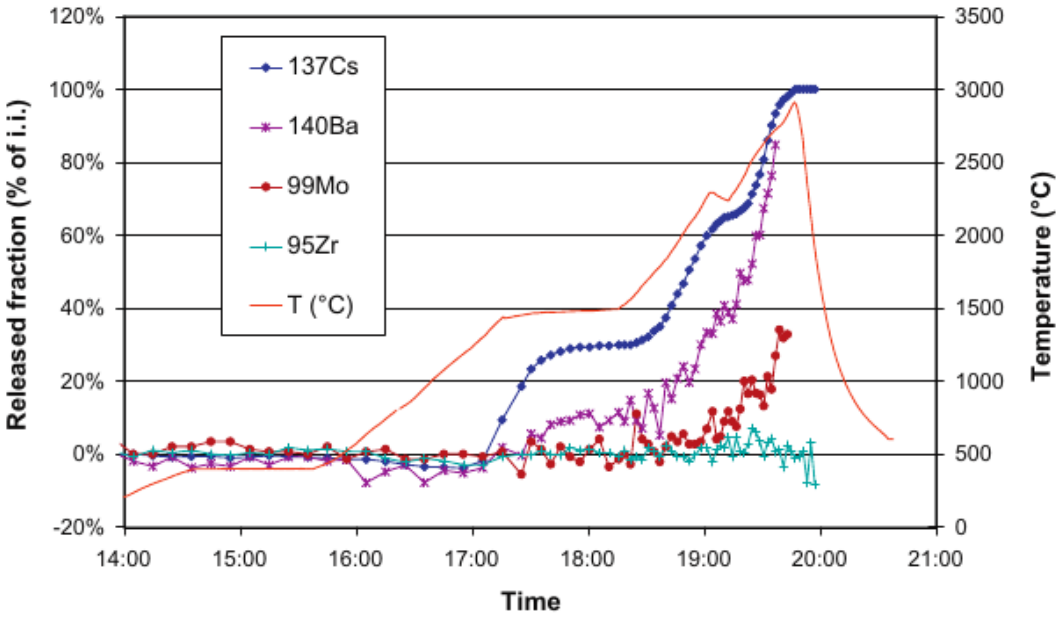

Figure 3.15. VERCORS RT3: release kinetics for ^{137}Cs during VERCORS RT3 out-of-pile test and transient temperature history [Pontillon and Ducros, 2010b]

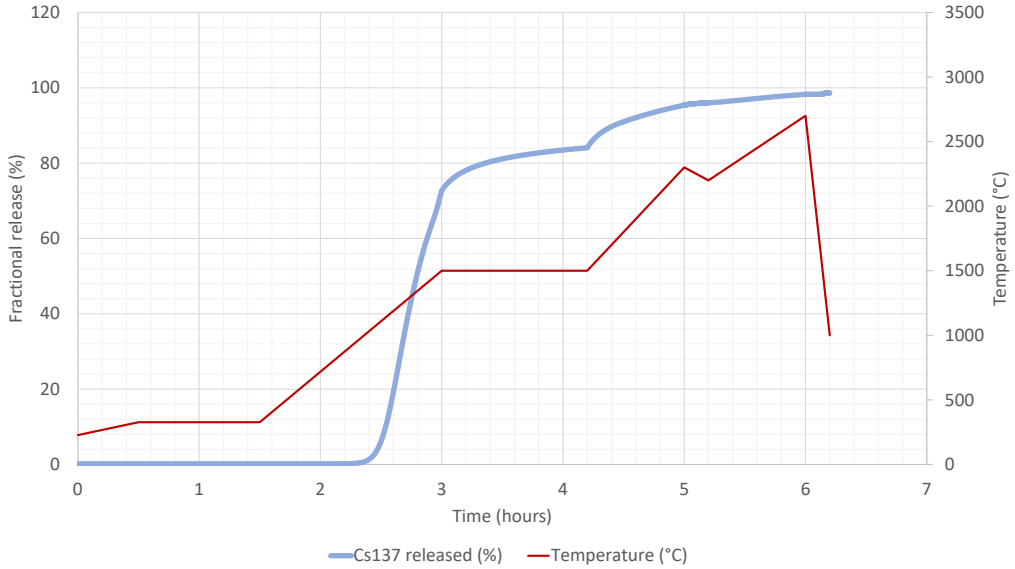

Figure 3.16. VERCORS RT3: SCIANTIX numerical prediction of the emission kinetics for ^{137}Cs, superimposed with the interpolated temperature history.

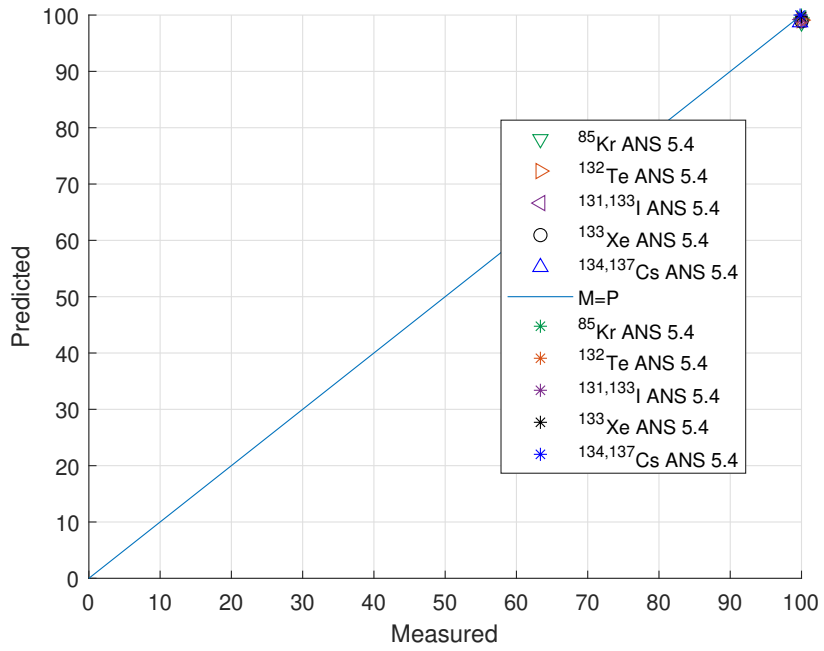

Figure 3.17. VERCORS RT3: measured vs. predicted plot for the final fractional releases of the radioactive gaseous and volatile FPs of interest. The results above the reference bisector line overestimate the experimental data, the results below underestimate the experimental data.

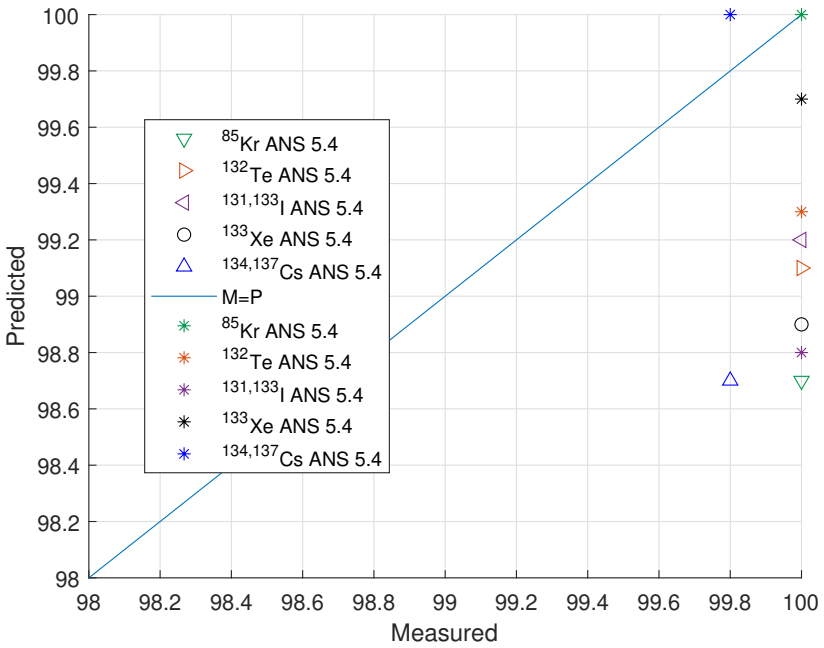

Figure 3.18. VERCORS RT3: enlargement of the measured vs. predicted plot for the final fractional releases of the radioactive gaseous and volatile FPs of interest.

VERCORS RT1 - RT6

VERCORS RT1 and VERCORS RT6 have been compared together, due to the similar temperature transients (Fig. 3.19).

Fuel melting, which causes the almost complete fractional releases, was again the target of the tests. The maximum temperature was respectively of about 2300 °C and 2200 °C, achieved through a sequence of successive plateau of 10 minutes every 100 °C, starting from 2000 °C. The plateaux succession has been interpolated with a single ramp, in line with the previous simulation (Figs. 3.15 and 3.16).

With respect to the other tests, VERCORS RT1 fuel sample did not undergo a re-irradiation phase. Only the long-lived FPs were controlled, i.e. ^{85}Kr and ^{137}Cs. Conversely VERCORS RT6 fuel sample underwent re-irradiation. The isotopes controlled were ^{85}Kr, ^{132}Te, ^{131}I, ^{133}I, ^{133}Xe, ^{134}Cs and ^{137}Cs. The observed fractional release for the isotopes was complete (Tab. 3.1).

The predicted fractional releases are about 98.8% for VERCORS RT1 and 97% for VERCORS RT6 simulations. The numerical results underestimate the observation. Once again, the reason probably is the storage of the intra-granular concentration in the intra-granular bubbles The error with respect to the measured releases roughly lie between 1.2% and 3%, a remarkable results for the model implemented in SCIANTIX.

The fractional release kinetics for ^{137}Cs are available in Figs. 3.19 and 3.20. For both the tests, the numerical predictions are very similar. As a consequence of the similar temperature transients.

- Firstly, it is evident that the both the numerical fractional releases are closely to the one measured in VERCORS RT6 test. The reason of this observation has to searched in the impact of the burn-up on the release kinetics. The global fractional release is not affected but the kinetics seem to be strongly dependent on the fuel burnup history [Pontillon and Ducros, 2010a]. The model implemented for the simulations, coherently with the basic assumptions, is not able to give a kinetics description.

- The fractional release observed in VERCORS RT1 and VERCORS RT6 are made of two clear burst releases. The first is activated at about 1200 °C, for both the tests. The second is activated more or less at 1800÷2000 °C.

- The numerical model is in line with VERCORS RT6 kinetics. But this agreement is not considered a consequence of the model description. Probably for fuel at higher burnup the caesium isotopes are released considerably faster.

With respect to the numerical values of the global fractional releases, the model is able to predict them. The underestimation is about 1.5 %, a remarkable result with reference to ANS 5.4 predictions.

Regarding the release kinetics, the intermediate transients are constantly overestimated, with a conservative approach. As a consequence, it seems that the model reasonably predict the fractional release until fuel melting. The phenomenon which causes the almost complete release of all volatile and gaseous FPs.

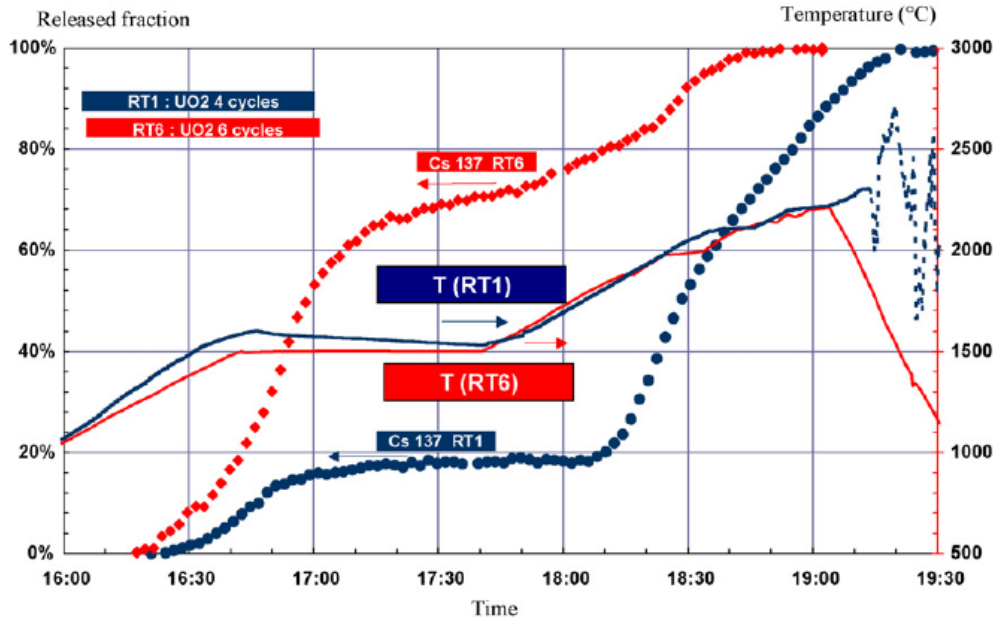

Figure 3.19. VERCORS RT1-6: observed release kinetics for ^{137}Cs and temperature histories of the transient phase [Ducros et al., 2001].

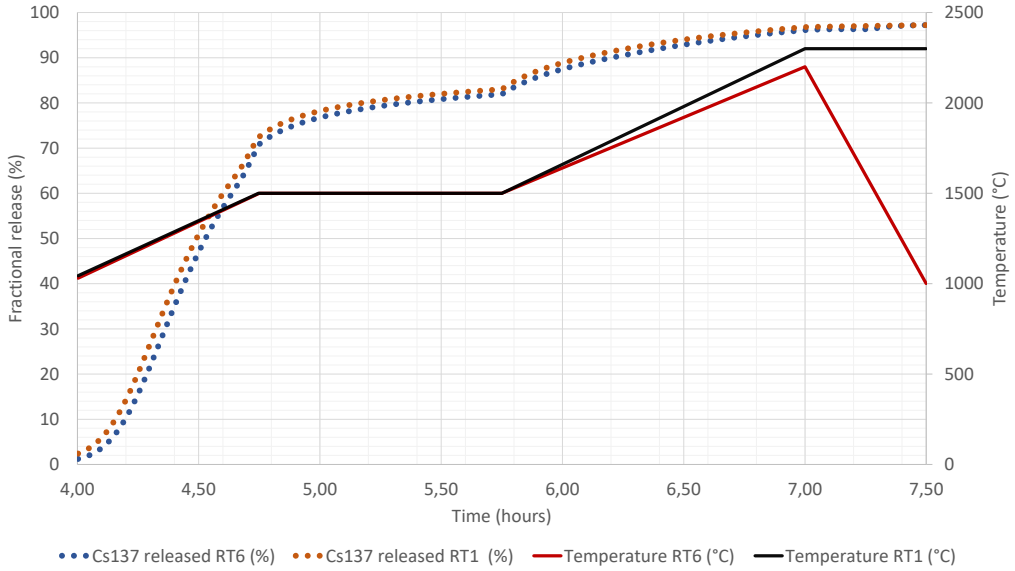

Figure 3.20. VERCORS RT1-6: SCIANTIX numerical predictions of the emission kinetics for ^{137}Cs, superimposed with the transient temperature histories.

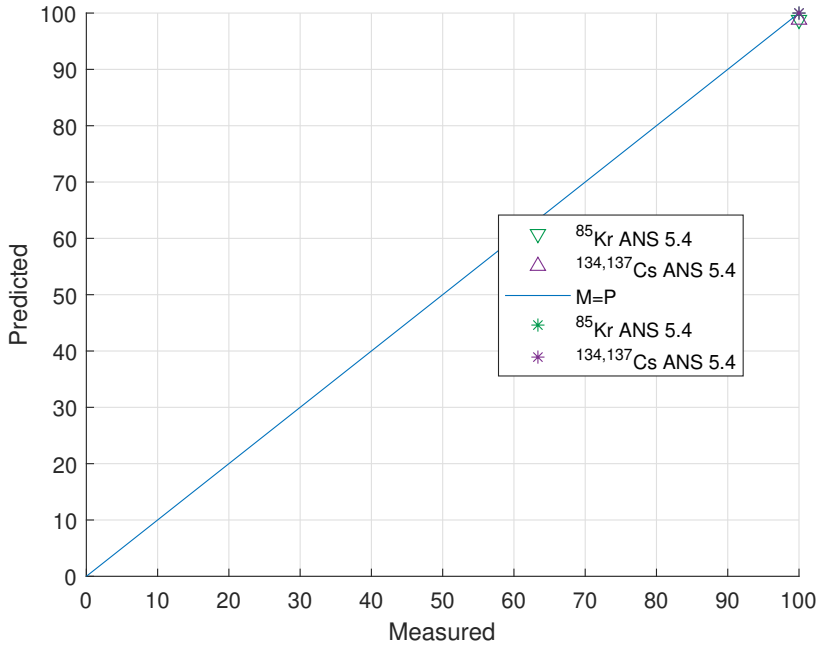

Figure 3.21. VERCORS RT1: measured vs. predicted plot for the final fractional releases of the radioactive gaseous and volatile FPs of interest. The results above the reference bisector line overestimate the experimental data, the results below underestimate the experimental data.

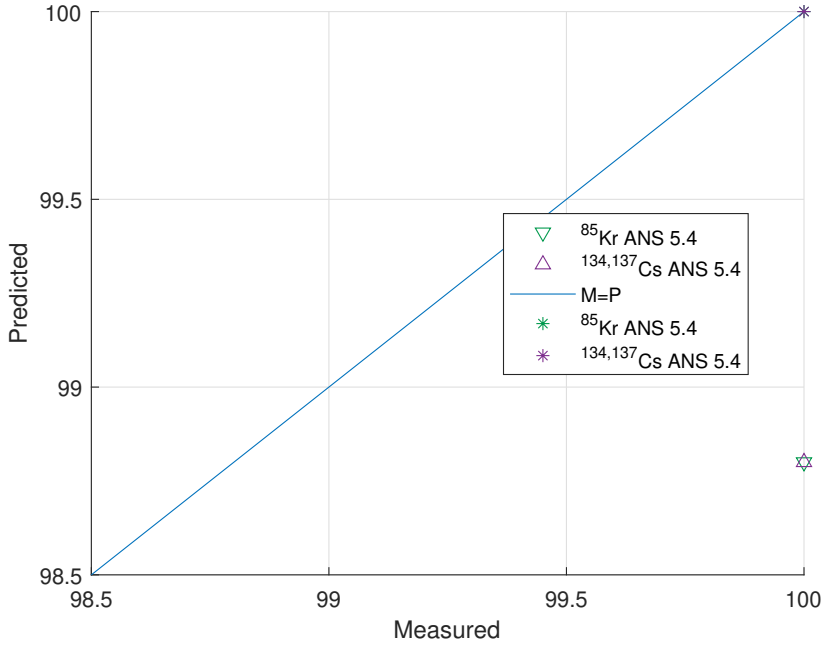

Figure 3.22. VERCORS RT1: enlargement of the measured vs. predicted plot for the final fractional releases of the radioactive gaseous and volatile FPs of interest.

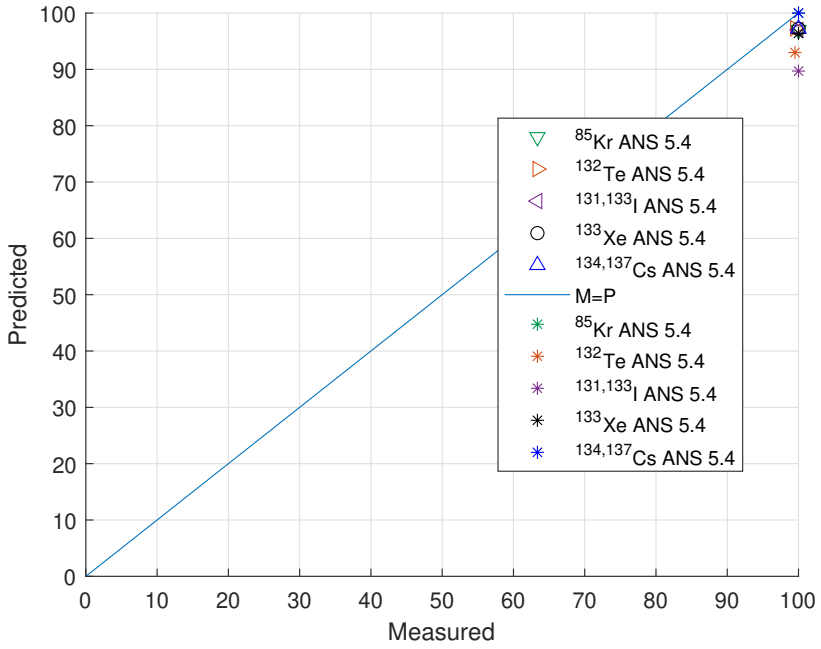

Figure 3.23. VERCORS RT6: measured vs. predicted plot for the final fractional releases of the radioactive gaseous and volatile FPs of interest. The results above the reference bisector line overestimate the experimental data, the results below underestimate the experimental data.

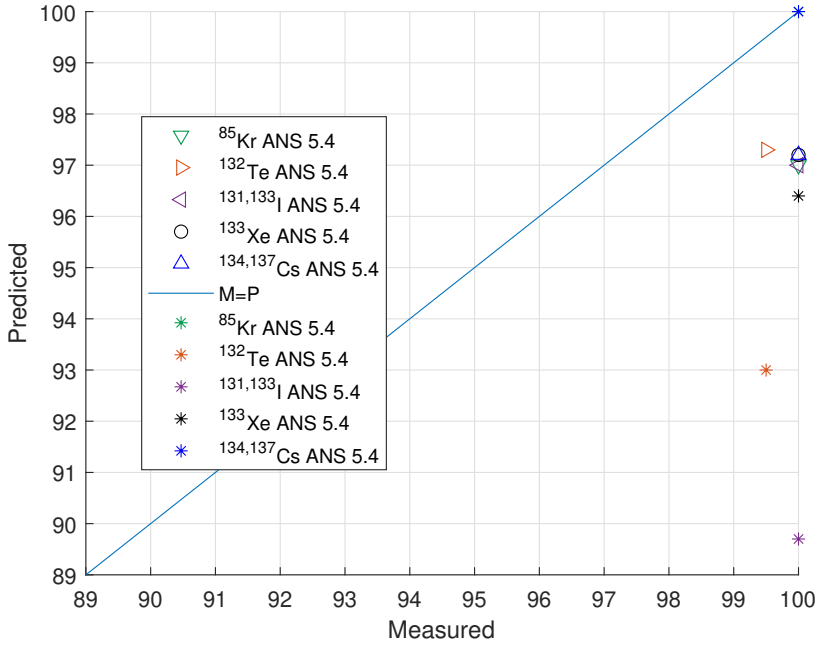

Figure 3.24. VERCORS RT6: enlargement of the measured vs. predicted plot for the final fractional releases of the radioactive gaseous and volatile FPs of interest.

3.6 Closing remarks

The employment of a physics-based description for the inter-granular bubble behaviour constitutes a key point in the radioactive release assessment. The interactions between bubbles have been included in the model, in terms of growth, coalescence and interconnection. The basic hypothesis which allows the development is that the radioactive isotopes of interest, namely the short-lived FPs, are negligible in mass with respect to the inert fission gases. As a consequence, they are not relevant in determining inter-granular bubble interconnection.

Once defined a suitable fractional release, it has been possible to compare the numerical predictions of the model with the measured fractional release of gaseous and volatile FPs during the experimental VERCORS tests.

The model implemented in SCIANTIX allows the evaluation of the fractional release throughout the transient, with respect to ANS 5.4 which computes the equilibrium fractional release. In particular, the measured emission kinetics have been compared to the model predictions.

At intermediate temperatures, i.e. between 1200 °C and 1500 °C, the predicted fractional releases reasonably anticipate and overestimate the observed one. The model indeed does not take into consideration chemical interactions, which may delay or modify the emission of certain isotopes. The retention phenomena are caused by chemical interactions with cladding or other structural elements. For example, the emission of volatile tellurium is caused by the presence of tin in the Zircaloy cladding. At higher temperature, the almost complete release is observed, activated by thermal diffusion, and correctly predicted for the radioactive isotopes.

The final fractional release, after the temperature transient, has been also evaluated with ANS 5.4 by assuming a constant temperature equal to the maximum one. ANS 5.4 and SCIANTIX model both predict the almost complete FPs release, forced by high temperatures, by committing an error lower then 1%.

Therefore, provided the final fractional release, the advantage of the model implemented in SCIANTIX is double. Firstly, a severe accident simulations supplies a conservative estimate of the radioactive release kinetics at intermediate (between 1200 °C and 1500 °C) temperature and the estimate becomes more accurate at high temperature. Secondly, SCIANTIX is a code which takes into consideration several mechanisms, in order to provide an accurate 0D description of the fuel pellet. From a single simulation, information about fuel swelling, inert gas behaviour, fission gas release, intra- and inter-granular bubble, are obtained. On the contrary, ANS 5.4 is a stand-alone methodology usable for fractional releases evaluation. It does not consider other nuclear fuel phenomena of interest and the description of long-lived FPs, stable isotopes or different fuel materials, such as MOX, necessarily requires other models.

Conclusions

The state-of-art methodology ANS 5.4 has been developed to evaluate the fractional release of radioactive gaseous and volatile FPs, of primary radiological importance. ANS 5.4 is tailored to stationary conditions of the reactor. Therefore, it should not be applied to accidents which involve abrupt temperature variations

From a review of the ANS 5.4 basic assumptions it has been derived the analytic fractional release employed in the model. The formula holds in stationary conditions and it is coupled with the Vitanza threshold in order to describe the inter-granular bubble interconnection. The latter phenomenon is responsible for the incubation period and the subsequent release of radioactive material from the fuel pellet.

The current work aims to provide a transient description of the release and a physics-based modeling of inter-granular bubble interconnection.

To solve the diffusion-decay equation, which rules the intra-granular behaviour of radioactive isotopes, it has been developed a spectral solver. Once implemented in the SCIANTIX meso-scale code, its consistency has been verified with Method of Manufactured Solutions (MMS).

The diffusion coefficient of the model has been modified in order to consider intra-granular repeated trapping and irradiation-induced resolution. The inter-granular bubble behaviour is determined by the amount of FG and FPs absorbed and released throughout irradiation. The majority of existent isotopes is composed by stable inert gases and long-lived FPs. Therefore it has been assumed that the concentration of short-lived FPs, of primary radiological interest, is negligible in determining inter-granular bubble interconnection and release.

By exploiting these assumptions, a complete intra- and inter-granular solver has been implemented in SCIANTIX and a suitable fractional release definition has been given. The latter allows an accurate description of the fractional release kinetics. The model predictions have been tested against the experimental database of the VERCORS tests, a series of experiments representative of LOCA transient conditions.

The results of the validation against experimental data highlighted several features of the model. Firs of all, fractional release measurements at the end of the transient are in line ANS 5.4 predictions. Both the methodologies commit an error lower than 1 % with respect to VERCORS results. In addition to the correct global release, at intermediate temperatures (between 1200 °C and 1500 °C) the model supplies a conservative estimate of the radioactive release kinetics. At higher temperature, where thermal diffusion constitutes the dominant mechanism, the predictions become more accurate.

A further advantage is that the employed code, SCIANTIX, takes into consideration several mechanisms, to allows an accurate description of the fuel pellet. The

information about fuel swelling, inert gas behaviour, fission gas release, intra- and inter-granular bubble, are obtained at the same time. On the contrary, ANS 5.4 is a stand-alone methodology usable only for radioactive releases evaluation. The description of long-lived FPs, stable isotopes or different fuel materials, such as MOX, necessarily requires other models.

The model implemented in SCIANTIX offers also several improvements with reference to the present description, e.g. the possibility of coupling several radioactive isotopes through a decay matrix, the inclusion of chemical interactions in the mechanistic equations of the model and the change to conduct a sensitivity analysis with adjoint models. In conclusion, it is possible to couple SCIANTIX with integral FPCs, e.g. TRANSURANUS or BISON, to extend the validation database with IFA irradiated fuel sample simulation.

Appendix A

Uniqueness of the solution

The mathematical problem (2.10), below repeated, belongs to the category of the well-posed problems. Under the reasonable assumptions of sufficient regularity of the data, the solution $C(r,t)$ exists in $\mathbb{R} \times (0,\infty)$. The uniqueness proof is a valid tool in order to confirm that the two approaches, the Fourier series and the spectral decomposition, must provide the same result, regardless the boundary condition in $r = 0$. Consider the problem

$$\begin{cases} \dfrac{\partial C}{\partial t} = \alpha D \nabla^2 C - \lambda C + B \\ C(r,0) = C_0, \quad 0 < r < a \\ C(a,t) = 0, \quad t > 0 \\ \nabla C|_{r=0} = 0, \quad t > 0 \end{cases} \tag{A.1}$$

defined on the domain $\Omega_r \times \Omega_t$. Assume that $\Omega_r = (0,a)$ and $\Omega_t = (0,\infty)$. Suppose the existence of two different solutions C_1 and C_2. For the difference $w = C_1 - C_2$, there is a homogeneous problem

$$\begin{cases} \dfrac{\partial w}{\partial t} - \alpha D \nabla^2 w + \lambda w = 0 \\ w(r,0) = 0, \quad 0 < r < a \\ w(a,t) = 0, \quad t > 0 \\ \nabla w|_{r=0} = 0, \quad t > 0 \end{cases} \tag{A.2}$$

Multiply the homogeneous equation by $w(r,t)$ and integrate on $\Omega_r \times \Omega_t$[1] to get

$$\int_0^\infty dt \int_0^a w \left(\frac{\partial w}{\partial t} - \alpha D \nabla^2 w + \lambda w \right) 4\pi r^2 dr = 0 \tag{A.3}$$

Exploiting the Green's identity

$$\int_V u \nabla^2 v \; dV = \int_S u \nabla v \cdot \mathbf{n} \; dS - \int_V \nabla u \cdot \nabla v \; dV \tag{A.4}$$

[1]Remember that the diffusion-decay equation is defined on a three-dimensional domain. Due to the spherical symmetry of the system there is only one independent, spatial, variable, and a volume integral must include the infinitesimal spherical surface element $4\pi r^2 dr$.

equation (A.3) becomes

$$\int_0^\infty dt \int_0^a \left(\frac{1}{2} \frac{\partial w^2}{\partial t} + \alpha D |\nabla w|^2 + \lambda w^2 \right) 4\pi r^2 dr = \int_0^\infty dt \int_S \alpha D \; w \nabla w \cdot \mathbf{n} \; dS \quad \text{(A.5)}$$

The right-hand side of (A.5) cancels, because $w(a,t) = 0, \forall t > 0$.

$$\int_0^\infty dt \int_0^a \left(\frac{1}{2} \frac{\partial w^2}{\partial t} + \alpha D |\nabla w|^2 + \lambda w^2 \right) 4\pi r^2 dr = 0 \quad \text{(A.6)}$$

Since $\alpha \geq 0$, $D \geq 0$, $\lambda \geq 0$ and the integrand is a sum of three non-negative terms, (A.6) holds only if $w \equiv 0$, namely $C_1 \equiv C_2$. In the end, the solution of (2.10) is unique. It is involved only the null boundary condition on $r = a$, then it does not depend whether $\nabla c|_{r=0} = 0$ or $c(0,t) < \infty$. The solution is the same and is unique. This conclusion is the expected one, since the important boundary condition is the one holding in $r = a$. In $r = 0$ a symmetry boundary condition is used, for convenience. Nevertheless, in line of principle, the same solution for $C(r,t)$ can be obtained by imposing $C(a,t) = C(-a,t) = 0$, considering an even domain $\Omega_r = (-a, a)$.

Appendix B

Dimensionless problem

In line of principle it is possible solve a dimensionless equation which depends only on one parameter. Let's consider the diffusion-decay equation

$$\frac{\partial C(r,t)}{\partial t} = \alpha D \nabla^2 C(r,t) - \lambda C(r,t) + B \tag{B.1}$$

and introduce the following dimensionless quantities:

$$\widetilde{r} = \frac{r}{a}, \quad \tau = \lambda t, \quad \phi = \frac{\lambda}{B} C \tag{B.2}$$

By simple calculations, the dimensionless equation for ϕ is

$$\frac{\partial \phi}{\partial \tau} = \frac{1}{\mu} \widetilde{\nabla}^2 \phi - \phi + 1 \tag{B.3}$$

Similarly to the previous discussions, by applying the spectral approach, the following equations are obtained

$$\phi(\widetilde{r},\tau) = \frac{2}{\pi} \sum_{k=1}^{\infty} \frac{\sin(k\pi\widetilde{r})}{\widetilde{r}} \frac{\mu k^{-1}(-1)^{k+1}}{\mu + \pi^2 k^2} \left(1 - e^{-\left(1+\pi^2 k^2/\mu\right)\tau}\right) \tag{B.4}$$

$$\bar{\phi}(\tau) = \frac{6}{\pi^2} \sum_{k=1}^{\infty} \frac{1}{k^2} \frac{\mu}{\mu + \pi^2 k^2} \left(1 - e^{-(1+\pi^2 k^2/\mu)\tau}\right) \tag{B.5}$$

$$\phi_\infty = 1 - \frac{3}{\sqrt{\mu}} \left(\coth\sqrt{\mu} - \frac{1}{\sqrt{\mu}}\right) \tag{B.6}$$

$$\frac{R}{B} = \frac{3}{\sqrt{\mu}} \left(\coth\sqrt{\mu} - \frac{1}{\sqrt{\mu}}\right) - 6e^{-\tau} \sum_{n=1}^{\infty} \frac{e^{-n^2\pi^2\tau/\mu}}{n^2\pi^2 + \mu} \tag{B.7}$$

$$\left(\frac{R}{B}\right)_\infty = 1 - \phi_\infty \tag{B.8}$$

The dimensionless equations reveal their utility every time that the dependence on μ appears. For example, in error analysis or in the previsions of the behaviour of problems characterized by high or low μ value.

Appendix C

Adjoint equation and perturbation theory

Adjoint equations are powerful tools of the mathematical physics. They are based on the Lagrange theory of the adjoint operators and are indispensable for the formulation of the small perturbation theory. Furthermore, nuclear reactor theory generated an important interest in adjoint equations and small perturbation theory, which have been essential for the development of the nuclear reactor physics and nuclear power projects.

Examine the diffusion-decay equation with external source, for the concentration of a single fission product, within a sphere of radius a. Referring to the adjoint equations theory, the *main problem* is

$$\begin{cases} \dfrac{\partial C}{\partial t} - \alpha D \nabla^2 C + \lambda C = B \\ C(r,0) = C_0, \quad 0 < r < a \\ C(a,t) = 0, \quad t > 0 \\ \nabla C|_{r=0} = 0, \quad t > 0 \end{cases} \tag{C.1}$$

We deal with a three-dimensional problem which depends only on one coordinate, thanks to the spherical symmetry. The concentration is defined in $\Omega_r \times \Omega_t = (0,a) \times (0,T)$.[1] Let us denote the second order operator

$$A = \frac{\partial}{\partial t} - \alpha D \nabla^2 + \lambda \tag{C.2}$$

which operates on real functions defined in $\Omega_r \times \Omega_t$, continuous and differentiable in all the internal point of the domain. The solution $C(r,t)$ must be quadratically summable on the domain, together with its partial derivatives $\partial C/\partial r$, $\partial^2 C/\partial r^2$ and $\partial C/\partial t$. Furthermore

$$B \in L_2(\Omega_r \times \Omega_t), \quad C_0 \in L_2(\Omega_r) \tag{C.3}$$

where L_2 is the Hilbert space of the functions quadratically summable. The domain of the operator A is labeled $D(A)$, set of $C(r,t)$ defined on $\Omega_r \times \Omega_t$ which fulfill the

[1] For convenience, the time domain $\Omega_t = (0,\infty)$ has been replaced with $\Omega_t = (0,T)$, if $T \to \infty$ the reasoning does not change.

previous conditions. The main equation can be simply written as

$$AC = B \tag{C.4}$$

Consider the following inner product

$$(v, w) = \int_{\Omega_t} dt \int_{\Omega_r} vw \; dV = \int_0^T dt \int_0^a vw \; 4\pi r^2 dr \tag{C.5}$$

Let's formulate the adjoint problem. Consider the inner product (AC, C^*), where C^* is the adjoint function. Within the adjoint equations theory, the adjoint function C^* is referred as *function of information importance* or *importance*, because it is responsible for the sensitivity analysis. The initial and boundary values for the adjoint concentration will be established during the derivation of the adjoint formulation. The starting inner product is

$$(AC, C^*) = (B, C^*) \tag{C.6}$$

which can be explicitly written as

$$\int_0^T dt \int_0^a \left(\frac{\partial C}{\partial t} - \alpha D \nabla^2 C + \lambda C \right) C^* 4\pi r^2 dr = \int_0^T dt \int_0^a BC^* 4\pi r^2 dr \tag{C.7}$$

We manipulate the left-hand side through an integration by parts. The first term becomes

$$\int_0^T dt \int_0^a C^* \frac{\partial C}{\partial t} 4\pi r^2 dr = \int_0^a \left(C^*(r,t) C(r,t) \right)_0^T 4\pi r^2 dr - \int_0^T dt \int_0^a C \frac{\partial C^*}{\partial t} 4\pi r^2 dr \tag{C.8}$$

The second term requires the Green's identity (A.4)

$$\int_0^T dt \int_0^a C^* \nabla^2 C 4\pi r^2 dr = \tag{C.9}$$

$$= \int_0^T dt \int_S C^* \nabla C \cdot \mathbf{n} dS - \int_0^T dt \int_0^a \nabla C \cdot \nabla C^* 4\pi r^2$$

$$= \int_0^T dt \int_S (C^* \nabla C - C \nabla C^*) \cdot \mathbf{n} dS + \int_0^T dt \int_0^a C \nabla^2 C^* 4\pi r^2 dr \tag{C.10}$$

The middle term $\int_0^T dt \int_S (C^* \nabla C - C \nabla C^*) \cdot \mathbf{n} dS$ is an integral evaluated on the spherical surface, namely at $r = a$, where the concentration is subjected to a null boundary condition. The term related to the adjoint concentration $C(a, t)$ is similarly put to zero. Analogously to what is common in neutron transport theory, it can be said that, in light of the meaning of the adjoint concentration, namely the importance function, the importance of a particle generated on the spherical surface is zero, since it diffuses immediately out from the sphere and an hypothetical measurement device will not detect it. In summary, $C^*(a, t) = 0$ and (C.10) simplifies in

$$\int_0^T dt \int_0^a C^* \nabla^2 C 4\pi r^2 dr = \int_0^T dt \int_0^a C \nabla^2 C^* 4\pi r^2 dr \tag{C.11}$$

which is the Lagrange identity for the self-adjoint diffusion operator. The integral (C.7) eventually can be written as

$$\int_0^T dt \int_0^a C \left(-\frac{\partial C^*}{\partial t} - \alpha D \nabla^2 C^* + \lambda C^* \right) 4\pi r^2 dr = \\ = -\int_0^a (C^*(r,t)C(r,t))_0^T \, 4\pi r^2 dr + \int_0^T \int_0^a BC^* 4\pi r^2 dr \tag{C.12}$$

or exploiting the inner product (C.5) and defining the adjoint operator A^* as

$$A^* = -\frac{\partial}{\partial t} - \alpha D \nabla^2 + \lambda \tag{C.13}$$

a compact formula is the following

$$(AC, C^*) = (C, A^* C^*) + \int_0^a (C^*(r,t)C(r,t))_0^T \, 4\pi r^2 dr \tag{C.14}$$

Assume the following *adjoint equation*

$$\begin{cases} -\dfrac{\partial C^*}{\partial t} - \alpha D \nabla^2 C^* + \lambda C^* = P(r,t) \\ C^*(r,T) = H(r), \quad 0 < r < a \\ C^*(a,t) = 0, \quad t > 0 \\ \nabla C^*|_{r=0} = 0, \quad t > 0 \end{cases} \tag{C.15}$$

Unlike the main problem (C.1), a final condition for the adjoint problem is given, at $t = T > 0$. The symmetry boundary condition is used for convenience. The useful boundary condition is the one holding in $r = a$, which is the same holding in $r = -a$. $P(r,t)$ and $H(r)$ are arbitrary functions.

The solution C^* is assumed to belong, at every t, to the domain of A^*, $D(A^*) \equiv D(A)$. With regarding the previous introductions

$$(C, A^* C^*) = (C, P) \tag{C.16}$$

and

$$(C, A^* C^*) = -\int_0^a H(r)C(r,T)4\pi r^2 dr + \int_0^a C^*(r,0)C_0 \, 4\pi r^2 dr + (B, C^*) \tag{C.17}$$

Then

$$(C, P) + \int_0^a H(r)C(r,T)4\pi r^2 dr = (B, C^*) + \int_0^a C^*(r,0)C_0 4\pi r^2 dr \tag{C.18}$$

It is commonly assumed, in adjoint equations theory, that we are not interest in the value of thee solution $C(r,t)$ but in a solution's functional J. We define J as

$$J = \frac{3}{4\pi a^3}(C, P) + \frac{3}{4\pi a^3} \int_0^a H(r)C(r,T)4\pi r^2 dr \tag{C.19}$$

or equivalently

$$J = \frac{3}{4\pi a^3}(B, C^*) + \frac{3}{4\pi a^3} \int_0^a C^*(r,0)C_0 4\pi r^2 dr \tag{C.20}$$

The functions $P(r,t)$ and $H(r)$ are said to be determined by the characteristic of a measurement instrument. Eq. (C.20) is important because it is more usable in computations, with respect to (C.19), in particular when values of J are needed for a large set of initial data B and C_0.

Let's assume that the initial and boundary conditions are such that $(C,P) = (B,C^*)$ and $P = 1$. Then J reduces to the expression

$$J = \frac{3}{4\pi a^3}\int_0^T dt \int_0^a C(r,t) 4\pi r^2 dr \tag{C.21}$$

By exploiting the average of $C(r,t)$ over the sphere, namely Eq. (1.22)

$$J = \int_0^T \bar{C}(t) dt \tag{C.22}$$

The last expression for the functional J is proportional to the temporal average of the concentration. The time domain $(0,T)$ may coincide with the simulated period.

As concerns the sensitivity analysis, let's consider now a perturbation of the inputs B and C_0. In the small perturbation theory, the functions become

$$B' = B + \delta B, \quad C_0' = C_0 + \delta C_0 \tag{C.23}$$

The perturbed main problem is

$$\begin{cases} \dfrac{\partial C'}{\partial t} - \alpha D \nabla^2 C' + \lambda C' = B \\ C'(r,0) = C_0', \quad 0 < r < a \\ C'(a,t) = 0, \quad t > 0 \\ \nabla C'|_{r=0} = 0, \quad t > 0 \end{cases} \tag{C.24}$$

The solution can be linearized with respect to the perturbation

$$C'(r,t) = C(r,t) + \delta C(r,t) \tag{C.25}$$

and similarly the perturbed functional is

$$J' = J + \delta J \tag{C.26}$$

The small change δJ is easy to find exploiting eqs. (C.19) and (C.20)

$$\delta J = \frac{3}{4\pi a^3}(\delta C, P) + \frac{3}{4\pi a^3}\int_0^a H(r)\delta C(r,T) 4\pi r^2 dr \tag{C.27}$$

$$\delta J = \frac{3}{4\pi a^3}(\delta B, C^*) + \frac{3}{4\pi a^3}\int_0^a C^*(r,0)\delta C_0 4\pi r^2 dr \tag{C.28}$$

The estimate of functional variation δJ with respect to δB and δC_0 descend from (C.28), where the importance function C^* appears as a weight function, in the frame of the small perturbation theory.

Appendix D

Spectral solver for a system of N coupled diffusion-decay equations

If one focuses on radioactive FPs then it is perfectly reasonable to consider that some isotopes may by related by a precursor-daughter relationship type. For example, this is the case of metastable nuclei, $^{135\mathrm{m}}$Xe and $^{85\mathrm{m}}$Kr which decay by isomeric transition (IT), an elecromagnetic process, respectively into ^{135}Xe and ^{85}Kr Another example is represented by an unstable iodine isotope that decays into a xenon one, through β^- decay, namely the emission of an electron and an anti-neutrino together with the conversion of a neutron of the nucleus into a proton

Let's group the concentrations of the radionuclides of interest in a vector $\mathbf{C} = \{C_i\}$, the subscript i browse the different isotopes. The intra-granular problem becomes

$$\mathbf{C}_t = \overline{\overline{D}} \cdot \mathbf{C} + \overline{\overline{\Lambda}} \cdot \mathbf{C} + \mathbf{S} \tag{D.1}$$

The diagonal matrix $\overline{\overline{D}}$ represents the diffusion operator $D_i \nabla^2$. The matrix $\overline{\overline{\Lambda}}$ is in general not diagonal. The source vector is $\mathbf{S} = \{y_i \dot{F}\}$. For a general system of N isotopes

$$\begin{bmatrix} \frac{\partial C_1}{\partial t} \\ \dots \\ \frac{\partial C_i}{\partial t} \\ \dots \\ \frac{\partial C_N}{\partial t} \end{bmatrix} = \begin{bmatrix} D_1\nabla^2 & \dots & 0 & \dots & 0 \\ 0 & \dots & \dots & \dots & 0 \\ 0 & \dots & D_i\nabla^2 & \dots & 0 \\ 0 & \dots & \dots & \dots & 0 \\ 0 & \dots & 0 & \dots & D_N\nabla^2 \end{bmatrix} \cdot \begin{bmatrix} C_1 \\ \dots \\ C_i \\ \dots \\ C_N \end{bmatrix} +$$

$$+ \begin{bmatrix} -\lambda_{1\to2} & 0 & \dots & 0 & 0 \\ \lambda_{1\to2} & -\lambda_{2\to3} & \dots & 0 & 0 \\ \dots & \dots & \dots & \dots & \dots \\ \dots & \dots & \dots & -\lambda_{N-1\to N} & \dots \\ 0 & 0 & \dots & \lambda_{N-1\to N} & -\lambda_N \end{bmatrix} \cdot \begin{bmatrix} C_1 \\ C_2 \\ \dots \\ C_{N-1} \\ C_N \end{bmatrix} + \begin{bmatrix} S_1 \\ \dots \\ S_i \\ \dots \\ S_N \end{bmatrix} \tag{D.2}$$

Within the decay matrix $\overline{\overline{\Lambda}}$, diagonal elements represent the radioactive decay loss, non-diagonal elements represent the positive contribute of production due to precursor decay. Note that it has been assumed an order in the vector $\mathbf{C}$ such that the i-th element decays into the (i+1)-th element. Moreover, for completeness reason, in the

decay matrix all the possible decay rates have been included. Obviously this matrix will be full of zero-terms. As a purely mathematical constraint we can state that the sum along the i-th column must be 0 or $-\lambda_i$.

From a numerical point of view, spectral discretization of the spatial dimension is again preferred. The modal decomposition reads

$$\mathbf{C} = \sum_{k=1}^{\infty} \mathbf{x}_k(t)\varphi_k(r) \tag{D.3}$$

The scalar eigenfunction $\psi_k(r)$ is again a sinc function, which respect the boundary conditions of the problem. For every vector $\mathbf{x}_k$ the following differential system has to be solved

$$\dot{\mathbf{x}}_k = (\overline{\overline{Y}}_k + \overline{\overline{\Lambda}}) \cdot \mathbf{x}_k + \mathbf{s}_k \tag{D.4}$$

where $\overline{\overline{Y}}_k$ is the spectral equivalent of the diffusion matrix $\overline{\overline{D}}$

$$\overline{\overline{Y}}_k = \begin{bmatrix} -\dfrac{D_1\pi^2k^2}{a^2} & \dots & 0 & \dots & 0 \\ 0 & \dots & \dots & \dots & 0 \\ 0 & \dots & -\dfrac{D_i\pi^2k^2}{a^2} & \dots & 0 \\ 0 & \dots & \dots & \dots & 0 \\ 0 & \dots & 0 & \dots & -\dfrac{D_N\pi^2k^2}{a^2} \end{bmatrix} \tag{D.5}$$

The spectral source vector is $\mathbf{s}_k = \{< \varphi_k | S_{i,k} >\}$. The system is solved with backward implicit Euler in time, then for every mode

$$(\mathbb{I} - \overline{\overline{M}}_k \Delta t) \cdot \mathbf{x}_k^{t+1} = \mathbf{x}_k^t + \mathbf{s}_k \Delta t \tag{D.6}$$

where $\overline{\overline{M}}_k = \overline{\overline{Y}}_k + \overline{\overline{\Lambda}}$. This is a linear system of the form $\overline{\overline{A}} \cdot \mathbf{x} = \mathbf{b}$. There are several ways to handle such a problem. In SCIANTIX it is possible to iterate a LU decomposition to get the solution $\mathbf{x}_k^{t+1}$, at every t. Once computed $\mathbf{x}_k$, the solution is obtained with the usual spatial average

$$\bar{\mathbf{C}}(t) \approx \frac{3}{4\pi a^3} \sum_{k=1}^{K} \mathbf{x}_k < \psi_k | 1 > \tag{D.7}$$

For example, a general case in which an iodine isotope decays into a xenon one, is written as

$$\begin{cases} \dfrac{\partial I}{\partial t} = D_I \nabla^2 I - \lambda_I I + S_I \\ \dfrac{\partial X}{\partial t} = D_X \nabla^2 X - \lambda_X X + \lambda_I I + S_X \end{cases} \tag{D.8}$$

or

$$\begin{bmatrix} I_t \\ X_t \end{bmatrix} = \begin{bmatrix} D_I\nabla^2 & 0 \\ 0 & D_X\nabla^2 \end{bmatrix} \cdot \begin{bmatrix} I \\ X \end{bmatrix} + \begin{bmatrix} -\lambda_I & 0 \\ \lambda_I & -\lambda_X \end{bmatrix} \cdot \begin{bmatrix} I \\ X \end{bmatrix} + \begin{bmatrix} S_I \\ S_X \end{bmatrix} \tag{D.9}$$

Bibliography

[American Nuclear Society, 2016] American Nuclear Society (2016). Glossary of definitions and units. Technical report, American Nuclear Society.

[Barnes, 1964] Barnes, R. S. (1964). A theory of swelling and gas release for reactor materials. *Journal of Nuclear Materials*, 2:135–148.

[Beck, 1960] Beck, S. D. (1960). The diffusion of radioactive fission products from porous fuel elements. *Physics and Mathematics (TID-4500, 15th Ed.)*.

[Bernard and Bonnaud, 1997] Bernard, L. C. and Bonnaud, E. (1997). Finite volume method for fission gas release modeling. *Journal of Nuclear Materials*, 244(1):75–84.

[Bernard et al., 2002] Bernard, L. C., Jacoud, J. L., and Vesco, P. (2002). An efficient model for the analysis of fission gas release. *Journal of Nuclear Materials*, 302(2-3):125–134.

[Booth, 1957] Booth, A. (1957). A method of calculating fission gas diffusion from UO2 fuel and its application to the X-2-f loop test. *Atomic Energy of Canada Limited*.

[Brown and Faircloth, 1976] Brown, P. E. and Faircloth, R. L. (1976). Metal fission product behaviour in high temperature reactors -UO2 coated particle fuel. *Journal of Nuclear Materials*, 59(1):29–41.

[Ducros et al., 2001] Ducros, G., Malgouyres, P. P., Kissane, M., Boulaud, D., and Durin, M. (2001). Fission product release under severe accidental conditions: General presentation of the program and synthesis of VERCORS 1-6 results. *Nuclear Engineering and Design*, 208(2):191–203.

[Ducros et al., 2013] Ducros, G., Pontillon, Y., and Malgouyres, P. P. (2013). Synthesis of the VERCORS experimental programme: Separate-effect experiments on Fission Product release, in support of the PHEBUS-FP programme. *Annals of Nuclear Energy*, 61:75–87.

[Friskney and Speight, 1976] Friskney, C. A. and Speight, M. V. (1976). A calculation on the in-pile diffusional release of fission products forming a general decay chain. *Journal of Nuclear Materials*, 62:89–94.

[Friskney and Turnbull, 1979] Friskney, C. A. and Turnbull, J. A. (1979). The characteristics of fission gas release from uranium dioxide during irradiation. *Journal of Nuclear Materials*, 79(1):184–198.

[Ham, 1958] Ham, F. S. (1958). Theory of diffusion-limited precipitation. *Journal of Physics and Chemistry of Solids*, 6(4):335–351.

[Housiadas et al., 2012] Housiadas, C., Kissane, M., Sehgal, R., and Ducros, G. (2012). *Fission product release and transport*. Elsevier Inc.

[IAEA, 2020] IAEA (2020). https://www-nds.iaea.org/sgnucdat/c3.htm.

[Johnson and Johnson, 1988] Johnson, I. and Johnson, C. E. (1988). Mass spectrometry studies of fission product behaviour I. Fission products released from irradiated LWR fuel. *Journal of Nuclear Materials*, 154:67–73.

[Kleykamp, 1985] Kleykamp, H. (1985). The chemical state of the fission products in oxide fuels. *Journal of Nuclear Materials*, 131(2-3):221–246.

[Kogai, 1997] Kogai, T. (1997). Modelling of fission gas release and gaseous swelling of light water reactor fuels. *Journal of Nuclear Materials*, 244(2):131–140.

[Lassmann, 1992] Lassmann, K. (1992). TRANSURANUS: a fuel rod analysis code ready for use. *Nuclear Materials for Fission Reactors*, pages 295–302.

[Lösönen, 2000] Lösönen, P. (2000). On the behaviour of intragranular fission gas in UO2 fuel. *Journal of Nuclear Materials*, 280(1):56–72.

[Oberkampf et al., 2004] Oberkampf, W. L., Trucano, T. G., and Hirsch, C. (2004). Verification, validation, and predictive capability in computational engineering and physics. *Applied Mechanics Reviews*, 57(1-6):345–384.

[Olander, 1976] Olander, D. R. (1976). *Fundamental Aspects of Nuclear Reactor Fuel Elements*. Technical lnformation Center Energy Research and Development Administration.

[Olander and Wongsawaeng, 2006] Olander, D. R. and Wongsawaeng, D. (2006). Resolution of fission gas - A review: Part I. Intragranular bubbles. *Journal of Nuclear Materials*, 354(1-3):94–109.

[Pastore et al., 2013] Pastore, G., Luzzi, L., Di Marcello, V., and Van Uffelen, P. (2013). Physics-based modelling of fission gas swelling and release in UO2 applied to integral fuel rod analysis. *Nuclear Engineering and Design*, 256:75–86.

[Pastore et al., 2018] Pastore, G., Pizzocri, D., Rabiti, C., Barani, T., Van Uffelen, P., and Luzzi, L. (2018). An effective numerical algorithm for intra-granular fission gas release during non-equilibrium trapping and resolution. *Journal of Nuclear Materials*, 509:687–699.

[Pizzocri et al., 2020] Pizzocri, D., Barani, T., and Luzzi, L. (2020). SCIANTIX: A new open source multi-scale code for fission gas behaviour modelling designed for nuclear fuel performance codes. *Journal of Nuclear Materials*, page 152042.

[Pizzocri et al., 2018] Pizzocri, D., Pastore, G., Barani, T., Magni, A., Luzzi, L., Van Uffelen, P., Pitts, S. A., Alfonsi, A., and Hales, J. D. (2018). A model describing intra-granular fission gas behaviour in oxide fuel for advanced engineering tools. *Journal of Nuclear Materials*, 502:323–330.

[Pontillon and Ducros, 2010a] Pontillon, Y. and Ducros, G. (2010a). Behaviour of fission products under severe PWR accident conditions: The VERCORS experimental programme - Part 2: Release and transport of fission gases and volatile fission products. *Nuclear Engineering and Design*, 240(7):1853–1866.

[Pontillon and Ducros, 2010b] Pontillon, Y. and Ducros, G. (2010b). Behaviour of fission products under severe PWR accident conditions. The VERCORS experimental programme - Part 3: Release of low-volatile fission products and actinides. *Nuclear Engineering and Design*, 240(7):1867–1881.

[Pontillon et al., 2010] Pontillon, Y., Ducros, G., and Malgouyres, P. P. (2010). Behaviour of fission products under severe PWR accident conditions VERCORS experimental programme - Part 1: General description of the programme. *Nuclear Engineering and Design*, 240(7):1843–1852.

[Pontillon et al., 2005] Pontillon, Y., Malgouyres, P. P., Ducros, G., Nicaise, G., Dubourg, R., Kissane, M., and Baichi, M. (2005). Lessons learnt from VERCORS tests.: Study of the active role played by UO2-ZrO2-FP interactions on irradiated fuel collapse temperature. *Journal of Nuclear Materials*, 344(1-3):265–273.

[Quarteroni et al., 2006] Quarteroni, A., Sacco, R., and Saleri, F. (2006). *Numerical Mathamatics*. Springer.

[R2CA, 2019] R2CA (2019). https://www.irsn.fr/EN/Research/Research-organisation/Research-programmes/R2CA-project/Pages/R2CA-project.aspx.

[Rest, 2003] Rest, J. (2003). The effect of irradiation-induced gas-atom re-solution on grain-boundary bubble growth. *Journal of Nuclear Materials*, 321(2-3):305–312.

[Setyawan et al., 2018] Setyawan, W., Cooper, M. W., Roche, K. J., Kurtz, R. J., Uberuaga, B. P., Andersson, D. A., and Wirth, B. D. (2018). Atomistic model of xenon gas bubble re-solution rate due to thermal spike in uranium oxide. *Journal of Applied Physics*, 124(7).

[Soffer et al., 1995] Soffer, L., Burson, S., Ferrell, C., Lee, R., and Ridgely, J. (1995). Accident Source Terms for Light-Water Nuclear Power Plants. Technical report, U.S. Nuclear Regulatory Commission.

[Speight, 1969] Speight, M. V. (1969). A Calculation on the Migration of Fission Gas in Material Exhibiting Precipitation and Re-solution of Gas Atoms Under Irradiation. *Nuclear Science and Engineering*, 37(2):180–185.

[Speight and Beeré, 1975] Speight, M. V. and Beeré, W. B. (1975). Vacancy potential and void growth on grain boundaries. *The Metal Society*, 9:190–191.

[Turnbull and Beyer, 2009] Turnbull, J. and Beyer, C. E. (2009). Background and Derivation of ANS-5 . 4 Standard Fission Product Release Model Office of Nuclear Regulatory Research. *Office of Nuclaer Regulatory Research*.

[Turnbull, 1971] Turnbull, J. A. (1971). The distribution of intragranular fission gas bubbles in UO2 during irradiation. *Journal of Nuclear Materials*, 38(2):203–212.

[Turnbull, 2001] Turnbull, J. A. (2001). The treatment of radioactive fission gas release measurements and provision of data for development and validation of the ANS-5.4 model. *OECD HALDEN REACTOR PROJECT*.

[Turnbull et al., 1982] Turnbull, J. A., Friskney, C. A., Findlay, J. R., Johnson, F. A., and Walter, A. J. (1982). The diffusion coefficients of gaseous and volatile species during the irradiation of uranium dioxide. *Journal of Nuclear Materials*, 107(2-3):168–184.

[Verma et al., 2020] Verma, L., Noirot, L., and Maugis, P. (2020). Modelling intragranular bubble movement and fission gas release during post-irradiation annealing of UO2 using a meso-scale and spatialized approach. *Journal of Nuclear Materials*, 528:151874.

[Veshchunov, 2008] Veshchunov, M. S. (2008). Modelling of grain face bubbles coalescence in irradiated UO2 fuel. *Journal of Nuclear Materials*, 374(1-2):44–53.

[Vitanza et al., 1979] Vitanza, C., Kolstad, E., and Graziani, U. (1979). Fission gas release from UO2 pellet fuel at high burn-up. *OECD HALDEN REACTOR PROJECT*, pages 361–366.

[Whapham, 1966] Whapham, A. D. (1966). Electron microscope observation of the fission-gas bubble distribution in UO2. *Nuclear applications*, pages 123–130.

[White, 2001] White, R. J. (2001). The fractal nature of the surface of uranium dioxide: A resolution of the short-lived/stable gas release dichotomy. *Journal of Nuclear Materials*, 295(2-3):133–148.

[White, 2004] White, R. J. (2004). The development of grain-face porosity in irradiated oxide fuel. *Journal of Nuclear Materials*, 325(1):61–77.

[White et al., 2006] White, R. J., Corcoran, R. C., and Barnes, R. S. (2006). A Summary of Swelling Data Obtained from the AGR/Halden Ramp Test Programme. *R&T/NG/EXT/REP/0206/02*.

[White and Tucker, 1983] White, R. J. and Tucker, M. O. (1983). A new fission-gas release model. *Journal of Nuclear Materials*, 118(1):1–38.